Copyright

by

Brenda Jean Postnikova

2003

The Dissertation Committee for Brenda Postnikova Certifies that this is the approved version of the following dissertation:

Synthesis of Organic Compounds for Two-photon Initiated Polymerization and Molecular Recognition

Committee:

Eric V. Anslyn, Supervisor

Michael J. Krische

John T. McDevitt

Rebecca Richards-Kortum

David A. Vanden Bout

Synthesis of Organic Compounds for Two-photon Initiated Polymerization and Molecular Recognition

by

Brenda Jean Postnikova, B.A., M.A.

Dissertation

Presented to the Faculty of the Graduate School of

The University of Texas at Austin

in Partial Fulfillment

of the Requirements

for the Degree of

Doctor of Philosophy

The University of Texas at Austin

August 2003

Dedication

To my husband, Серёжа

Acknowledgements

My deepest thanks go to my advisor, Professor Eric V. Anslyn. Your guidance and enthusiasm have been most inspiring to me throughout my graduate career. I have sincerely appreciated the opportunity to work in your research group.

I also would like to thank all of my research collaborators on the two-photon project, Professor David A. Vanden Bout, Professor Jason B. Shear, Dr. Robert E. Hanes, Thomas Doyle and John Currie. Particularly, I would like to thank Professor Vanden Bout for enlightening discussions which have expanded my understanding of my research.

I am grateful to the members of the Anslyn research group, past and present for their helpful advice and thoughtful discussions. Of special mention are Dr. Anna Piątek for your helpful suggestions, Ron Houk for your assistance with computer-related issues, Frantz Andersen for reading this dissertation, Dr. Robert E. Hanes for "initiation" into the two-photon project and for your advice on chemistry in general, and especially, Dr. Shawn McCleskey for your friendship and support.

I want to thank my family, Mom, Dad, my brother Allan, and most of all, my husband, Sergei, for your enduring love, patience and support.

To our God and Father be glory for ever and ever. Amen. Philippians 4:20

Synthesis of Organic Compounds for Two-photon Initiated Polymerization and Molecular Recognition

Publication No._____

Brenda Jean Postnikova, Ph. D.

The University of Texas at Austin, 2003

Supervisor: Eric V. Anslyn

In section I, three-dimensional polymeric objects were fabricated using two-photon initiated polymerization (TPIP) with a two-photon absorbing chromophore and an acrylate resin. The feasibility of fabricating polymeric features on the nanoscale was explored using an enhanced field generated at the apex of a gold tip as the excitation source, as used in near-field excitation (NFE). In section II, C_3-symmetric chiral receptors were used to direct enantioselective enolate alkylation. A series of host compounds was synthesized and 1:1 host to enolate binding was observed by ^{1}H NMR titration experiments. A moderate increase in the enantioselectivity of the alkylation of 2-acetylcyclohexanone was observed in the presence of host **2.22**. Also in section II, the use of enolate stabilization *via* charge-pairing was investigated for the reduction of the pK_a of 2-

acetylcyclopentanone. In the presence of host **3.12**, the pK_a of 2-acetylcyclopentanone was reduced by 10 pK_a units. In comparison with the 2.9 pK_a unit shift observed with host **3.11**, this result suggests that charge-pairing is more effective in stabilizing enolates in enzyme active sites than traditional hydrogen bonding.

Table of Contents

List of Figures

List of Tables

SECTION I

DEVELOPMENT OF MATERIALS AND METHODS FOR THE FABRICATION OF NANOSCALE THREE-DIMENSIONAL STRUCTURES USING TWO-PHOTON INITIATED POLYMERIZATION

Chapter 1

1.1 INTRODUCTION

Photoinitiated polymerization is a well-documented and widely used method for preparing polymeric materials, particularly for the fabrication of integrated circuits and microelectromechanical systems (MEMS). An advantage of photoinitiated polymerization (as opposed to thermally initiated polymerization, for example) is the spatial control of the reaction to regions exposed to light, thus providing a method to generate polymeric patterns on surfaces. Polymerization initiated by single-photon absorption, as used in standard photolithographic techniques, is inherently two-dimensional and three-dimensional structures required for MEMS are built up by iterative photolithographic steps. Due to the increasing complexity of MEMS devices, the use of two-photon absorption should offer several advantages over conventional lithographic techniques in MEMS fabrication, particularly a more direct route to three dimensional polymeric structures and also, the incorporation of chemical functionality into polymeric structures. The goal of this project is to develop methods to fabricate polymeric structures on the nanoscale and incorporate chemical functionality, such as molecular recognition and color, into nanoscale three-dimensional polymeric structures for potential application as sensors.

1.2 PHOTOCHEMISTRY

The absorption of light by organic compounds can initiate many chemical processes including luminescence, ionization, isomerization and free-radical formation. These processes are useful in both organic synthesis and in chemical analysis. The field of photochemistry describes these processes in terms of quantum theory[1] in which light is composed of discrete packets of energy called photons wherein the energy of a photon is related to its wavelength as follows:

$$\mathscr{E} = \frac{hc}{\lambda}$$

The absorption of a single photon by a molecule may be thought of as a chemical reaction in which the photoactivated compound is the product of a photon ($h\nu$) and the chromophore (M) as shown in Equation 1.1.[2]

$$M + n(h\nu) \rightleftharpoons M^*$$

Equation 1.1

A rate expression for the rate of formation of the activated species, M*, defined by Equation 1.1 may then be written as shown in Equation 1.2.

$$d[M^*]/dt = k[h\nu]^n[M]$$

Equation 1.2

This expression relates the rate of formation of the photoactivated chromophore (M*) to the light intensity ($h\nu$), the number of photons involved in the excitation event (n), and the concentration of the chromophore (M). The rate constant, k, describes the sensitivity of a chromophore to photon absorption.

1.2.1 Single Photon Excitation

One photon excitation (OPE) of a molecule occurs through the absorption of a single photon by a chromophore and, from Equation 1.2 where $n = 1$, excitation is linearly proportional to the light intensity ($h\nu$). Upon absorption of a photon, an electron is promoted from a bonding orbital to an antibonding molecular orbital, for example from the ground state, S_0, to the first excited stated, S_1 (Figure 1.1). The absorption of light is quantized in that only photons carrying exactly the same energy as the energy difference between the ground and an excited state are absorbed (S_{n+1} - S_0). Increasing the light intensity only increases the number of molecules undergoing a certain transition (as would be observed in a second order chemical reaction between two molecules A and B, where increasing the concentration of one of the reactants increases the rate of reaction), but does not affect the nature of the transition.

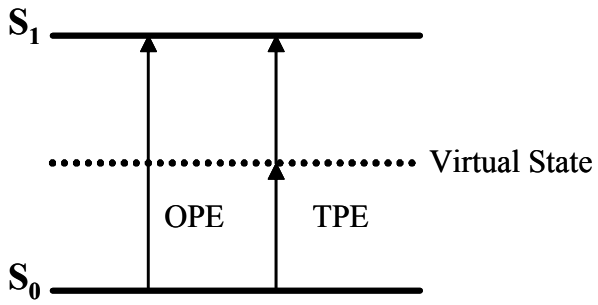

Figure 1.1 Joblanski Diagram of the Operative Photophysics of a Chromophore; OPE, one-photon excitation, TPE, two-photon excitation.[1]

The transitions available to a chromophore are observed in the UV-Vis absorption spectrum of a chromophore. The UV-Vis spectrum of an organic compound appears as a continuous function (rather than a set of distinct lines) spanning wavelengths in the electromagnetic spectrum because of the multitude of transitions that exist for an organic compound. The optimal wavelength for exposure to bring about a photochemical reaction is the wavelength with the highest absorbance in the UV spectrum of a chromophore.

1.2.2 Two-photon Excitation

As shown in Figure 1.1, a chromophore may also be promoted to an excited state through two-photon excitation (TPE). In multiphoton excitation processes involving two or more photons, the excitation of a molecule from the ground state

(S_0) to an excited state (S_1) is achieved by the near-simultaneous absorption of two or more photons (within approximately one femtosecond), each carrying a fraction of the energy required for excitation with a single photon. Whereas single-photon absorption is linearly proportional to light intensity, the probability for absorption of two photons is quadratically dependent on the light intensity, as can be seen in Equation 1.2 where $n = 2$, and therefore requires high instantaneous intensity to occur.

Absorption of a photon of an energy not equal to the energy difference between the ground state and an excited state of a molecule cannot occur, except under special conditions when narrow bandwidth, high intensity radiation is used. According to the Heisenberg uncertainty principle, an electron may occupy intermediate energy levels ("virtual states") between the ground and excited state, resulting from a broadening of energy levels between the states. The energy and lifetime of the "virtual" states can be found through the Heisenberg uncertainty principle, Equation 1.3.[2]

$$\Delta t = h \diagup 2\pi \cdot \Delta E$$

Equation 1.3

Each energy level can be thought of as consisting of many energy levels, with less stable states having a larger energy distribution. As can be seen from Equation 1.3, when the energy level broadens, the lifetime of the energy level becomes shorter. The lifetime of the virtual states has been determined to be on the order

of one femtosecond.[2] As seen in Figure 1.1, for two-photon absorption, a photon one-half the energy required for single-photon excitation must be absorbed, promoting the molecule to one of these short-lived "virtual" excited states of an energy halfway between the ground state and an excited state. Within the one femtosecond lifetime of this energy state, a second photon must be absorbed to promote the molecule into the more stable, higher energy excited state, S_1, otherwise, the molecule relaxes back to the ground state.

The λ_{max} for single photon excitation cannot simply be doubled to find the optimal wavelength for two-photon excitation because selection rules for excitation depend on the molecular properties of the chromophore and the number of photons required for excitation. The absorption spectrum for a two-photon absorbing chromophore may be found experimentally and the absorption spectra of several two-photon absorbing chromophores have been reported.[3]

1.3 TWO-PHOTON ABSORBING CHROMOPHORES

The two-photon absorption cross-section of a molecule, δ, quantifies the intensity dependent probability of two-photon absorption (TPA) and is proportional to the rate constant, *k*, in Equation 1.2 and has units dependent on the number of photons involved in excitation ($cm^{2n}(s/photon)^{n-1}$). In single photon absorption, the λ_{max} may be predicted according to the functional groups in a molecule and is easily found from the UV spectrum of the chromophore.

Similarly, the δ for two-photon absorbing chromophores is connected to the extent of conjugation of the π-system and the presence of electron donating or withdrawing groups conjugated to the π-system, as found both experimentally and by theoretical calculations by Albota *et al*.[4] Symmetrically substituted compounds having the general structure donor-π-donor were found to have large δ values. The large δ values for such compounds is correlated with intramolecular charge redistribution that occurs within the molecule upon excitation that takes place with symmetric charge transfer from the donor groups to the π-conjugated bridge.

A series of two-photon absorbing chromophores, designed by Albota *et al*, with successively extended π-systems, revealed an increase in the two-photon absorption cross-section from the parent chromophore, *trans*-stilbene.[4] Likewise, the addition of donating groups such as amines, or electron accepting groups such as cyano groups, increased the two-photon sensitivity, as illustrated in Table 1.1. Additionally, it was found that these modifications resulted in a shift of the λ_{max} for two-photon absorption to longer wavelengths. Based on the concept that enhanced δ values may be obtained *via* symmetric charge transfer upon excitation, several groups have also developed two-photon photoactive compounds with large TPA cross-sections.[5]

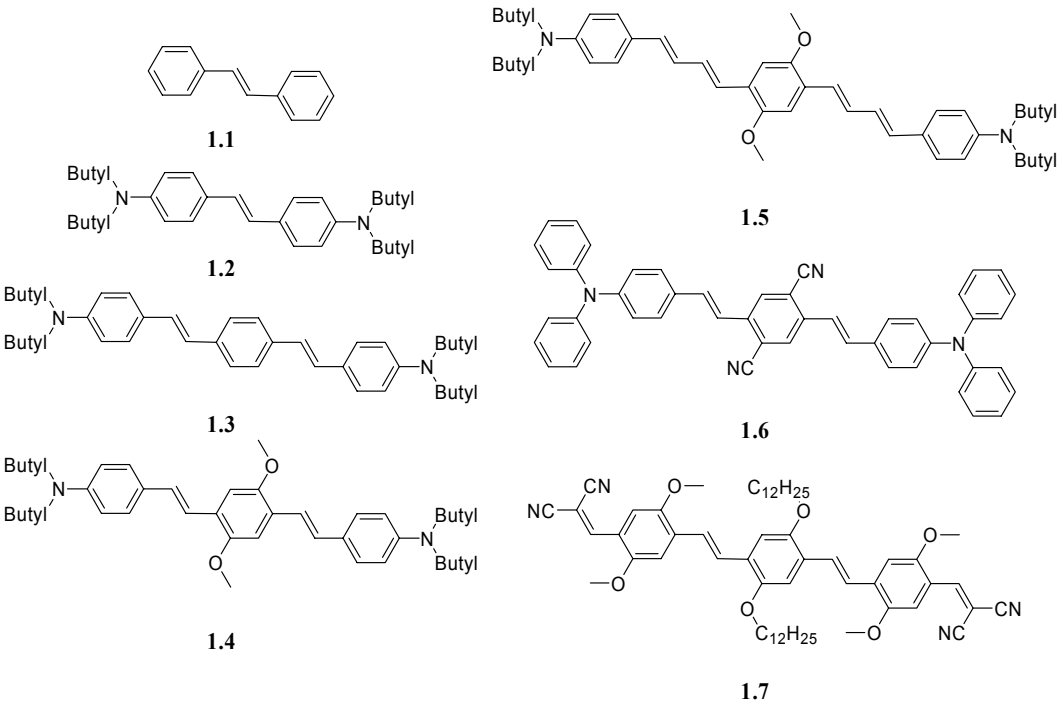

Compound	TPA λ_{max} (nm)	δ (10^{-50} cm^4 s photon^{-1})
1.1	514	12
1.2	605	210
1.3	730	995
1.4	730	900
1.5	775	1250
1.6	835	1940
1.7	825	480

Table 1.1 Experimental Two-photon Excitation Cross Sections (δ) and Peak Positions (TPA λ_{max}) for *Trans*-stilbene Based Chromophores.

1.4 APPLICATIONS OF TWO-PHOTON ABSORPTION

Multiphoton excitation was first proposed by Maria Göppert-Mayer in 1931, who examined the photon absorption of different materials and predicted their nonlinear resonance.[6] However, practical applications were limited due to the high intensity necessary for the process to take place. With the advent of high instantaneous intensity lasers, in 1961[7] and thereafter, this process was explored for a variety of applications, including fluorescence imaging and polymerization.

1.4.1 Fluorescence Spectroscopy with Two-photon Excitation

Two key aspects of multiphoton excitation make it desirable for fluorescence spectroscopy in bioanalytical chemistry.[8] It can be concluded from Figure 1.1 that longer wavelengths (lower energy photons) are used for multiphoton excitation. The longer wavelengths used for excitation allow penetration into highly absorbing biological samples and eliminate scattering associated with the use of UV and visible excitation light. Since biological samples do not absorb longer wavelengths, a sample may be examined without excessive heating.

Another advantage of two-photon excitation for fluorescence imaging is the ability of obtain three-dimensional images. Single photon excitation generates photochemical reactions in every plane perpendicular to the propagation of light through a photoactive material because each plane experiences the same total

photon flux (photons sec^{-1}). In contrast, when the excitation rate has a quadratic dependence on light intensity, as observed with two-photon excitation from Equation 1.2, excitation events occur predominantly in regions where the light intensity is high, particularly near the center of the focal point of a laser beam. Therefore, a three-dimensional image at the focal point of a tightly focused laser may be obtained because excitation of two-photon absorbing chromophores is confined to the focal point. A three-dimensional image of a biological sample may then be obtained by raster-scanning the focus of the laser within an "*x*-y" plane and repeating scans of the same area along the *z* axis. The three-dimensional array of points produces the image of a volume rather than a surface, as obtained with single photon fluorescence imaging.

1.4.2 Two-Photon Initiated Polymerization

Two-photon absorption (TPA) relies on the near-simultaneous absorption of two photons and consequently, is a process that requires extremely high peak intensities. The rate of TPA is quadratically dependent on intensity, and therefore TPA can be confined to high numerical aperture focal volumes of ~ 1 μm^3 when using pulsed near-infrared laser light.[2] Because single photon absorption scales linearly with excitation intensity, the excitation rate for a homogeneous chromophore solution is the same in all sample planes that intersect the propagation axis. Chemical processes initiated by TPA, such as polymerization,

can be confined to coordinates near the focal volume, allowing three-dimensional polymeric structures to be fabricated by translating a tightly focused laser beam within a material.

The quadratic dependence of TPA probability on excitation intensity allows the fabrication of polymeric structures with feature sizes that are smaller than the diffraction limit.[9] The resolution of an optical system is defined by the Rayleigh criterion as follows:

$$\Phi = 1.22\lambda / N.A.$$

Equation 1.4

where *N. A.* is the numerical aperture of the lens, λ is the wavelength of light used by the lens and Φ is the diameter of an object that is resolved. As shown in Figure 1.2, light from a point source passing through a lens creates a pattern of concentric circles of high and low light intensity, known as Airy circles. The distance from the center of the highest intensity circle at the focal point to the first node was defined by Abbe (Equation 1.4).[10] According to the Rayleigh criterion, if two point sources of light are resolved by an optical system, the distance between them is at least equal to the distance Φ.[11] Thus, the use of smaller wavelengths and lenses with high numerical apertures results in better resolution (and thus smaller feature sizes), as is the strategy in optical lithography. However, optical lithography relies on single photon excitation and thus excitation occurs throughout the focal plane of a lens. Two-photon excitation,

however, is quadratically dependent on the light intensity and therefore, exclusively occurs in regions where the intensity is highest, in the center of the focal point (Figure 1.2).

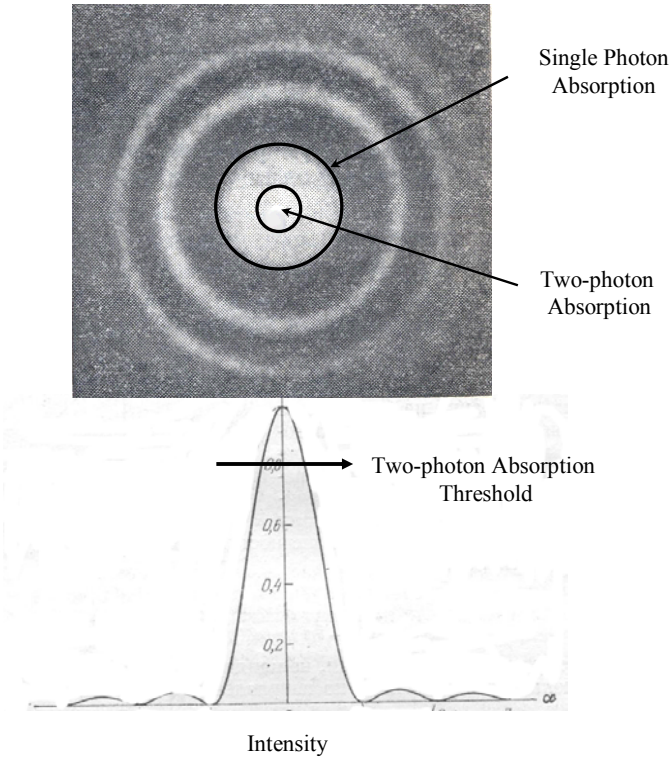

Figure 1.2 Intensity Distribution at the Focal Point of a Lens (Airy Circles) Illustrating the Threshold for Two-photon Absorption.[12]

This leads to a reduction in the area of excitation, and thus polymerization. All other factors being equal, smaller polymeric features should be possible with two-photoinitiated polymerization. The caveat however is that longer wavelengths are used for two-photon excitation (λ_{max}, Table 1.1). The use of larger wavelengths

leads to an increase in the diameter of the focal volume, thus reducing the potential benefit of the quadratic dependence of TPA.

Two-photon initiated polymerization (TPIP) has been demonstrated to occur in a localized area using a highly focused laser beam.[13, 14, 15, 16, 17, 18, 19, 20, 21, 22, 23, 24, 25, 26] Three-dimensional microstructures, which would be either difficult or time-consuming to fabricate using two-dimensional lithography, have been fabricated using TPIP in a single step by scanning a laser beam through a photopolymerizable resin along the *x*, *y* and *z* axis. A polymeric "micro bull", 10 μm long and 7 μm high (approximately the size of a red blood cell) was fabricated using TPIP from a commercially available urethane acrylate resin.[9] A minimum feature size of 120 nm was reported using a fabrication wavelength of 780 nm demonstrating that TPIP is not limited by the diffraction limit imposed by the Rayleigh criterion.

1.5 POLYMERIZATION WITH OPTICALLY ABSORBING MONOMERS

Photopolymerization using single-photon absorption is typically limited to surface-type applications because penetration of light through a thickness of absorbing material is low. In two-dimensional photolithography, fabrication of polymeric structures using highly absorbing materials is accomplished through the use of a sacrificial layer that is relatively non-absorbing (top-surface imaging).[27] Although a polymer matrix may incorporate UV absorbing additives,

since red or near-infrared light is used for TPIP, light attenuation is minimal because the polymer matrix does not effectively absorb red or near-infrared light. As a result, fabrication using TPIP is not as limited by the absorbance of a material compared to single photon excitation and structures can be built from the ground up in a material, instead of through the stacking of layers of material.

The utility of TPIP in generating three-dimensional objects is well documented.[13-26] However, the ability to polymerize materials with chemical functionality has not yet been exploited using TPIP. A practically unlimited range of materials can be utilized in micro and nano scale three-dimensional polymeric structures that respond to external stimuli in a controlled and reproducible manner ("smart" materials) using TPIP.

1.5.1 Monomer Desgin and Synthesis

To demonstrate the feasibility of incorporating monomers capable of molecular recognition into a three-dimensional polymeric structure fabricated using TPIP, colored and fluorescent monomers **1.8** and **1.9** were synthesized for use in a photopolymerizable matrix. Monomers **1.8** and **1.9** were proposed to model the incorporation of monomers capable of molecular recognition, as they can be detected using spectroscopic methods. Monomer **1.8** was synthesized

from Disperse Orange 13 by nucleophilic displacement of chloride in acryloyl chloride (Figure 1.3) in the presence of triethylamine.

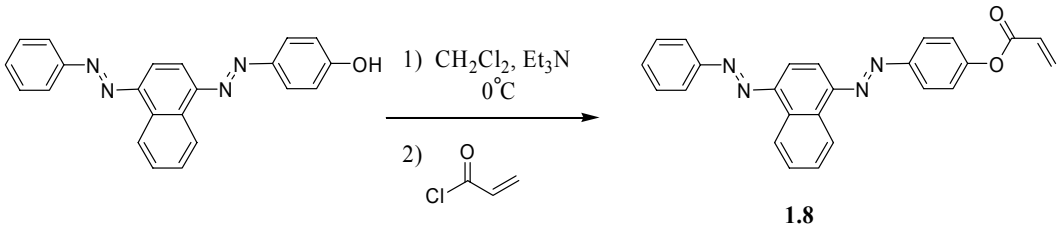

Figure 1.3 Synthesis of Disperse Orange Acrylate Monomer.

The single photon absorption spectrum of monomer **1.8** is shown in Figure 1.4. The λ_{max} of **1.8** is 420 nm with an extinction coefficient of 2.0 x 10^4.

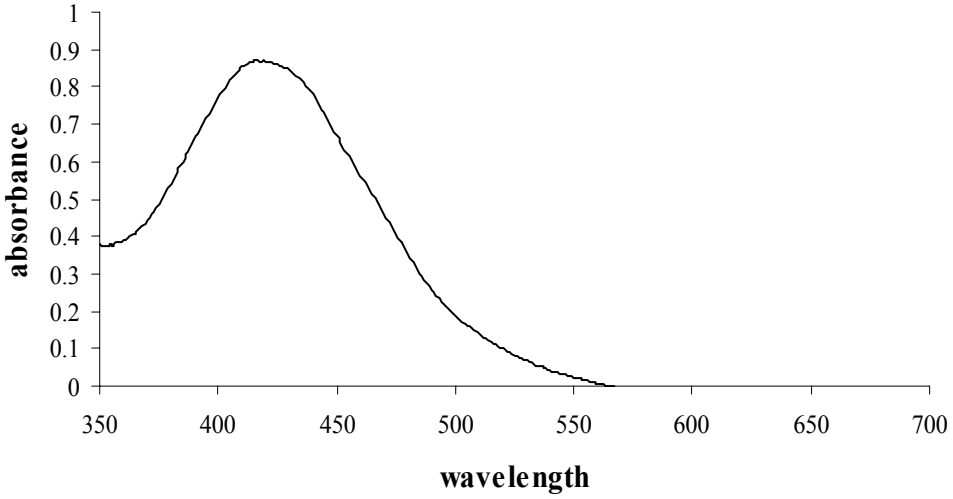

Figure 1.4 Linear Absorption Spectrum of **1.8** (6.1 x 10^{-2} mM in acetonitrile).

Monomer **1.9** was synthesized from Nile Blue A in two steps by first deprotonating Nile Blue A using aqueous sodium hydroxide, followed by nucleophilic displacement of chloride with acryloyl chloride (Figure 1.5).

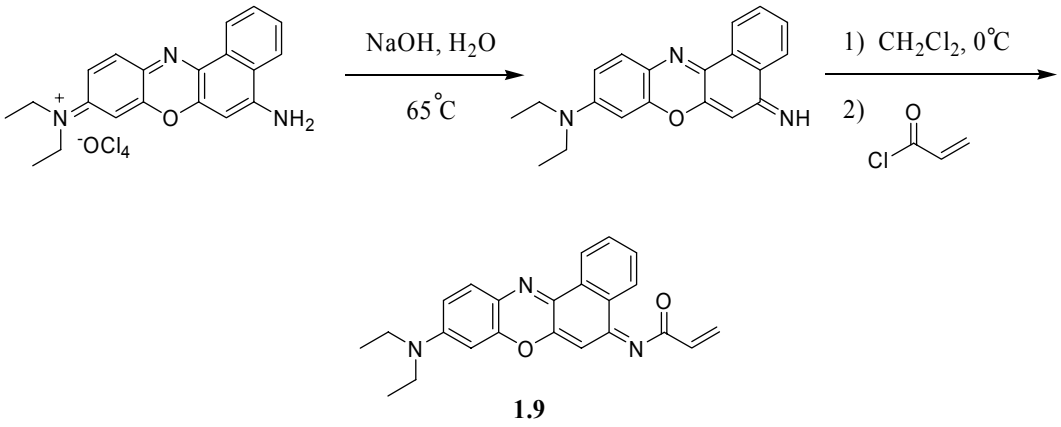

1.9

Figure 1.5 Synthesis of Nile Blue A Acrylate Monomer.

The single photon absorption spectrum of **1.9** is shown in Figure 1.6. An extinction coefficient of 3.8 x 10^4 was found at a λ_{max} of 610 nm.

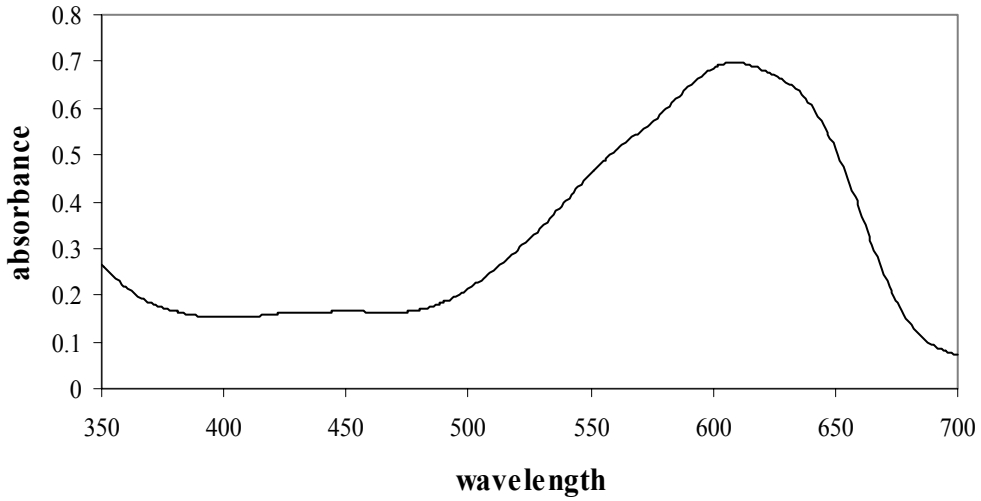

Figure 1.6 Linear Absorption Spectrum of **1.9** (2.0 x 10^{-2} mM in acetonitrile).

1.5.2 Two-photon Initiated Polymerization

1.5.2.1 Photoinitiator Selection and Synthesis

For the purpose of constructing small-scale polymeric structures incorporating chemically functionalized monomers, an initiator suitable for two-photon absorption was necessary. As compound **1.4** is electron rich (Table 1.1), it was postulated by Cumpston *et al.* that photoinduced electron transfer from **1.4** to an acrylate acceptor could result in polymerization of acrylate monomers.[17] Steady-state fluorescence quenching experiments revealed electron transfer

following the photoexcitation of **1.4**. The growth rate of polymerization of acrylate monomers as a function of intensity was found to be linearly dependent upon the incident laser intensity at 600 nm, as expected for two-photon initiated polymerization by a free-radical mechanism.[17]

Due to its well characterized utility in initiating the polymerization of acrylates, **1.4** was selected for our study. However, at the time of our study, the synthesis of **1.4** had not been reported. Retrosynthetic analysis suggested that the key carbon-carbon bond forming step could be accessible *via* a double Wittig reaction[28] from (*N*,*N*-di-*n*-butylamino)benzaldehyde and [(2,5-dimethoxy-1,4-phenylene)bis-(methylene)]bistriphenyl-phosphonium dibromide (**1.14)**. It was envisioned that 1,4-bis-bromomethyl-2,5-dimethoxybenzene could be prepared from 1,4-dimethoxybenzene by bromomethylation. Using this reaction sequence, compound **1.4** was obtained in 20% yield after chromatographic purification (Figure 1.7).[29] The synthesis of **1.4** from (*N*,*N*-di-*n*-butylamino)benzaldehyde and [(2,5-dimethoxy-1,4-phenylene)bis-(methylene)]bistriphenyl-phosphonium dichloride under Wittig reaction conditions (22.4% yield) has since been reported by Rumi *et al*.[30]

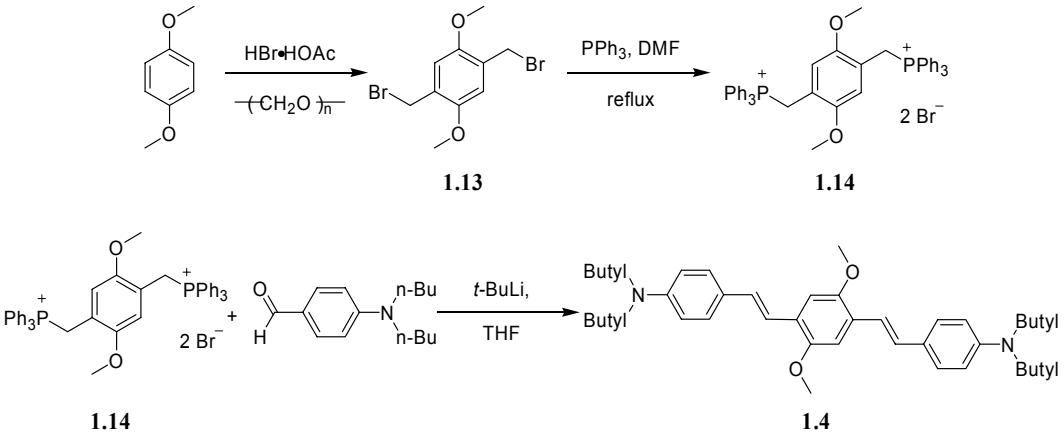

Figure 1.7 Synthesis of Two-photon Absorbing Photoinitiator **1.4**.

The single photon absorption spectrum of initiator **1.4** is shown in Figure 1.8. The λ_{max} appears at 430 nm. At the wavelength of two-photon excitation (780 nm), no linear absorbance is observed. The two-photon absorbing monomers **1.8** and **1.9** show overlapping linear absorption, and therefore photoexcitation using single photon excitation would be expected to be limited to the surface of a material due to attenuation of light into the film. However, using two-photon excitation of **1.4**, the fabrication of polymeric structures in the presence of **1.8** and **1.9** should be possible.

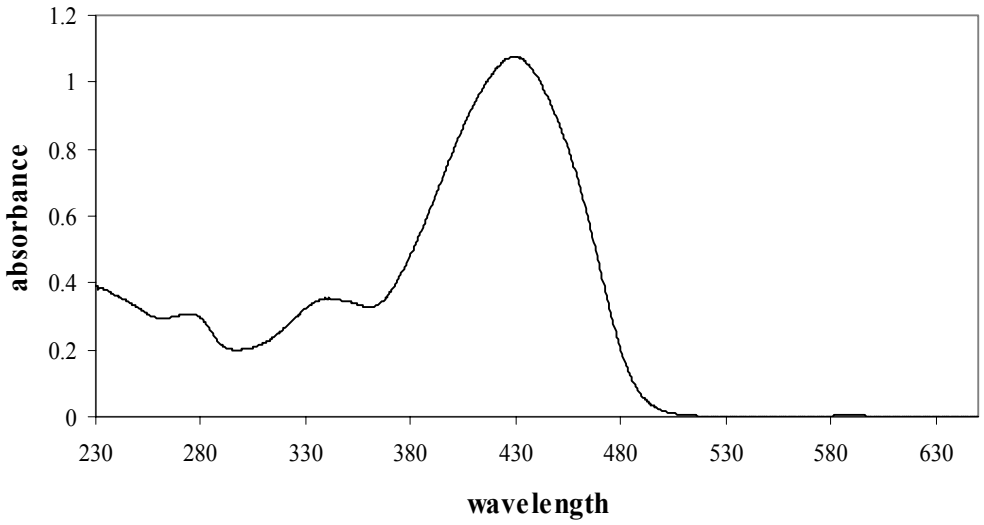

Figure 1.8 Linear Absorption Spectrum of Initiator **1.4** (8.5 x 10^{-3} M).

1.5.2.2 Fabrication of Polymeric Structures

Prior to incorporating functionalized monomers **1.8** and **1.9** into three-dimensional polymeric structures using two-photon initiated polymerization (TPIP), the results for TPIP using initiator **1.4** and commercially available triacrylate monomers (Figure 1.9), as described by Cumpston *et al.*[17] were reproduced using our instrumentation.

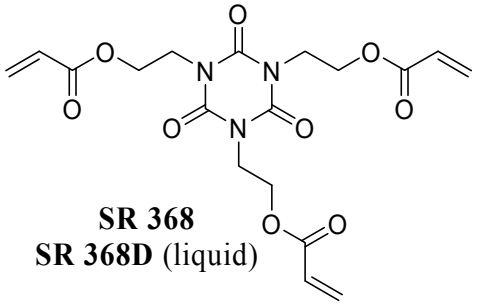

SR 368
SR 368D (liquid)

Proprietary
Structure

SR 9008

Figure 1.9 Triacrylate Monomers Used in to Fabricate Polymeric Structures.

Monomer solutions comprised of commercially available triacrylate monomers, initiator **1.4** and poly(styrene-*co*-acrylonitrile (75:25)) in toluene were prepared in ratios of approximately 70%, 0.1% and 29.9%, respectively, as reported.[17] The solution was spun-coat onto a glass microscope slide and exposed with a laser beam at 780 nm focused through a microscope objective. The beam was manually scanned in the *x* and *y* direction through the resin. Polymerization was noted visually (either through the eyepiece of the microscope or using a CCD camera) due to a change in the refractive index of the material. After the removal of unpolymerized resin by washing the glass coverslip with dichloromethane, no polymeric structures were found. It was determined that initial experiments were unsuccessful because polymerized material was removed during the development process.

Silylation of the glass coverslip with a monomeric trichlorosilane prior to application of the monomer resin was proposed to provide a monomer surface on the glass to covalently bind the structures to the glass surface. If the laser is focused at the interface of the glass coverslip and monomer solution, the resulting polymeric structure should be cross-linked to the silylated glass surface *via* free-

radical copolymerization of the triacrylate monomers and the surface monomers. Silylation reactions with glass coverslips were preformed using either 5-hexenyltrichlorosilane (**1.15**) or 3-acryloxypropyltrichlorosilane (**1.16**) in a solution of water (0.15%) in toluene (Figure 1.10).[31]

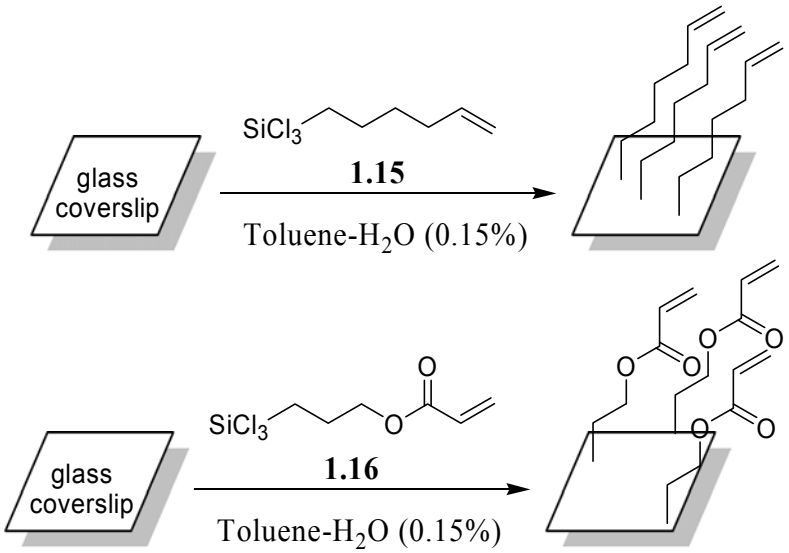

Figure 1.10 Silylation of Glass Coverslips.

Silylation of the glass coverslips prevented the removal of polymeric structures during development with dichloromethane, as predicted. Qualitative characterization of the silylated glass coverslips was made by a comparison of the contact angle of derivatized and clean glass coverslips and by IR spectroscopy. A comparison of the surface roughness of silylated and clean glass coverslips was made by SEM.[32] No significant increase in surface roughness was observed.

Several structures were fabricated using TPIP with our instrumentation; initially lines (of approximately 5 to 10 μm as determined by comparison with a stage micrometer) were fabricated by manually scanning the laser (Figure 1.11, a). More sophisticated three-dimensional platforms were fabricated by raster-scanning a focused laser beam across the surface of the monomer solution in the *x* and *y* direction and through the material along the *z* axis. A "stepped" pyramid was fabricated using the two-photon active resin described previously on a silylated glass coverslip, demonstrating our ability to construct three-dimensional features with TPIP and our instrumentation (Figure 1.11, b). Optically, this structure was fabricated using a 1.3 numerical aperture 100x objective by performing raster scans while moving the focal plane away from the surface along the *z*-axis. Fabrication of the structure required approximately 45 seconds to complete and the lateral dimensions are on the order of 32 x 21 μm. The total height of the structure is less than 11 μm. The structures remained intact and adhered to the surface after removal of the unpolymerized material.

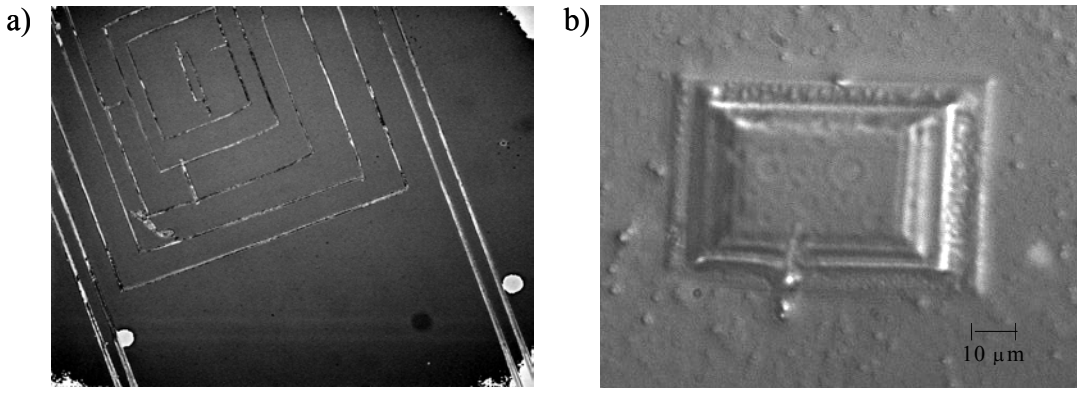

Figure 1.11 Differential Interference Contrast (DIC) Images of Polymeric Structures Fabricated Using Two-Photon Initiated Polymerization; a) Lines, 5 to 10 μm and b) Three-dimensional "Stepped" Pyramid.

Additionally, polymeric lines were fabricated using monomer solutions consisting of optically absorbing monomers **1.8** and **1.9** (29.9% binder, 69% triacrylate monomer, 0.1% **1.4** and 1% additive (**1.8** or **1.9**) by weight in dichloromethane). Visual inspection with an optical microscope revealed orange-colored lines from solutions incorporating **1.8** and blue, fluorescent lines from solutions incorporating **1.9**.

1.5.3 Results and Discussion

The qualitative incorporation of optically absorbing monomers into polymeric structures fabricated using two-photon initiated polymerization was

accomplished. However, it was not established whether monomers **1.8** and **1.9** were incorporated *via* copolymerization with the triacrylate monomers or simply entangled in the matrix. Under the same reaction conditions, polymerization experiments were performed with the unfunctionalized dyes, Nile Blue and Disperse Orange 13, and colored features were produced. Attempts at "leaching" the unfunctionalized dyes from the polymeric structures did not result in removing the color from the structures. While this does not exclude the possibility that the acrylate dyes are covalently bonded within the polymeric structure, it cannot be concluded that they were copolymerized. The conclusion is that it may not be necessary to design monomers to incorporate chemical functionality into polymeric structures fabricated using TPIP. Chemical functionality may be incorporated more conveniently through doping the photopolymerizable resin with the desired compound or using surface functionalization.[33] Ongoing experiments are aimed at functionalizing the surface of the acrylate structures with fluorescent dyes capable of conjugate addition, such as 5-aminofluorescein.

1.5.4 Summary

The fabrication of polymeric features was accomplished using two-photon initiated polymerization under the conditions described by Cumpston *et al.*[17] Optically absorbing colored monomers were incorporated in polymeric features

fabricated using TPIP, suggesting the potential to incorporate various chemical functionalities into small polymeric structures. This technique provides promise for the fabrication of chemically responsive micro and nano scale MEMS devices.

1.5.5 Experimental

1.5.5.1 Synthesis

General Considerations. All chemicals were obtained from Aldrich and used as received otherwise indicated. Dichloromethane was distilled from calcium hydride. Triethylamine was distilled from calcium hydride. Tetrahydrofuran was distilled from sodium benzophenone ketyl. Preparative flash chromatography was performed on Natland International 200-400 mesh silica gel. ^{1}H and ^{13}C NMR were obtained on a Varian Unity Plus-300 MHz spectrometer. A Finnigan VG analytical ZAB2-E spectrometer was used to obtain high resolution mass spectra. *t*-Butyl lithium was titrated with *N*-benzylamide in THF immediately prior to use.[34]

Acrylic acid-4-*p*-{[4-(phenylaxo)-1-napthyl]azo}-phenyl ester (1.8)

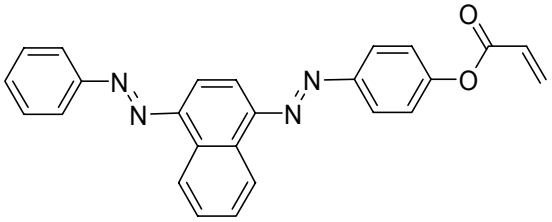

Into a 500 mL, three neck, round-bottomed flask equipped with a pressure-equilibrating addition funnel was added Disperse Orange 13 (1.08 g, 3.1 mmol) under argon with 300 mL anhydrous CH_2Cl_2. Triethylamine (0.85 mL, 6.1 mmol) was added to the solution with stirring. Acryloyl chloride (0.25 mL, 3.06 mmol) in 50 mL of CH_2Cl_2 was added slowly at 0 $^{\circ}$C. When the reaction was judged complete by TLC, (silica, 33% ethyl acetate in hexanes), the solution was washed with water and the organic phase separated, dried over $MgSO_4$, filtered, and the solvent removed under reduced pressure to give **1.8** as a red powder (1.015 g, 82% yield). Mp. 133-134 $^{\circ}$C. ^{1}H NMR (300 MHz, $CDCl_3$) δ 9.05 (m, 2H), 8.16-7.36 (m, 13H), 6.68 (dd, 1H, J_1 = 17.7 Hz, J_2 = 0.9 Hz), 6.39 (dd, 1H, J_1 = 17.4 Hz, J_2 = 10.5 Hz), 6.08 (dd, 1H, J_1 = 10.5 Hz, J_2 = 1.2 Hz); ^{13}C NMR (75 MHz, $CDCl_3$) δ 164.44, 151.21, 133.44, 132.46, 131.73, 129.48, 127.95, 127.58, 124.86, 123.96, 123.66, 122.60, 112.54, 112.49, 57.33; HRMS (CI^+) calcd for $C_{25}H_{18}N_4O_2$: 407.150; found 407.151.

1,2-Benzo-7-(diethylamino)-3-(acryloylimino)phenoxazine (1.9):

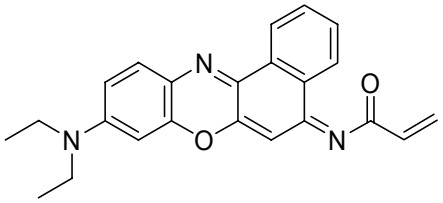

A suspension of Nile Blue A perchlorate (1.16 g, 2.78 mmol) was stirred with 100 mL of 0.5 M aqueous sodium hydroxide at 65 °C for 35 minutes. The aqueous solution was extracted with CH_2Cl_2, dried over $MgSO_4$, filtered, and the solvent was removed under reduced pressure to give a 0.80 g of a red powder in 77% yield.[35] Without further purification, the basic form of Nile Blue A (0.32 g, 1.0 mmol) was dissolved in 30 mL of anhydrous CH_2Cl_2 in a 50 mL, round-bottomed flask equipped with a pressure equilibrating addition funnel under argon. Acryloyl chloride (0.20 mL, 2.5 mmol) in 10 mL CH_2Cl_2 was added slowly at 0 °C. The reaction solution was allowed to stir for two hours at room temperature. The solution was then washed with saturated aqueous sodium bicarbonate, followed by water. The organic phase was separated, dried over $MgSO_4$, filtered and the solvent removed under reduced pressure to give **1.9** as a blue powder (0.32 g, 86% yield). Mp. 129-130 °C. ^{1}H NMR (300 MHz, $CDCl_3$) δ 8.56 (apparent d, 1H, J = 7.8 Hz), 8.39 (m, 1H), 7.55 (m, 3H), 6.57 (m, 1H), 6.32 (m, 4H), 5.82 (apparent d, 1H, J = 12 Hz), 3.28 (q, 4H, J = 7.2 Hz), 1.18 (t, 3H, J = 6.9 Hz); HRMS (CI^+) calcd for $C_{23}H_{21}N_3O_2$: 372.171; found 372.171.

1,4-*Bis*-bromomethyl-2,5-dimethoxybenzene (1.13)[36]

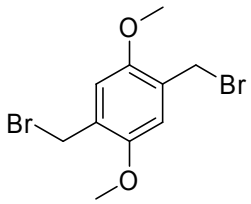

Into a 100 mL, three neck, round-bottomed flask was added 1,4-dimethoxybenzene (5.0 g, 0.036 mol) and paraformaldehyde (2.7 g, 0.091 mol) under argon. To the stirred solution was added 25 mL (0.36 mol) of glacial acetic acid and the solution was allowed to stir under argon for 15 minutes. To this solution was added 20 mL of a solution of 31% HBr-HOAc. TLC analysis (silica, 20% ethyl acetate in hexanes) of the product with an original sample revealed formation of the desired compound. The precipitate was washed with water and filtered. The resulting white solid was dissolved in CH_2Cl_2 and the organic layer washed with 1M aqueous sodium hydroxide, followed by water. The organic layer was separated and the solvent removed under reduced pressure. The residue was then purified by recrystallization from ethyl acetate in hexanes to give **1.13** as a white powder (8.60 g, 73% yield). Mp. 194-195 $^{\circ}C$.[37] ^{1}H NMR (300 MHz, $CDCl_3$) δ 6.87 (s, 2H), 4.54 (s, 4H), 3.87 (s, 6H); ^{13}C NMR (75 MHz, $CDCl_3$) δ 151.51, 127.64, 114.66, 56.49, 28.85; HRMS (CI^+) calcd for $C_{10}H_{12}O_2Br_2$: 321.920; found 321.920.

[(2,5-dimethoxy-1,4-phenylene)bis-(methylene)]bistriphenyl-phosphonium dibromide (1.14)

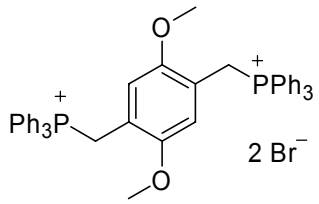

To **1.13** (343 mg, 1.06 mmol, 1.0 eq.) dissolved in DMF, triphenyl phosphine (611 mg, 2.33 mmol, 2.2 eq.) was added and the solution was stirred and heated to reflux under argon. After stirring for 12 hours, the solution was cooled to room temperature and a white precipitate was observed. The precipitate was filtered and rinsed with DMF. The diphosponium dibromide salt was purified by heating it to 120 ºC under high vacuum using a Kugelrohr apparatus. ^{1}H NMR (300 MHz, $CDCl_3$) δ 7.32-7.59 (m, 30H), 6.94 (s, 2H), 5.21 (d, 4H, J = 12.9 Hz), 2.94 (s, 6H); ^{13}C NMR (75 MHz, $CDCl_3$) δ: 150.89, 134.82, 134.82, 130.06, 129.91, 118.24, 117.55, 116.19, 116.17, 115.89, 55.47, 25.37, 24.99; ^{31}P NMR (200 MHz, $CDCl_3$, ext. ref. to 85% H_3PO_4) δ 22.43.

***E*,*E*-1,4-*Bis*[4'-(*N*,*N*-di-*n*-butylamino)styryl]-2,5-dimethoxybenzene (1.4)**

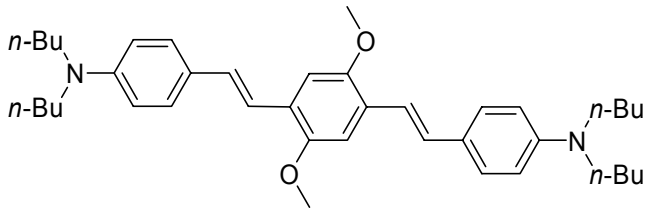

An average concentration of *t*-BuLi was determined to be 0.98 M from the titration of *t*-BuLi with *N*-benzylbenzamide. (*N*,*N*-di-*n*-butylamino)benzaldehyde was purified by short path column chromatography (silica, CH_2Cl_2). [(2,5-dimethoxy-1,4-phenylene)bis-(methylene)]bistriphenyl-phosphonium dibromide (**1.14**) (237 mg, 0.28 mmol, 1.0 eq.) was added to a flame dried flask containing a stir bar. Anhydrous tetrahydrofuran (25 ml) was added to the salt and the heterogeneous mixture was stirred. A 600μL solution of 0.98 M *t*-BuLi in

hexanes was added dropwise and a dark purple solution was observed. The solution was stirred for 30 minutes before a solution containing purified 4-dibutylamino benzaldehyde (140 mg, 0.6 mmol, 2.1 eq.) in 10 mL of dry THF was added dropwise *via* an addition funnel under argon. As the aldehyde solution was added to the Wittig reagent the color of the solution changed from purple to orange to bright yellow over 12 hours. The reaction solution was concentrated *in vacuo* and the residue dissolved in CH_2Cl_2 and water added. The organic layer was removed and extracted with CH_2Cl_2. The organic layer was washed with water, brine and dried over $MgSO_4$ and evaporated *in vacuo*. The product was purified by column chromatography (alumina, 20% CH_2Cl_2, 78% hexanes and 2% triethylamine) to afford **1.4** as a yellow crystalline solid (33.5 mg, 20% yield). ^{1}H NMR (300 MHz, $CDCl_3$) δ 7.38 (d, 4H, *J* = 8.1 Hz), 7.21 (d, 2H, *J* = 16.4 Hz), 7.11 (s, 2H), 7.07 (d, 2H, *J* = 16.4 Hz), 6.63 (d, 4H, *J* = 8.1 Hz), 3.90 (s, 6H), 3.28 (t, 8H, *J* = 7.6 Hz), 1.58 (p, 8H, *J* = 7.2 Hz), 1.36 (s, 8H, *J* = 7.4 Hz), 0.96 (t, 12H, *J* = 7.3 Hz); ^{13}C NMR (75 MHz, $CDCl_3$) δ 151.25, 147.68, 128.59, 127.76, 126.65, 128.28, 118.26, 111.67, 108.78, 56.56, 50.79, 29.51, 20.35, 14.00; HRMS (CI^+) calcd for $C_{40}H_{57}N_2O_2$: 597.442; found 597.443.

1.5.5.2 Instrumentation for Two-photon Polymerization

A solid state Tsunami Ti:Sapphire laser (Spectra-Physics) was used as an excitation source. A schematic is shown in Figure 1.12. The laser was operated at 780 nm with a repetition rate of 80 MHz; pulses were ~ 100 fs in duration. If

the power of the incident light (as measured from the microscope objective) is 10 mW, then the instantaneous intensity at the focal point is given by the following equation:

$$\mathrm{I} = \frac{\Delta E}{\Delta t \cdot A}$$

where ΔE is the laser-pulse energy, Δt is the duration of the pulse and A is the area of the focal point.

$$\mathrm{I} = \frac{1.5x10^{-10} J}{10^{-13} s \cdot (10^{-6} m)^2} \approx 10^{11} \; W/cm^2$$

The polarization of the excitation light was controlled with a half-wave plate before coupling the light into a laser scanning confocal microscope (Biorad MRC 600) equipped with a 1.3 numerical aperture objective (Zeiss, 100x). The laser scanner is configured to perform line and raster scans. Transmitted light microscopy was used for observing polymerization by a change in refractive index of the resin. After fabrication, polymeric structures were analyzed using transmission and differential interference contrast microscopy (Zeiss, Axiovert 135) and atomic force microscopy (AFM) (Digital Instruments, Nanoscope III).

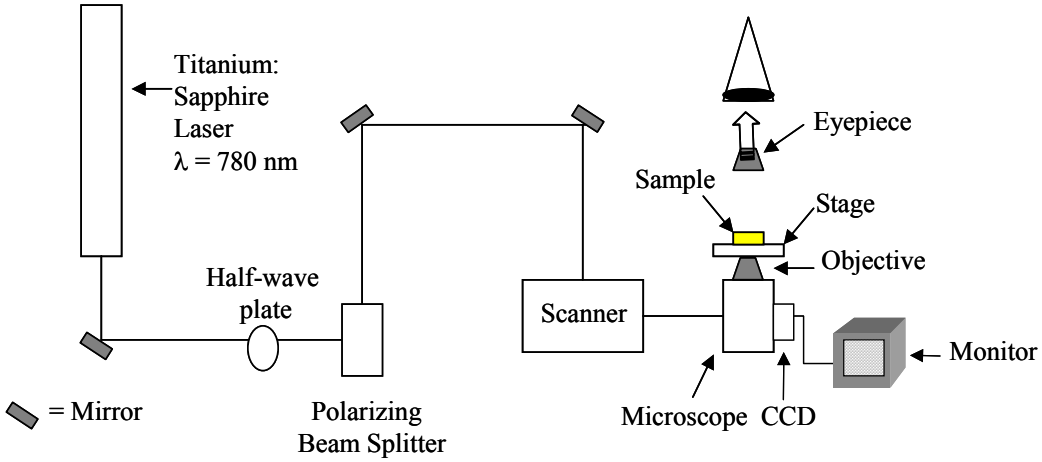

Figure 1.12 Schematic of the Instrument Used for Two-photon Initiated Polymerization.

1.5.5.3 General Method for Polymerization Experiments

General Considerations. *Tris*(2-hydroxy ethyl)isocyanurate triacrylate esters, SR 368, SR 368D and SR 9008 (CASRN: proprietary), were used as purchased from Sartomer. Poly(styrene-*co*-acrylonitrile) (75:25) was used as purchased from Aldrich. Toluene (EM Science) was used without further purification. Glass microscope coverslips were obtained from American Scientific Products. 5-Hexenyltrichlorosilane and 3-acryloxypropyl trichlorosiliane were used as purchased from Gelest.

Sample Preparation. Films of two-photon excitable resins were prepared from toluene solutions by spin coating onto silylated glass coverslips at 2500 rpm

for 20 s. A typical resin consists of 0.1 wt % two-photon absorbing chromophore (**1.4**), 29.9 wt % poly(styrene-*co*-acrylonitrile) and 70 wt % reactive trifunctional acrylate monomer (SR 368, SR 368D or SR 9008). Colored monomers **1.8** and **1.9** were added to the resin in 1 wt % while decreasing the wt % of the trifunctional acrylate to 69 %. Prior to silylation, glass coverslips were activated by sonication for 30 minutes in solutions of sodium hydroxide (aqueous), followed by deionized water, and finally concentrated nitric acid.[31] The activated glass coverslips were then silylated using either 5-hexenyltrichlorosilane or 3-acryloxypropyl trichlorosilane in a solution of water (0.15%) in toluene for 10 minutes. The silylated glass coverslips were then rinsed with chloroform and dried. Prior to application of the monomer solution, the glass plates were rinsed with acetone, water, isopropanol and again with acetone and dried. Qualitative characterization of the silylated glass coverslips was made by a comparison of the contact angle of derivatized and clean glass coverslips and by IR spectroscopy. A comparison of the surface roughness of silylated and clean glass coverslips was made by SEM.[32] No significant increase in surface roughness was observed.

1.6 NANOSCALE FABRICATION USING TWO-PHOTON EXCITATION

In conventional optical lithography, the minimum feature size that can be printed is limited by the exposure wavelength. Two-photon initiated polymerization (TPIP) is a non-linear process, and therefore provides the potential for the fabrication of smaller feature sizes using the same exposure wavelength. However, the size of features reported using TPIP is comparable to those attainable by conventional methods.[20] In this section, the use of non-conventional optical imaging techniques such as near-field scanning optical microscopy (NSOM) and apertureless NSOM is proposed to confine exposure to extremely localized positions with resolution below 100 nanometers in diameter[38,39] and subsequently, allow the fabrication of polymeric features on the nanometer scale.

1.6.1 Near-field Scanning Optical Microscopy

The spatial resolution of conventional optical techniques, as defined by the Rayleigh criterion (Equation 1.4), is limited to approximately half the wavelength of the light source used for imaging. Due to the increasing interest in imaging smaller objects, alternative methods of imaging have emerged, including scanning electron microscopy (SEM), atomic force microscopy (AFM) and near-field

scanning optical microscopy (NSOM). Of these methods, NSOM provides the advantages of optical imaging (sensitivity, specificity and flexibility) while surpassing the resolution limit.

The theory of near-field imaging, upon which modern day NSOM is based, was first proposed by Synge.[40] Near-field imaging relies on exposure through a subwavelength aperture (Figure 1.13).

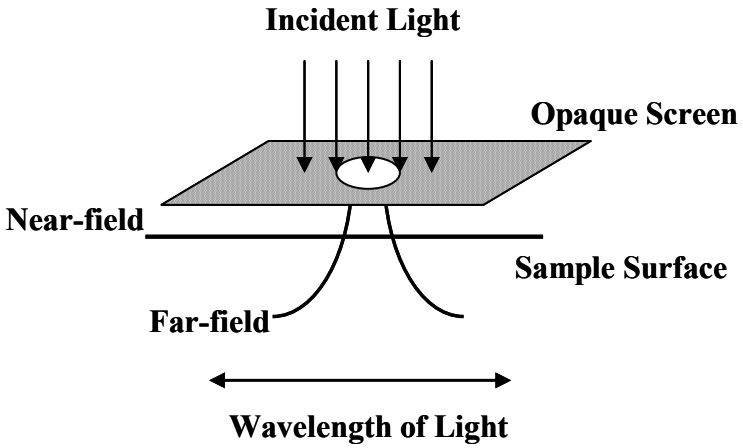

Figure 1.13 Schematic Diagram of Near-field Imaging.[41]

As light passes through a hole less than its wavelength, it is confined to the dimensions of the hole. The light intensity initially emerging from the opening is high enough to image a sample at close range (near-field), but due to interference, the intensity rapidly decreases with the distance from the opening. The concept of near-field imaging is relatively straightforward; however the implementation is problematic for two main reasons: formation of a subwavelength aperture and controlling the distance between the aperture and the surface of a sample with nanometer precision.

Significant advances have been made in both of these areas such that optical imaging using NSOM has many applications.[41] A schematic of a typical near-field microscope is illustrated in Figure 1.14. The basic components are a light source (laser), an NSOM tip (aperture) for excitation (and/ or collection), a piezo stage for sample positioning and a method of collecting light from the sample.

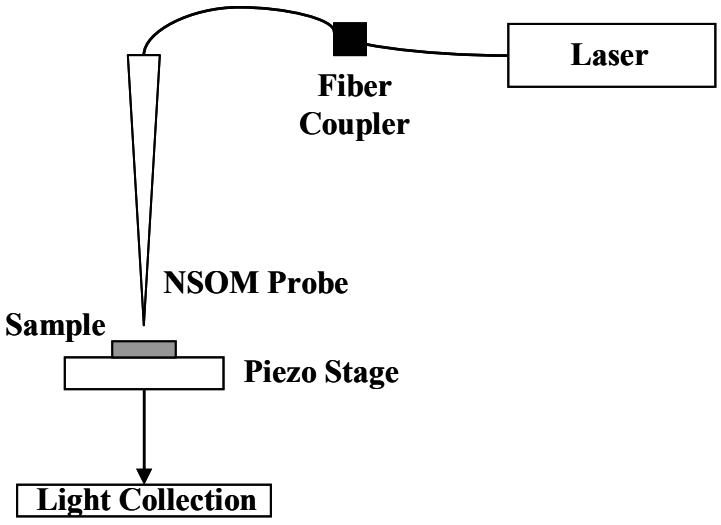

Figure 1.14 Schematic Diagram of an Illumination Mode Near-field Microscope.

There are several methods to fabricate NSOM tips, yet all NSOM tips share two common characteristics: a nanometer diameter opening and a metal coating on the tip to prevent light from escaping from the sides of the tip. NSOM tips with subwavelength apertures are typically fabricated by heating and pulling single mode optical fibers to a fine point with a mechanical micropipette puller.[42] The metal coating, usually aluminum or silver, can be applied through vacuum vapor deposition.

Maintaining a constant tip-sample distance is of paramount importance to the tip function as contact with the surface of a sample may damage the tip. Controlling the tip sample distance on the nanometer scale often relies on shear-force feedback as used in AFM microscopes. This technique relies on recording changes in the oscillation of a tip as the tip approaches a surface either optically with an external light source[38] or through the use of a tuning fork.[43] The tip is made to oscillate and the oscillation is monitored for a dip in amplitude, signaling that the tip is positioned within nanometers of the sample surface. The small scale movements required for the shear-force method of positioning a sample are controlled by a piezo electric stage. Nanoscale movements are regulated by the controlled expansion of ceramic material in the stage when an electric current is applied. Due to the feedback used for controlling the tip-sample distance, NSOM produces not only spectroscopic information about the sample, but also topographic information.

The resolution obtainable using NSOM is limited to approximately 50 nm.[44] Higher resolution is difficult because of low light intensity at the tip. With the use of alternative probe designs, specifically apertureless probes, spatial resolution on the nanometer scale is possible. Apertureless probes are sharpened metal tips (usually gold) that, when placed in the focus of a laser, create an enhanced field. The enhanced field may be more than 1000 times greater than the incident light intensity.[45]

1.6.2 Polymerization Using an Enhanced Field

By reducing of the area of exposure using non-conventional optics, the minimum feature size may potentially be greatly reduced in comparison to those previously reported using TPIP. The goal of our work is to eventually use the radiation generated at the tip of an NSOM probe to excite two-photon absorbing chromophores and subsequently, fabricate free-form polymeric structures. The difficultly with tip-sample alignment coupled with the uncertainties of using the tips on a viscous surface prompted us to first demonstrate that near-field excitation could be used to initiate TPIP through the use of a model system.[46]

1.6.2.1 Design and Fabrication of a Model System

In order to demonstrate that the enhanced field generated at the apex of a gold tip, as used in apertureless NSOM, may be used for initiating polymerization, a model system of an array of gold tips using nanosphere lithography[47] was constructed.[46] A solution of polymeric microspheres was deposited onto a silylated glass coverslip. Upon evaporation of the solvent, a closely packed hexagonal array of spheres was formed. Vapor deposition of gold into the triangular void spaces between the spheres and subsequent removal of the spheres resulted in an array of gold "tips" on the surface of the glass coverslip.

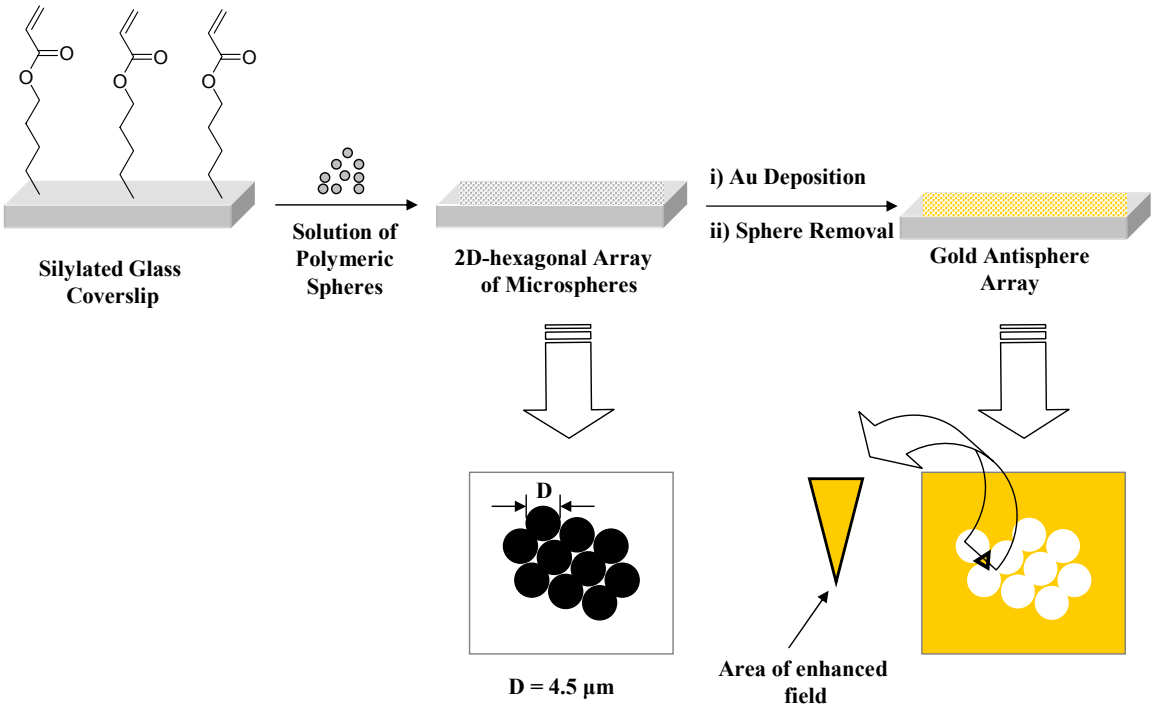

Figure 1.15 Fabrication of a Model System for Two-photon Excitation in the Presence of an Enhance Field.

A contact tapping-mode AFM height image was obtained of a 15 x 15 µm section of the gold antisphere array (Figure 1.16). The lightly shaded areas are the areas where gold was deposited in the interstices between the spheres, whereas the darkly shaded areas are "voids" where there is only silylated glass surface. The distance between the gold antispheres (optimally isosceles triangles) is approximately 2.6 µm.[47] The corner of each regularly formed triangle should mimic the apex of an apertureless NSOM probe by forming an enhanced field when placed in the focus of a laser beam. This enhanced field is expected to locally initiate polymerization *via* TPE.

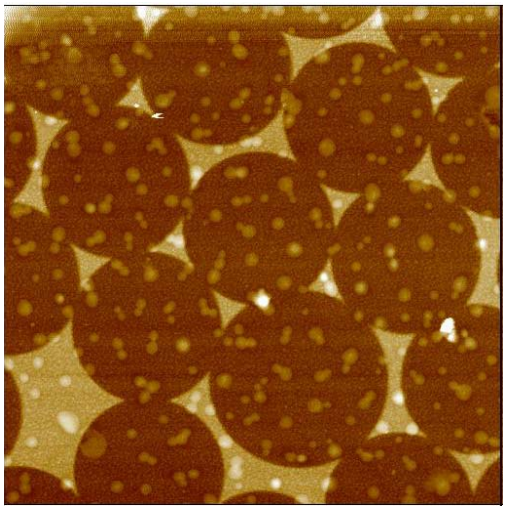

Figure 1.16 Contact, Tapping Mode AFM Height Image of an Array of Gold Tips. Scan Area is 15 x 15 μm.[48]

1.6.2.2 Polymerization using the Model System

In order to maximize polymerization in the vicinity of the enhanced field using the model system, the intensity at the focus of the laser should be below the threshold for two-photon excitation. Determination of the minimum exposure dose required to achieve TPIP using our instrument and the two-photon active resin described previously was accomplished by constructing a series of polymeric lines at successively lower laser powers.[49] The power of the beam was measured at the back aperture of the microscope objective (Figure 1.12). Line scans were performed at successively lower powers from 19 mW to below 5 mW

until polymerization was no longer observed optically *via* a change in the refractive index of the resin (Figure 1.17). While polymerization may occur prior to becoming optically apparent, our goal was to establish a minimum power for visible "writing". This power was determined at less than 5 mW measured through the microscope objective. The lines fabricated at the highest power, 19 mW were less than 1 μm in width and the width decreased with lower exposure doses (Figure 1.17).

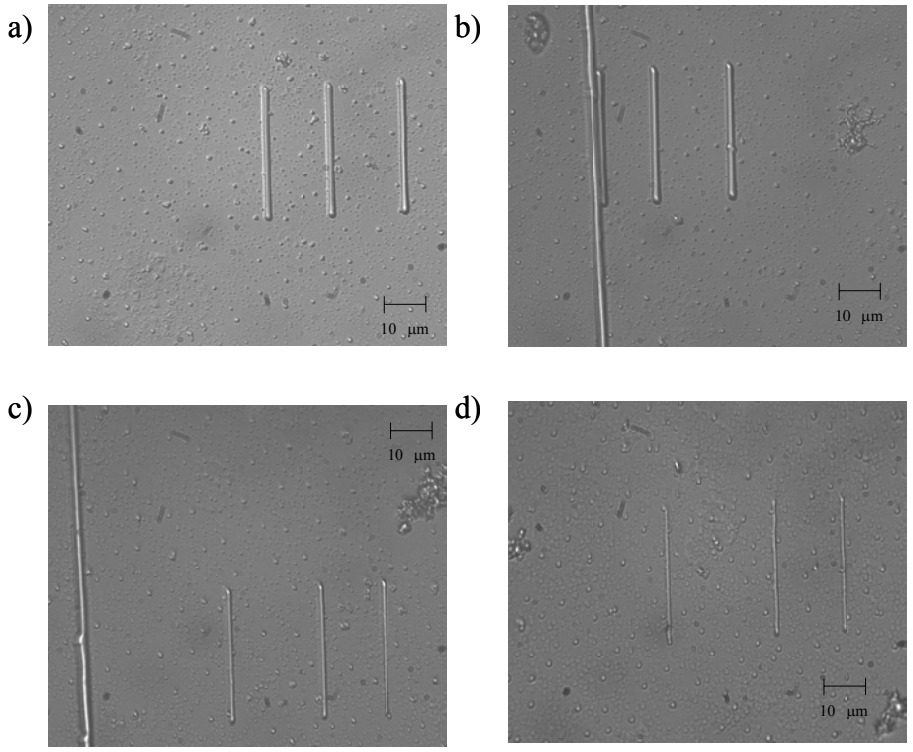

Figure 1.17 Differential Interference Contrast (DIC) Images of Polymeric Lines Fabricated using a) 19 mW, b) 13 mW, c) 9 mW, and d) 5 mW.

A two-photon active resin consisting of 70 wt % SR 368, 29.9 wt % poly(styrene-co-acrylonitrile) and 0.1 wt % **1.14** was spun on the gold antisphere array. A 32 x 21 μm platform was fabricated by raster scanning a laser beam of 780 nm light using an exposure dose of 5 mW, as described previously (Figure 18).

Figure 1.18 Sample Preparation.

After removal of the unexposed resin, a contact tapping-mode AFM height image (Figure 1.19) of the area in the vicinity of the platform was obtained. The scan area containing the polymeric platform was 75 x 75 μm. In Figure 1.19, height is illustrated by a variation of color as shown by the scale bar. Lightly shaded areas represent taller features, whereas darkly shaded areas represent shorter features. The AFM image shown in Figure 1.19 reveals that polymerization occurs in the area of the gold antispheres (the circular areas which are lightly shaded) and notably accumulates in the vicinity of the gold, where white "halos" are visible. No polymerization is observed above the gold (dark patches surrounded by white halos), most likely because the light is blocked from the polymer resin.

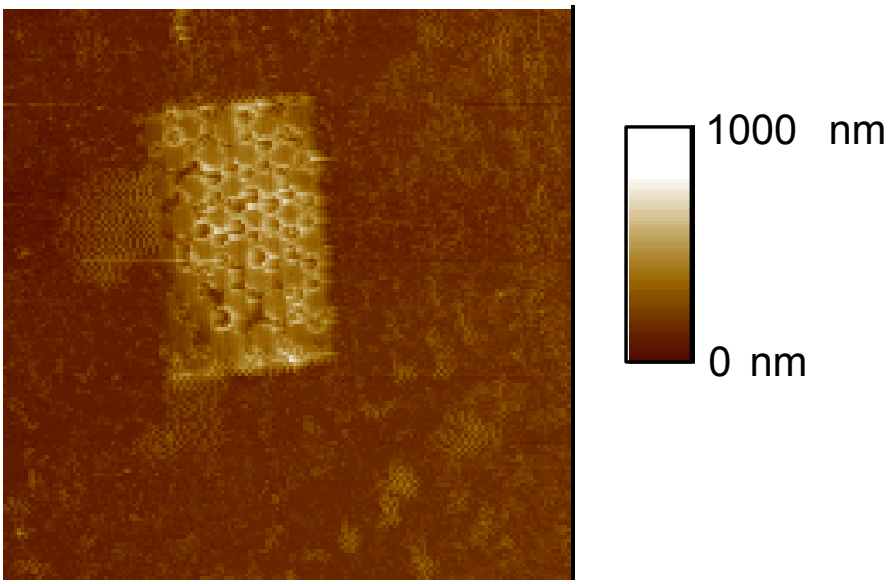

Figure 1.19 Contact, Tapping Mode AFM Height Image of a Three-dimensional Polymeric "Platform" Fabricated Using TPIP on a Gold Antisphere Array With Height Scale Bar. Scan Area is 75 x 75 μm.

1.6.3 Summary

A model system to study two-photon initiated polymerization using near-field excitation was fabricated. Using our instrumentation and a two-photon absorbing chromophore with an enhanced two-photon absorption cross section, results suggest an enhancement of polymerization at the edges of the gold features. Future work will focus on whether polymeric structures can be generated reproducibly on the gold antisphere array using powers incapable of producing optically visible photopolymerization to enhance the difference in the

extent of polymerization in the vicinity of the gold tips. Future work will also include characterizing the potentially enhanced field created by our model system and the use of scanning apertureless NSOM to produce three-dimensional structures for application in the fabrication of MEMS devices.

1.6.4 Experimental

General Considerations. The two-photon absorbing chromophore, *E*,*E*-1,4-*bis*[4'-(*N*, *N*-di-*n*-butylamino) styryl]-2,5-dimethoxybenzene (**1.4**) was synthesized *via* a double Wittig coupling (Section 1.5.5.1). *Tris*(2-hydroxy ethyl)isocyanurate triacrylate ester, SR 368, was used as purchased from Sartomer. Poly(styrene-*co*-acrylonitrile) (75:25) was used as purchased from Aldrich. Toluene (EM Science) was used without further purification. Glass microscope coverslips were obtained from American Scientific Products. 3-Acryloxypropyl trichlorosiliane was used as purchased from Gelest.

1.6.4.1 Fabrication of Gold Antisphere Array

For the model system for near-field experiments, an array of gold tips was formed on the surface of silylated glass coverslips as follows: Polymeric microspheres , 4.5 μm (Polybead® polystyrene, 2.7% solids-latex, Polysciences, Inc.) were deposited from an aqueous solution onto a silylated glass coverslip

(*vide supra*). The solvent was evaporated, leaving a regular hexagonal array of microspheres on the glass substrate. Gold was then deposited on the array *via* thermal vapor deposition. The microspheres were removed by dissolving them in dichloromethane, leaving a pattern of gold antispheres on the glass substrate. The gold antisphere array was found to vary in thickness from approximately 70 to 100 nm.[46]

1.6.4.2 Sample Preparation

Films of two-photon excitable resins were prepared from toluene solutions by spin coating onto silylated glass coverslips at 2500 rpm for 20 s. The resin consists of 0.1 wt % two-photon absorbing chromophore (**1.14**), 29.9 wt % poly(styrene-*co*-acrylonitrile) and 70 wt % reactive trifunctional acrylate monomer (SR 368).

1.7 REFERENCES AND NOTES

[1] Lowry, T. H.; Richardson, K. S. In *Mechanism and Theory in Organic Chemistry,* 3rd Edition; Haper Collins Publishers: New York, 1987; Chapter 12.

[2] Shear, J. B. *Anal. Chem. News and Features A* **1999**, 598-605.

[3] a) Xu, C.; Guild, J.; Webb, W. W.; Denk, W. *Opt. Lett.* **1995**, *20*, 2372-2374. b) Xu, C.; Webb, W. W. *J. Opt. Soc. Am. B* **1996**, *13*, 481-491. d) Xu, C.; Zipfel, W. Shear, J. B.; Williams, R. M.; Webb, W. W. *Proc. Natl. Acad. Sci. U. S. A.* **1996**, *93*, 10763-10768. d) Feneyrou, P.; Doclot, O.; Block, D.; Baldeck, P. L.; Delysse, S.; Nunzi, J. M. *Opt. Lett.* **1997**, *22*, 1132-1134. e) Rehms, A. A.; Callis, P. R. *Chem. Phys. Lett.* **1993**, *208*, 276-282. f) Maiti, S.; Shear, J. B.; Williams, R. M.; Zipfel, W. R.; Webb, W. W. *Science* **1997**, *275*, 530-532. g) Kierdaszuk,

B.; Gruczynski, I.; Modrak-Wojcik, A.; Bzowska, A.; Shugar, D.; Lakowicz, J. R. *Photochem. Photobiol.* **1995**, *61*, 319-324.

[4] Albota, M.; Beljonne, D.; Bredas, J.-L.; Ehrlich, J. E.; Fu, J.-Y.; Heikal, A. A.; Hess, S. E.; Kogej, T.; Levin, M. D.; Marder, S. R.; McCord-Maughon, D.; Perry, J. W.; Rockel, H.; Rumi, M.; Subramaniam, G.; Webb, W. W.; Wu, X.-L.; Xu, C. *Science* **1998**, *281*, 1653-1656.

[5] a) Cho, B. R.; Son, K. H.; Lee, S. H.; Song, Y.-S.; Lee, Y.-K.; Jean, S.-J.; Choi, J. H.; Lee, H.; Cho, M. *J. Am. Chem. Soc*. **2001**, *123*, 10039-10045. b) Andronov, A.; Fréchet, J. M. J. *Chem. Mater.* **2000**, *12*, 2838-2841. c) Ventelon, Z.; Charier, S.; Moreaux, L.; Mertz, J.; Blanchard-Desce, M. *Angew. Chem. Int. Ed.* **2001**, *40*, 2098-2100. d) Abbotto, A.; Beverina, L.; Bozio, R.; Facchetti, A.; Ferrante, C.; Pagani, G. A.; Pedron, D.; Signorini, R. *Org. Lett.* **2002**, *4*, 1495-1498.

[6] Göppert-Mayer, M. *Ann. Phys.* **1931**, *9*, 273-295.

[7] Kaiser, W.; Garrett, C. G. B. *Phys. Rev. Lett.* **1961**, *7*, 229-231.

[8] Denk, W.; Strickler, J. H.; Webb, W. W. *Science*, **1990**, *248*, 73-76. b) Denk, W.; Svoboda, K. *Neuron* **1997**, *18*, 351. c) Köhler, R. H.; Cao, J.; Zipfel, W. R.; Webb, W. W.; Hansen, M. R. *Science* **1997**, *276*, 2039. d) Kleinfeld, D.; Mitra, D. P.; Helmchen, F.; Denk, W. *Proc. Natl. Acad. Sci. U. S. A.* **1998**, *95*, 15741-15746.

[9] Kawata, S.; Sun, H.-B.; Tanaka, T.; Takada, K. *Nature* **2001**, *412*, 697-698.

[10] Abbe, E. *Arch. Mikrosk. Anat.* **1873**, *9*, 413-468.

[11] Bueche, F. J. In *Principles of Physics*, 5th Edition; McGraw-Hill: New York, 1988; Chapter 24.

[12] Sivukhin, D. V. In *General Course of Physics: Thermodynamics and Molecular Physics*, Vol II; Nauka: Moscow, 1990.

[13] Wu, E. S.; Strickler, J. H.; Harrell, W. R.; Webb, W. W. *Proc. SPIE*, **1992**, *1674*, 776-782.

[14] Maruo, S.; Nakamura, O.; Kawata, S. *Optics Letters* 1997, *22*, 132-134.

[15] Sun, H.-B.; Matsuo, S.; Misawa, H. *Appl. Phys. Lett.* **1999**, *74*, 786-788.

[16] Witzgall, G.; Vrijen, R.; Yablonovitch, E.; Doan, V.; Schwartz, B. J. *Optics Letters* **1998**, *23*, 1745-1747.

[17] Cumpston, B. H.; Ananthavel, S. P.; Barlow, S.; Dyer, D. C.; Ehrlich, J. E.; Erskine, L. L.; Keikal, A. A.; Kuebuler, S. M.; Lee, I.-Y. S.; Maugon, D. M.; Quin, J.; Rokel, H.; Rumi, M.; Wu, X.; Marder, S. R.; Perry, J. W. *Nature* **1999**, *398*, 51-54.

[18] Sun, H.-B.; Kawakami, T.; Xu, Y.; Ye, J.-Y.; Matsuo, S.; Misawa, H.; Meiwa, M.; Kaneko, R. *Optics Letters* **2000**, *25*, 1110-1112.

[19] Campagnola, P. J.; Delguidice, D.; Epling, G. A.; Hoffacker, K. P.; Howell, A. R.; Pitts, J. P.; Goodman, S. L. *Macromolecules* **2000**, *23*, 1511-1513.

[20] Pitts, J. D.; Campagnola, P. J.; Epling, G. A.; Goodman, S. L. *Macromolecules* **2000**, *23*, 1514-1523.

[21] Belfield, K. D.; Schafer, K. J.; Liu, Y.; Liu, J.; Ren, X.; Van Stryland, E. W. *J. Phys. Org. Chem.* **2000**, *13*, 837-849.

[22] Sun, H.-B.; Xu, Y.; Juodkazis, S.; Sun, K.; Watanabe, M.; Matsuo, S.; Misawa, H.; Nishii, J. *Optics Letters* **2001**, *26*, 325.

[23] Luo, L.; Li, C.; Wang, S.; Huang, W.; Wu, C.; Yang, H.; Jiang, H.; Gong, Q.; Yang, Y.; Feng, S. J. *Opt. A: Pure Appl. Opt*. **2001**, *3*, 489-492.

[24] Sun, H.-B.; Mizeikis, V.; Xu, Y.; Juodkazis, S.; Ye, J.-Y.; Matsuo, S.; Misawa, H. *Appl. Phys. Lett.* **2001**, *79*, 1-3.

[25] Sun, H.-B.; Tanaka, T.; Takada, K.; Kawata, S. *Appl. Phys. Lett.* **2001**, *79*, 1411-1413.

[26] Zhou, W.; Kuebler, S. M.; Braun, K. L.; Yu, T.; Cammack, J. K.; Ober, C. K.; Perry, J. W.; Marder, S. R. *Science* **2002**, *296*, 1106-1109.

[27] Willson, C. G.; Thompson, L. F.; Bowden, M. J. In *Introduction to Microlithography*; American Chemical Society: Washington D. C., 1994.

[28] Vedejas, E.; Marth, C. F. *J. Am. Chem. Soc.* **1988**, *110*, 3948.

[29] The reaction conditions for the synthesis of **1.14** were provided by Dr. Robert E. Hanes while a postdoctoral research associate at The University of Texas at Austin.

[30] Rumi, M.; Ehrlich, J. E.; Heikal, A. A.; Perry, J. W.; Barlow, S.; Hu, Z.; Maughon-McCord, D.; Parker, T. C.; Röckel, H.; Thayumanavan, S.; Marder, S. R.; Beljonne, D.; Brédas, J.-L. *J. Am. Chem. Soc.* **2000**, *122*, 9500-9510.

[31] McGovern, M. E.; Kallury, K. M. R.; Thompson, M. *Langmuir* **1994**, *10*, 3607-3614.

[32] SEM images of the silylated glass coverslip and underivatized glass coverslip were obtained by Thomas Doyle.

[33] Walchuk, G.; Gray, H. N.; Holtzman, B.; Bergbreiter, D. E. *Macromolecules*, **1998**, *31*, 3417-3423.

[34] Burchat, A. F.; Chong, J. M.; Nielsen, N. *J. Organomet. Chem.* **1997**, *542*, 281-285.

[35] Morb, W. E.; Seiler, K.; Rusterholz, B.; Simon, W. *Anal. Chem.* **1990**, *62*, 738-742.

[36] van der Made, A. W.; van der Made, R. H. *J. Org. Chem*. **1993**, *58*, 1262-1266.

[37] Literature Mp. 201-203 ºC. Shanmugan, P. *Synth. Commun.* **1999**, *29*, 4409-4416.

[38] Paesler, M. A.; Moyer, J. P. In *Near Field Optics: Theory, Instrumentation and Applications;* John Wiley and Sons: New York, 1996.

[39] Sanchez, E. J.; Novotny, L.; Xie, X. S. *Phys. Rev. Lett.* **1999**, *82*, 4014-4017.

[40] Synge, E. H. *Philos. Mag.* **1928**, *6*, 356-362.

[41] Dunn, R. C. *Chem. Rev.* **1999**, *99*, 2891-2927.

[42] Betzig, E.; Trautman, J. K.; Harris, T. D.; Weiner, J. S.; Kostelak, R. L. *Science* **1991**, *251*, 1468-1470.

[43] Karrai, K.; Grober, R. D. *Ultramicroscopy* **1995**, *61*, 197-205.

[44] Bouwkamp, C. J. *Rep. Prog. Phys.* **1954**, *17*, 35-100.

[45] Novotny, L.; Sanchez, E. J.; Xie, X. S. *Phys. Rev. Lett.* **1997**, *79*, 645-648.

[46] The fabrication of the gold nanosphere array was performed by Thomas Doyle in collaboration with the Vanden Bout research group.

[47] Xia, Y.; Gates, B.; Yin, Y.; Lu, Y. *Adv. Mater.* **2000**, *12*, 693-713.

[48] AFM images were taken by Thomas Doyle in collaboration with the Vanden Bout research group.

[49] The optimization of the laser power was performed by John Currie in collaboration with the Shear group.

SECTION II

MOLECULAR RECOGNITION OF ENOLATES OF ACTIVE METHYLENE COMPOUNDS FOR STEREOSELECTIVE SYNTHESIS AND SHIFTING THE pK_a OF CARBON ACIDS

Chapter 2: Chiral Receptors for Asymmetric Enolate Alkylation

2.1 INTRODUCTION

Stereoselectivity is an important aspect of reactions involving enolates, as enolates are synthetically useful intermediates in carbon-carbon bond forming reactions, such as Michael additions, aldol reactions, and alkylation.[1] Controlling the stereoselectivity of enolate alkylation has received considerable attention, as this reaction is often used in the synthesis of natural products.[2] In most reactions involving enolates, the chirality of the carbon α to a carbonyl is lost upon conversion to the corresponding enolate due to the planar nature of the enolate π-system. Subsequent reaction with an electrophile results in a racemic product. An enantiomerically enriched product is typically obtained from enolate alkylation through the use of an auxiliary source of chirality. The following examples illustrate recent approaches to enantioselective enolate alkylation.

2.2 ASYMMETRIC ENOLATE ALKYLATION

The approaches to asymmetric induction can be grouped into two major classes: diastereoselective asymmetric synthesis and enantioselective asymmetric

synthesis. Diastereoselective asymmetric synthesis involves either the simultaneous generation of more than one stereogenic center in an achiral substrate, or the introduction of a new stereogenic center in a substrate through the use of a pre-existing stereogenic center (usually a covalently attached chiral auxiliary). For this method, the chiral product is isolated after diastereomer separation and cleavage of the auxiliary. Enantioselective asymmetric synthesis involves the intermolecular induction of a stereogenic center in an achiral substrate. The substrate is usually transformed into a chiral product in the presence of a chiral auxiliary that does not form covalent bonds with the substrate.

2.2.1 Chiral Auxiliaries

Much effort has been devoted to the synthesis of enantiomerically enriched products from enolate alkylation, particularly to the synthesis of diastereomers through the use of chiral auxiliaries.[3] The general procedure for the formation of a stereogenic center using a chiral auxiliary is illustrated in Figure 2.1.

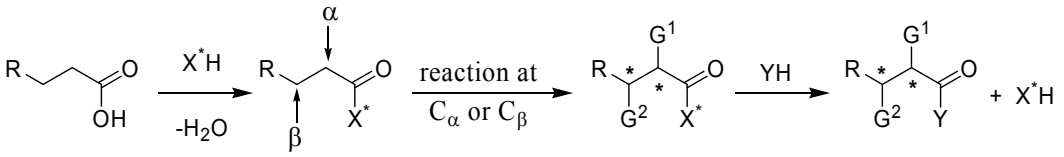

Figure 2.1 General Procedure for Auxiliary Controlled Asymmetric Reactions.

As shown, the chiral auxiliary, X^*H, is covalently attached to the substrate. Addition of other groups to the α and β positions are expected to proceed with stereoselectivity, generating an excess of one diastereomer (for either G^1 or G^2). Removal of the auxiliary generates the chiral product and preferably the auxiliary is recovered with its stereocenter intact.

There are several successful examples of chiral auxiliaries used for distereoselective enolate alkylation, including Meyer's use of chiral enamines,[4] imines[5,6] and oxazoline,[7] Evan's use of valinol or prolinol derived amides[8], Ender's use of asymmetric hydrazones,[9] Koga's use of enamines[10] and Whitesell's use of chiral enamines.[11] Most notably, Evan's chiral auxiliaries have received widespread use in asymmetric alkylation of enolates (Figure 2.2).[12]

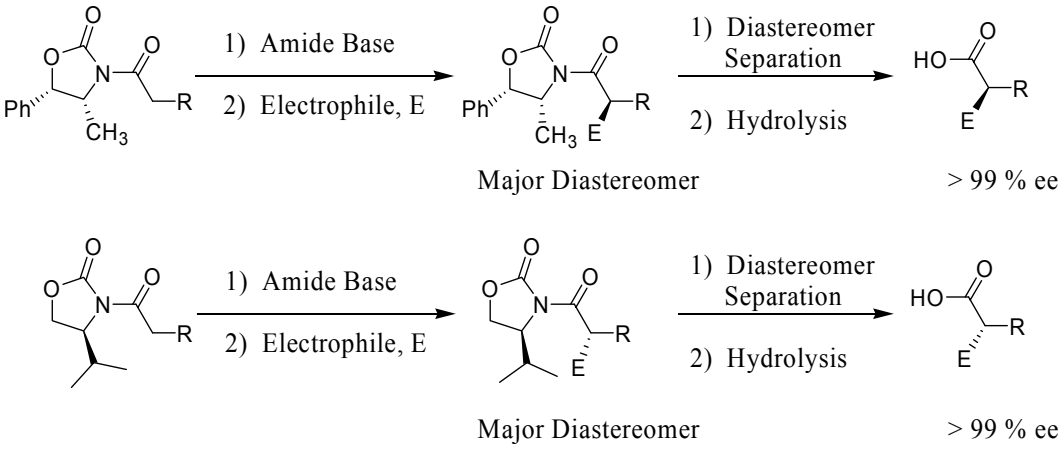

Figure 2.2 Asymmetric Enolate Alkylation Using Evan's Oxazolidone Chiral Auxiliaries.

The sense of asymmetric induction in these two alkylation reactions is complementary. The observed selectivity is easily rationalized by the approach of the attacking electrophile from the less hindered face of the enolate. Separation of the diastereomers and subsequent cleavage of the chiral auxiliaries not only generates the chiral products in greater than 99% ee, but also regenerates the auxiliaries intact (persistent auxiliaries).

Although the use of chiral auxiliaries provides a straightforward approach to stereoselective enolate alkylation, there are some disadvantages. First, at least two extra synthetic steps must be added to an overall synthetic route in which the chiral auxiliary is attached and removed. This inevitably reduces the yield of the product. Secondly, the chiral auxiliary should be recycled. Finally, since a stoichiometric amount of auxiliary is required, this method is not catalytic.

2.2.2 Chiral Noncovalent Complexes

In comparison to obtaining enantiomeric alkylation products with covalently attached chiral auxiliaries, a more economical and elegant method to obtain enantiomeric enrichment is through the use of a catalytic amount of a chiral additive. However, relatively few examples of highly enantioselective alkylation reactions employing chiral ligands are known. The rational design of ligands for enantioselective asymmetric synthesis is difficult due to a lack of precise knowledge of the interactions and associations of molecules in solution.

Noncovalent complexes often utilize hydrogen bonding between a chiral ligand and an achiral reactant. Hydrogen bonding stabilizes reactive intermediates and influences conformational preferences. Additionally, complexes may be formed through hydrophobic, van der Waals and electrostatic interactions, as seen in the following examples.

A method which has been extensively studied by Koga *et al.* employs chiral lithium amide bases.[13] In these reactions, it is assumed an achiral lithium enolate, prepared using a chiral lithium amide, exists in a chiral environment due to complex formation between the enolate and chiral amine. Enantioselective alkylation of cyclohexanone and 1-tetralone was obtained using chiral lithium amides (b-e) shown in Table 2.1.[13h]

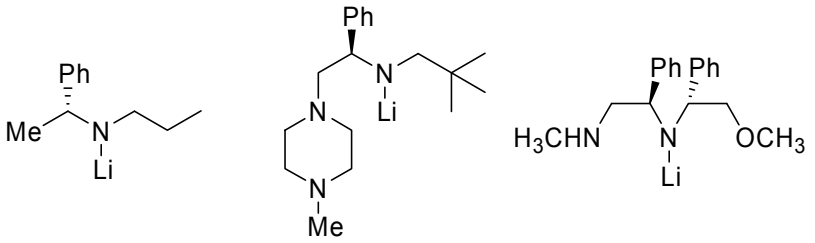

a **b** **c**

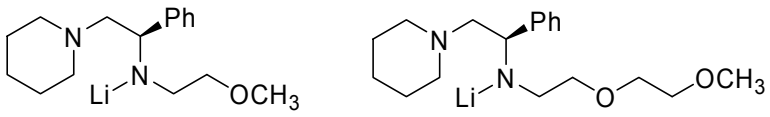

d **e**

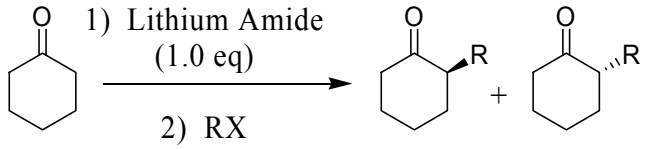

Ketone	Lithium Amide	RX	E.e (%)
cyclohexane	**a**	$PhCH_2Br$	0
cyclohexane	**b**	$PhCH_2Br$	1
cyclohexane	**c**	$PhCH_2Br$	6
cyclohexane	**d**	$PhCH_2Br$	27
cyclohexane	**e**	$PhCH_2Br$	58
cyclohexane	**e**	$PhCH_2Br$	92*
1-tetralone	**e**	PhCH2Br	62
1-tetralone	**e**	PhCH2Br	92*

* with LiBr (1.0 equiv)

Table 2.1 Enantioselective Alkylation *via* Deprotonation Using Chiral Lithium Amides.

An increase in enantioselectivity was reported upon the addition of lithium bromide. The use of lithium bromide enhances the coordinating ability of the ligands. Enantioselective alkylation of lactams and lactones was also obtained with chiral tetradentate lithium amide **2.1**.[13i]

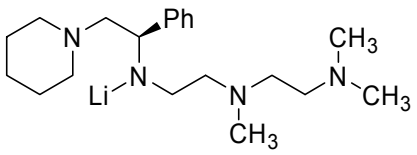

2.1

Again, the enatioselectivity of the reactions was enhanced by the presence of lithium bromide. Evidence of the importance of complex formation in directing the enantioselective alkylation reactions comes from a decrease in the enantiomeric excess when hexamethylphosphoramide and solvents such as ether, dimethoxyethane and tetrahydrofuran were used. These coordinating solvents are assumed to compete with the tetradentate amine for binding of the lithium enolate. Likewise, toluene was found to be a superior solvent for the alkylation because it is noncoordinating. However, the precise reaction mechanism remains to be solved.

Other studies utilizing chiral lithium amide bases have been reported.[14,15,16] In order to obtain high enantioselectivity, these studies also rely on the optimization of amide bases and reaction conditions. For example, pentamine ligand **2.2** was shown to be effective in directing the alkylation of lithium amide enolates. The highest enantiomeric excess reported was 84% in the

reaction shown in Figure 2.3. Ligand **2.2** was selected from a library of ligands obtained through solid phase organic synthesis.

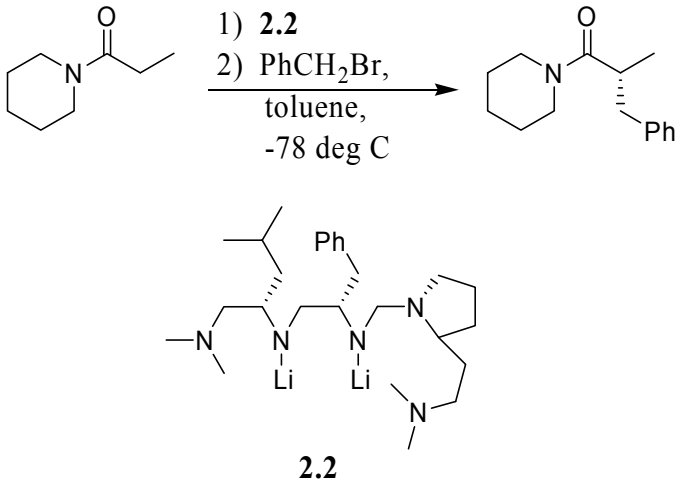

2.2

Figure 2.3 Chiral Pentamine Ligand for Enantioselective Alkylation of a Lithium Amide Enolate.

Other methods of alkylating enolates enantioselectively have appeared, however, they are not generally as applicable as of the use of chiral lithium amides. The chiral ketones **2.4 a-d** were obtained from the potassium enolate of the chiral ketone **2.3** in the absence of chiral additives, such as chiral ligands, chiral auxiliaries or chiral electrophiles.[17] The asymmetric induction is explained by preservation of the chirality of the carbon α to the carbonyl group in the enolate, due to steric interactions between the naphthalene ring and methoxy group (or the phenyl group). Although a novel method to obtain enantioselective enolate alkylation, this method is unique to ketone **2.3**.

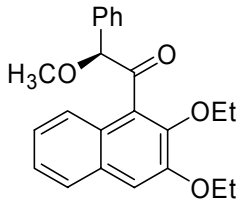

2.3

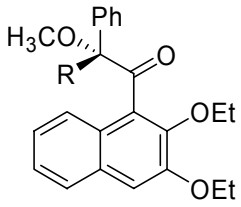

2.4 **a**: R = Me
b: R = Et
c: R = CH_2Ph
d: R = $CH_2CH{=}CH2$

Figure 2.4 Chiral Ketone and Chiral Alkylated Ketones Prepared From an Asymmetric Carbon Adjacent to a Carbonyl Group.

The previous examples illustrate that the current approach to enantioselective enolate alkylation relies on empirical and systematic screening of ligands and experimental conditions to obtain highly enantiomerically enriched products. Ideally, a rationally designed, versatile ligand generally applicable to a variety of reactions is necessary to promote the widespread use of noncolvalent chiral ligands in asymmetric synthesis.

2.3 CATALYTIC ENANTIOSELECTIVE ENOLATE ALKYLATION

The most efficient catalysts for enolate alkylation are enzymes. However enzymes are not generally useful in many applications. For chiral noncoordinating ligands to rival enzyme function, they must exhibit high

enantioselectivity and catalytic activity. In response to the need for catalysts capable of catalytic asymmetric alkylation, several systems have been designed, of which the most widely studied utilize phase-transfer catalysis.

Phase-transfer reactions are conducted in bi-phasic media. A substrate is deprotonated in the aqueous phase and transferred to the organic phase through ion pairing interactions with a cationic phase-transfer catalyst. In asymmetric phase-transfer reactions, reaction occurs enantioselectively because steric interactions between a chiral catalyst and the substrate block one face of a prochiral substrate from reaction.

Chiral quaternary ammonium salts, particularly *cinchona* alkaloids, have been used to direct enantioselective enolate alkylation.[18] Three generations of chiral *cinchona* alkaloids have produced successively higher enantiomeric excesses in enolate alkylations, as the mechanism of the enantioselectivity was elucidated,[18f] resulting in catalyst modification and subsequent improvement in the enantioselectivity. One of the first *cinchona* alkaloid systems used to catalyze asymmetric alkylation with high enantioselectivity was reported by Dolling *et al.*[18a] Methylation of 6,7-dichloro-5-methoxy-2-phenyl-1-indanone in the presence of phase-transfer catalyst *N*-(*p*-(trifluoromethyl)benzyl) cinchoninium bromide afforded the alkylation product with up to 92% enantiomeric excess and 95% yield. The observed enantioselectivity was explained by tight ion pairing between the enolate and the catalyst. Three-point binding was proposed to control the coordination. Hydrogen bonding between the hydroxyl group of the catalyst and the enolate oxygen contribute one point of interaction. The other two binding

interactions are contributed through the π-stacking of the aromatic rings in both the substrate and catalyst (Figure 2.5).

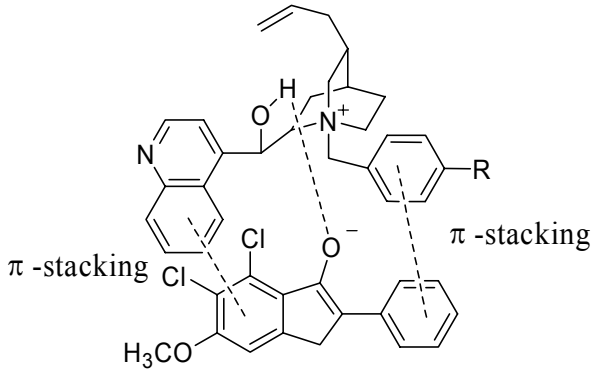

Figure 2.5 Three-point Binding Between Benzyl Cinchoninium Catalyst and Enolate Substrate.

The third generation phase-transfer cinchonidinium salt (**2.5**), synthesized by Corey *et al*., was used to obtain (*S*)-α-amino acid derivatives through the alkylation of *tert*-butyl glycinate-benzophenone Schiff base (Figure 2.6). Enantioselectivities of 94% to 99.5% were reported, indicating reaction occurs through a highly organized transition state.[18f]

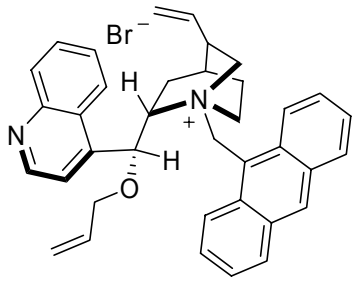

2.5

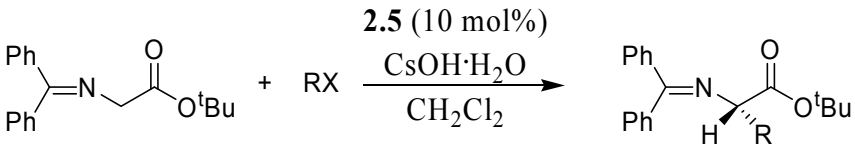

Figure 2.6 Enantioselective Catalytic Phase Transfer Alkylation *via O*(9)-Allyl-*N*-(9-anthracenylmethyl)-cinchonidinium bromide.

The high enantioselectivity obtained with chiral phase-transfer salt **2.5** is explained by three factors: First, the fixed orientation of the bulky *N*-9-anthracenylmethyl substituent orients the approaching enolate by steric interaction and restricts the conformation of the cation. Second, ion pairing occurs between the enolate and the ammonium nitrogen such that the enolate oxygen coordinates to the less sterically hindered face of the cation. Additionally the ion pair-complex forms to maximize van der Waals attraction. The enolate, therefore, preferably binds such that only the *si* face is subject to electrophilic attack, resulting in products with (*S*) configuration. It was also found by Corey *et al.* that electron donating substituents on the enolate increased the enantioselectivity of the reaction. This was explained by the formation of tighter contact ion pairs between the counterions.[18f]

A trimeric *cinchona* alkaloid phase-transfer catalyst, α,α',α''-tris[*O*(9)-allylcinchonidinium]mesitylene tribromide, was subsequently reported by Park *et al*.[19] Phase-transfer alkylation of *N*-(diphenylmethylene)glycine *tert*-butyl ester using 3 mol% of the catalyst (**2.6**) resulted in enantiomeric excesses comparable to those obtained using catalyst **2.5** (90-97%) with the same stereochemical outcome, the (*S*) alkylation product.

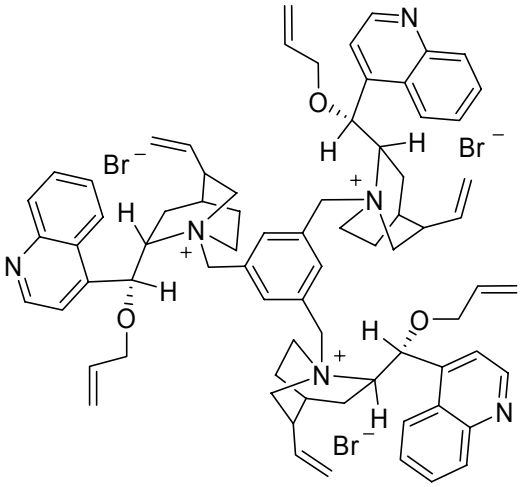

2.6

Chiral phase-transfer catalysis has also been used to produce α,α–dialkyl-α-amino acids through the use of C_2-symmetric chiral quaternary ammonium salt, **2.7**.[20] The double alkylation of an aldimine Schiff base of glycine *tert*-butyl ester proceeds with enantioselectivities of 92% to 98% (Figure 2.7). The reaction utilizes five equivalents of cesium hydroxide to deprotonate the substrate in the aqueous phase. The stereochemistry of the quaternary carbon center is

determined in the second alkylation, as was shown by the inversion of stereochemistry depending on the order of addition of alkylating agents.

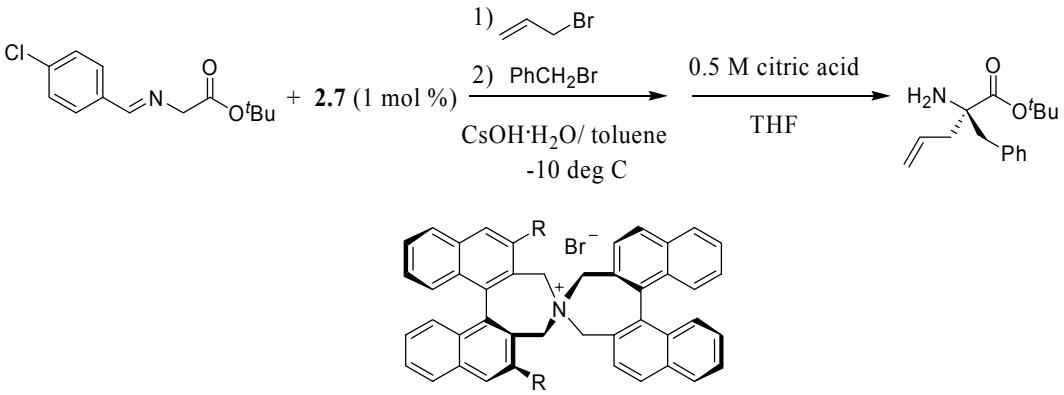

Figure 2.7 Catalytic Enantioselective Double Alkylation of Aldimine Schiff Base using a Chiral Quaternary Ammonium Salt.

In addition to the use of chiral phase-transfer catalysts, the use of an asymmetric binding pocket **2.8** in the alkylation of β-ketoesters has been described by Trost *et al.*[21] The stereochemistry of quaternary carbon centers was controlled through the use of ligand **2.8** in which the chirality of the ligand was transmitted to a prochiral nucleophile, 2-alkoxycarbonylcyclohexanone (Figure 2.8).

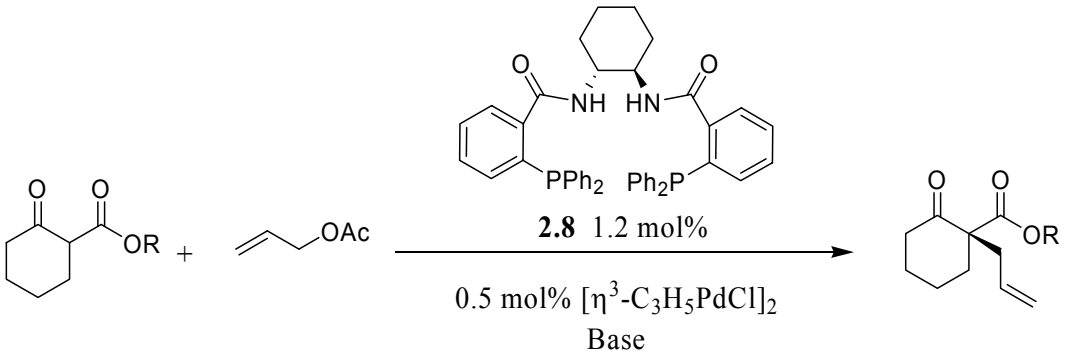

Figure 2.8 Palladium Catalyzed Asymmetric Alkylation of β-ketoesters Using a Chiral Binding Pocket.

The enantioselectivity of the reaction was shown to be dependent on the base used for deprotonation of the β-ketoesters, with *N*,*N*,*N*',*N*'-tetramethylguanidinium (TMG) giving the highest enantiomeric excesses compared to sodium hydride, *n*-butyl lithium, or sodium carbonate. Contrary to the previous examples, this catalytic system uses a chiral ligand to bind the electrophile rather than the nucleophile. The approach of a prochiral nucleophile is controlled by the stereochemistry of the ligand coordinated to the electrophile. Importantly, the use of the *S*,*S* ligand for the allylic alkylation in place of the *R*,*R* ligand reversed the stereochemistry of the product while the enantiomeric excess of the product remained the same, 86%.

The previous examples illustrate chiral catalysts which utilize an external base to form an enolate. In these examples, the pK_a of the conjugate acid of the base is larger than the pK_a of the substrate, thus the substrate exists in the reaction as the enolate. In phase-transfer catalysis, only the bound enolate is available to react with the nucleophile in the organic phase, thus resulting in enolate alkylation

products with high enantiomeric excess. In the example illustrated in Figure 2.8, only the bound electrophile is activated towards nucleophile attack, therefore the chirality of the ligand is transferred to the reaction product as the free electrophile is unreactive. In summary, in order for catalytic reactions to be highly enantioselective, product formation should result selectively from the substrate (or reactant) intimately coordinated with the chiral catalyst.

2.4 CHIRAL ENOLATE RECEPTOR DESIGN

2.4.1 Design Goal

The results of previous studies in our group suggest that catalysis may be achieved by a receptor that increases the acidity of a carbon acid substrate with respect to the unbound substrate. Selective deprotonation of the bound substrate is proposed in the presence of a base with a smaller pK_a value for its conjugate acid than the pK_a of the carbon acid substrate. The acidity of carbon acids may be increased by stabilizing the conjugate base through hydrogen bonding. The stabilization of enolates by hydrogen bonding was studied using receptors **2.9**[22] and **2.10** (Figure 2.9).[23]

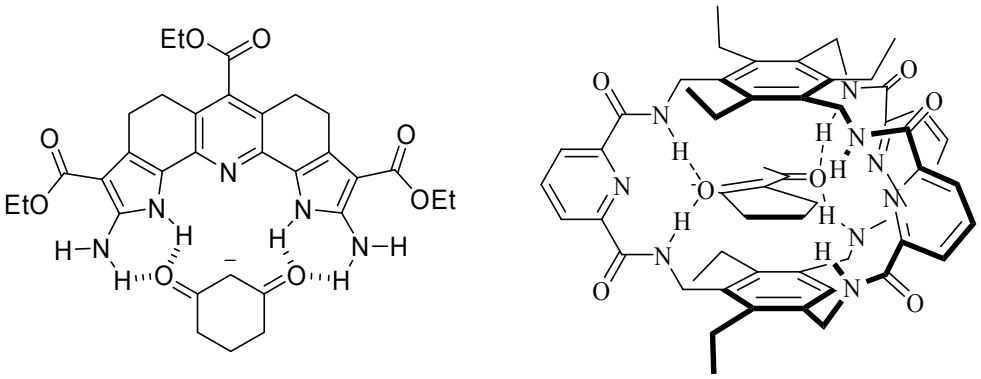

2.9 **2.10**

Figure 2.9 Synthetic Receptors Utilizing Hydrogen Bonding to Reduce the pK_a of Active Methylene Compounds.

Polyazacleft **2.9** utilizes two pairs of hydrogen bonds directed towards the lone pair electrons of dicarbonyl compounds. Upon binding 1,3-cyclohexanedione, the pK_a of the carbon acid was reduced by approximately one pK_a unit. Although promising, this moderate pK_a shift did not result in the desired catalysis of enolate alkylation with this receptor.[24] It was determined that a more significant reduction in the pK_a of carbon acids was necessary to obtain catalytic enolate alkylation. Subsequently, it was proposed that stronger hydrogen bonds may be formed through hydrogen bond donation to an enolate π-system with receptor **2.10**, as negative charge is concentrated in the π-system of the enolate. A 2.9 pK_a unit reduction was obtained for 2-acetylcyclopentanone in the presence of receptor **2.10** relative to the pK_a of the free dione.[23] The larger reduction in pK_a observed with receptor **2.10**, compared to **2.9**, is attributed to the hydrogen bond geometry between the enolate and the receptor, as predicted. Molecular modeling

supports encapsulation of the enolate of 2-acetylcyclopentanone between the aromatic rings of receptor **2.10**, thus positioning the π -system of the enolate for stabilization by the amide hydrogen bonds rather than the oxygen lone pairs.

The results of our studies with receptor **2.10** led us to design C_3-symmetric chiral receptors where binding, and thus stabilization, of active methylene enolates is proposed to result from the donation of hydrogen bonds to the π -system of the enolate. The design of our receptors includes six amide hydrogen bond donors prearranged to one face of an aromatic ring (**2.11**).

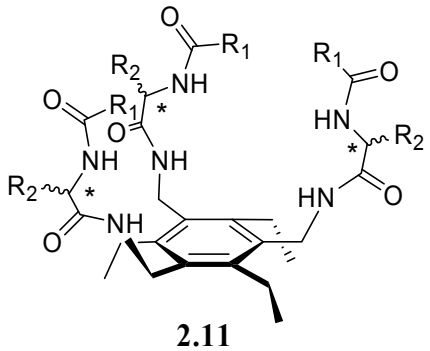

2.11

R_1 = Protecting group

R_2 = Alkyl group

The alternating geometrical pattern (*ababab*) of the chiral substituents on the benzene ring results from steric interactions of 1,3,5-tri(substituted)-2,4,6-triethylbenzene[25] and is supported by molecular modeling. The chiral ligands on the 1, 3, and 5 positions of the benzene scaffold are expected to provide a chiral pocket for guest binding. The C_3-symmetry of our host design increases the probability of chiral recognition because the number of possible binding modes is decreased to two possibilities with an enantiomeric substrate.[26] It has been

demonstrated that macrocyclic receptors possessing C_3-symmetry are more enantioselective than receptors possessing C_1 or D_3 symmetry.[27]

Binding of a prochiral enolate and a chiral host is proposed to produce a pair of diastereomers, depending on the facial orientation of the enolate guest with respect to the benzene ring of the host. It is postulated that the lower energy diastereomeric complex will predominate in solution and result in a face selective approach of an alkylating agent. Another possibility is that the lower energy diastereomeric complex will be less reactive, and alkylation will occur with an opposite sense of enantioselectivity from the higher energy diastereomeric complex. Enantiomeric enrichment of the alkylation product is, therefore, expected using the host design in either case.

A related example of a C_3-symmetric host utilizing a hexasubstituted benzene scaffold for asymmetric Michael addition of enolate substrates has been reported.[28] Mesitylene-based* host **2.12** was used to obtain catalytic asymmetric Michael addition of the potassium enolate of methyl phenylacetate and methyl acrylate.

* Mesitylene-based hosts do not exhibit the conformational control as do hexasubstituted benzene derivatives resulting in substituents alternating above and below the benzene ring (Hennrich, G.; Anslyn, E. V. *Chem. Eur. J.* **2002**, *8*, 2219-2224). Thus, this host does not utilize preorganization of alternate substituents as our proposed host design.

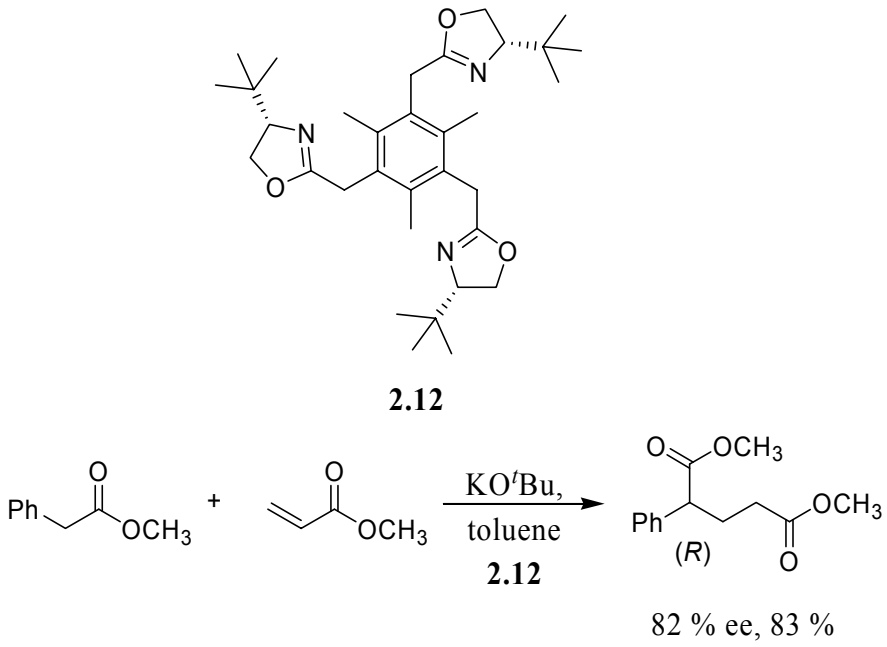

Figure 2.10 Chiral C_3-symmetric Oxazoline-potassium *Tert*-butoxide Complex Used to Catalyze Enantioselective Michael Addition.

The exact mechanism of asymmetric induction in the Michael reaction was not determined, but coordination of the potassium ion with the oxazoline nitrogens of the chiral ligand was proposed to place the enolate in a chiral environment, resulting in a face-selective approach of the Michael acceptor. An explanation of the observed catalysis was not reported.

In summary, using our host design, catalytic asymmetric enolate alkylation may be achieved from a carefully designed system in which a base selectively deprotonates only the bound substrate as a result of the reduction in the pK_a when bound verses the free substrate. Alkylation should result in a chiral product because only the bound substrate in a chiral environment is reactive.

2.4.2 Design Criteria

The scaffold of our host design, 1,3,5-tri(substituted)-2,4,6-triethylbenzene, has been utilized in our group and by others as a platform for synthetic receptors.[29] Specifically, 1,3,5-tris(aminomethyl)-2,4,6-triethylbenzene is used for our host design because the primary amine moieties provide a facile route to functionalization *via* nucleophilic substitution. An essential part of our design is the use of chiral substituents on the 1, 3 and 5 positions of the benzene ring. Our design incorporates α-amino acids due to their availability in optically pure form.

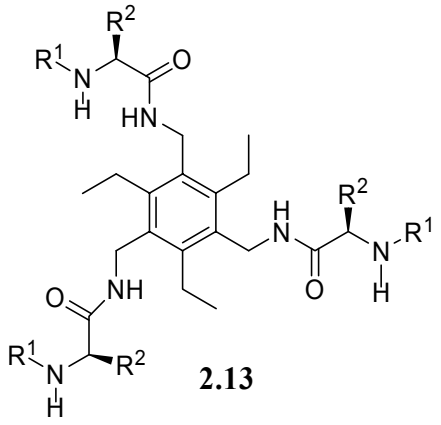

2.13

Additionally, it has been reported that tripodal peptides derived from chiral α-amino acids and 1,3,5-tris(aminomethyl)benzene form interstrand hydrogen bonds in apolar solvents.[30] Depending on the directionality of these bonds, a right-handed or a left-handed helix is formed in solution. Since the peptides are chiral,

the two alternatives are diastereomeric and one of the two arrangements is formed preferentially in solution. It was determined by theoretical calculations that when L-amino acids are used as substituents of 1,3,5-tris(aminomethyl)benzene, the right-handed helical structures are energetically favored over the left-handed helical structures. It is proposed in our design that this helical structure of our host will result in facially discriminatory binding of prochiral enolates.

2.5 SYNTHESIS OF CHIRAL RECEPTORS

2.5.1 α-Amino Acid-Based Receptors

The synthesis of hosts **2.13 a-c** was achieved according to the general reaction sequence depicted in Figure 2.11. 1,3,5-Tris(chloromethyl)-2,4,6-triethylbenzene (**2.14**) was synthesized from 1,3,5-triethylbenzene by electrophilic aromatic substitution in one step using chloromethyl methyl ether and tin tetrachloride.[31]

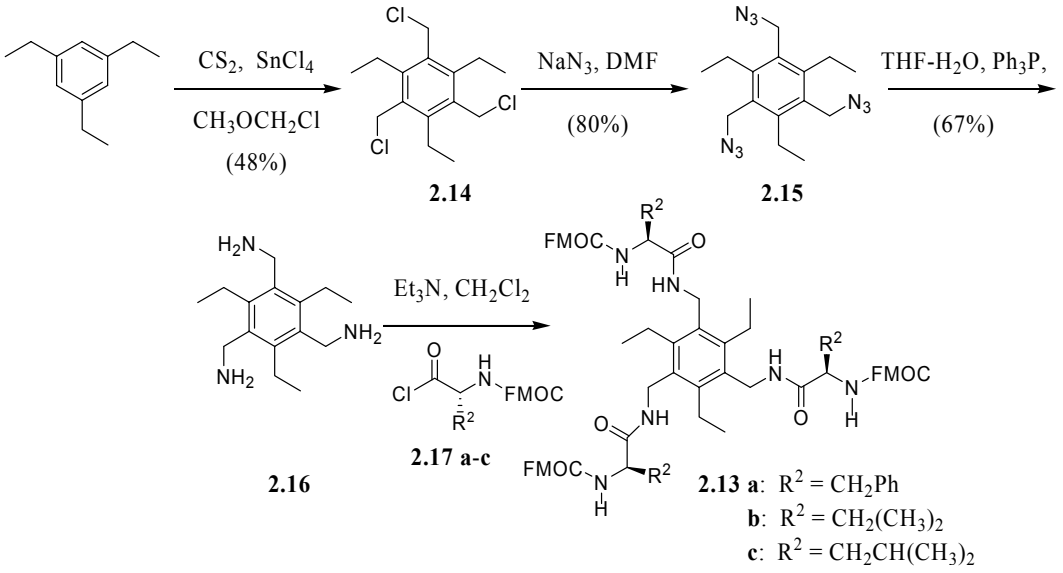

Figure 2.11 General Synthesis of α-Amino Acid-Based Receptors.

1,3,5-Tris(aminomethyl)-2,4,6-triethylbenzene (**2.16**) was synthesized in two steps from **2.14**. First, **2.14** was converted to 1,3,5-tris(azidomethyl)-2,4,6-triethylbenzene (**2.15**) by nucleophilic displacement of chloride with azide using sodium azide.[32] A Staudinger reduction[33] of the tris(azidomethyl) compound produces **2.16**. FMOC- protected L-phenylalanine (**2.17 a)**, L-valine (**2.17 b)** and L-leucine (**2.17 c**) were converted to acid chlorides with thionyl chloride (Figure 2.12).

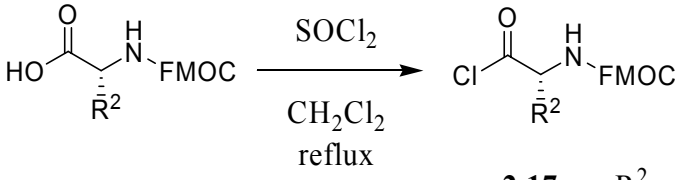

2.17 **a**: $R^2 = CH_2Ph$
b: $R^2 = CH_2(CH_3)_2$
c: $R^2 = CH_2CH(CH_3)_2$

Figure 2.12 Synthesis of L-Amino Acid Chlorides **2.17 a-c**.

The conversion of FMOC-protected amino acids to acid chlorides using thionyl chloride has been reported to retain the stereochemistry of the chiral center.[34] Coupling reactions of the acid chlorides with the tris(aminomethyl) scaffold (**2.16**) completes the synthesis of FMOC-protected *C_3*-symmetric receptors **2.13 a**, **b** and **c**. Although the FMOC-protected receptors fulfill our design criteria (three pairs of amide bonds), these receptors have limited solubility in organic solvents. Therefore, a series of receptors were synthesized by first removing the FMOC protecting group with piperidine in *N*, *N*'-dimethylformamide followed by protection of the amines with various protecting groups, as summarized in Table 2.2.

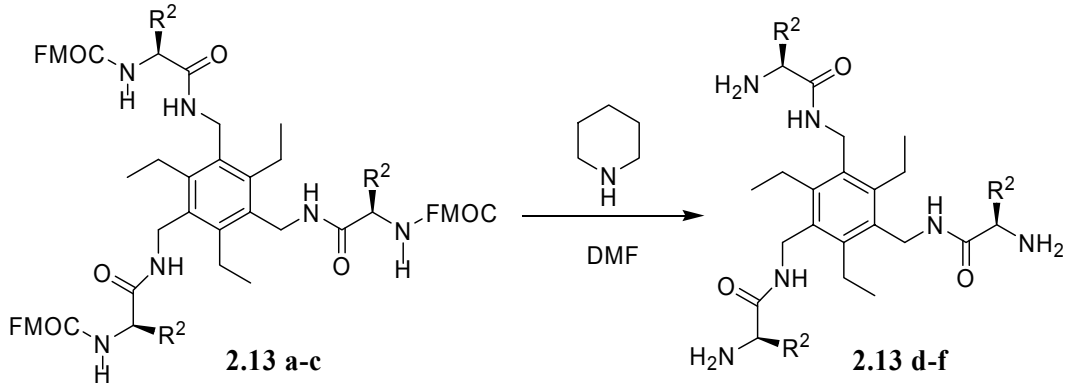

2.13 a-c **2.13 d-f**

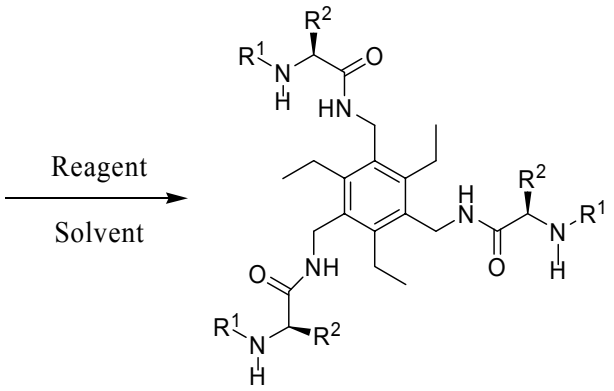

2.18 - 2.25

Entry	Reagent	Solvent	R^1	R^2	Yield (%)
2.18	Acetyl Chloride	CH_2Cl_2, Et_3N	$-CH_2Ph$		79
2.19	Valeryl Chloride	CH_3CN, Et_3N	$-CH_2Ph$	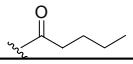	15
2.20	Hexanoyl Chloride	CH_2Cl_2, Et_3N	$-CH_2Ph$	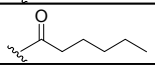	94
2.21	3,5-bis(trifluoromethyl) benzyl chloride	CH_2Cl_2, Et_3N	$-CH_2Ph$	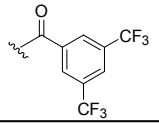	91
2.22	di-*tert*-butyl dicarbonate	CH_2Cl_2	$-CH_2Ph$		75
2.23	3,5-bis(trifluoromethyl) benzyl chloride	CH_2Cl_2, Et_3N	$-CH(CH_3)_2$	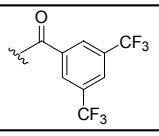	92
2.24	di-*tert*-butyl dicarbonate	CH_2Cl_2	$-CH(CH_3)_2$		65
2.25	di-*tert*-butyl dicarbonate	CH_2Cl_2	$-CH_2CH(CH_3)_2$		74

Table 2.2 Synthesis of α-Amino Acid-Based Hosts- Protecting Group Variation.

Receptors **2.18**-**2.21** are soluble only in dimethyl sulfoxide. Receptor **2.22** is sparingly soluble in tetrahydrofuran with sonication. Receptor **2.23** is also only soluble in dimethyl sulfoxide. Receptors **2.24** and **2.25** are soluble in tetrahydrofuran, toluene and dichloromethane, solvents suitable for enolate binding and alkylation studies. The enhanced solubility of hosts **2.24** and **2.25** may arise from the steric interactions of the valine and leucine amino acid ligands, as well as the BOC protecting groups, which prevent intermolecular hydrogen bonding.

2.6 ENOLATE BINDING STUDIES

2.6.1 Enolate Guest Selection

For enolate binding and alkylation studies, we chose cyclic enolates of active methylene compounds 2-acetylcyclopentanone (**2.26**), 2-acetylcyclohexanone (**2.27**) and 2-acetyl-1-tetralone (**2.28**).

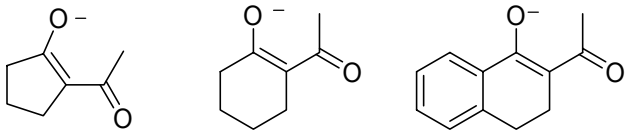

2.26 **2.27** **2.28**

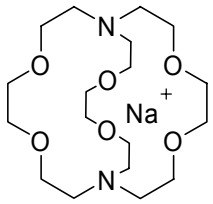

sodium-[2.2.1]cryptand counterion

Figure 2.13 Proposed Enolates of Cyclic Active Methylene Compounds for Binding and Alkylation Studies.

The use of enolates of active methylene compounds is advantageous to our study for two reasons. First, two carbonyl groups increase the number of potential binding sites for hydrogen bonding to our receptors and should serve to increase

the binding constant between the receptor and the guest (through cooperative binding[35]). Second, the carbon acidity of the methylene carbon between two activating groups, such as a carbonyl group, is greater than the carbon acidity of a methylene carbon adjacent to only one activating group. For example, the pK_a of cyclohexanone is 16.7 in water, whereas the pK_a of 1,3-cyclohexanedione is 5.25.[36] Cyclic active methylene compounds were chosen because the conformation of these enolates is restricted to either the *Z,E* or *Z,Z* conformation, out of the possible *E,E*; *E,Z*; *Z,E* and *Z,Z* conformations available to acyclic enolates of active methylene compounds (Figure 2.14).[37]

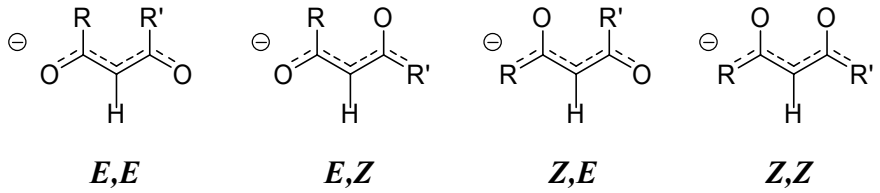

Figure 2.14 Conformations of Acyclic β-dicarbonyl Enolates.

For cyclic β-dicarbonyl enolates, the *Z,E* conformation, with the oxygen atoms anti to each other, is formed preferentially as the *Z,Z* form experiences repulsive dipole-dipole interactions between the carbonyl oxygen-carbon bonds.[38] Restriction of the conformation reduces the potential binding modes of these enolates to the receptor in solution, increasing the opportunity of stereoselective alkylation. Additionally, the use of [2.2.1]cryptand to complex the sodium counterion of the enolate generates a "free" enolate in solution.[39] Coordination of the carbonyl oxygens of active methylene compounds to the counterion generates

the *Z,Z* form, however, the non-coordinated enolate assumes the lowest energy conformation, *Z,E*.[40]

2.6.2 Binding Studies

Before evaluating the utility of our α-amino acid-based C_3-symmetric receptors in directing enantioselective enolate alkylation, we determined the binding stoichiometry and association constants of receptors **2.24** and **2.25** with enolate guest **2.26** by plotting the ^{1}H NMR shifts of the ArCH_2*NH* and BOC*NH* signals of the hosts as a function of the enolate guest concentration (THF-d_8, CD_3CN). For host **2.24**, the concentration of the host was held constant at 6.4 x 10^{-3} M by titrating a solution of **2.24** (6.4 x 10^{-3} M) and enolate-[2.2.1]cryptand guest, **2.26** (0.12 M) in deuterated acetonitrile into the host solution. A 1:1 host-guest binding stoichiometry was found between receptor **2.24** and enolate-[2.2.1]cryptand guest **2.26** by the downfield shift of the host amide *NH* resonances (Figure 2.15). For receptor **2.25**, a 1:1 binding stoichiometry was also found, as shown in Figure 2.16. The host concentration was kept constant at 4.7 x 10^{-3} M during the titration of a solution of the enolate-[2.2.1]cryptand guest **2.26** (5.9 x 10^{-2} M) and host **2.25** (4.7 x 10^{-3} M) solution in deuterated acetonitrile. An association constant of 6.0 x 10^3 ± 1.0 x 10^3 was found by analysis of the ^{1}H-NMR shift of the resonances of the host as a function of the guest concentration.

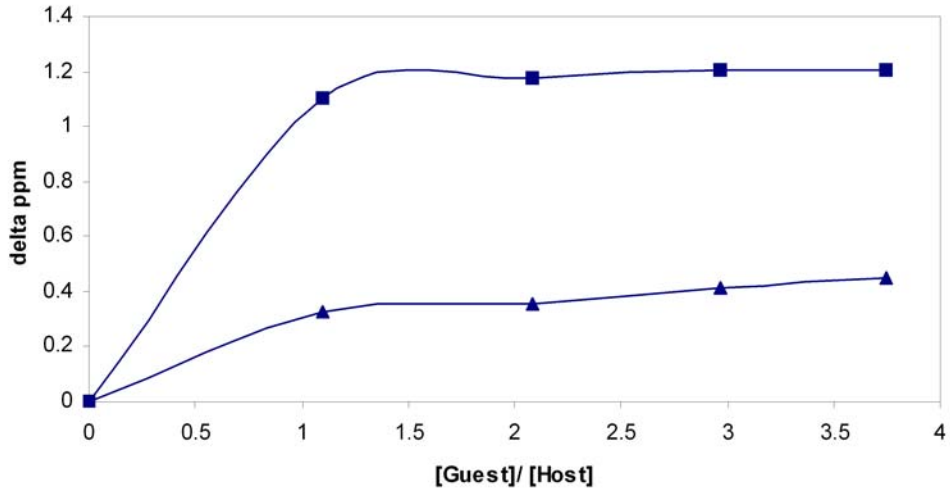

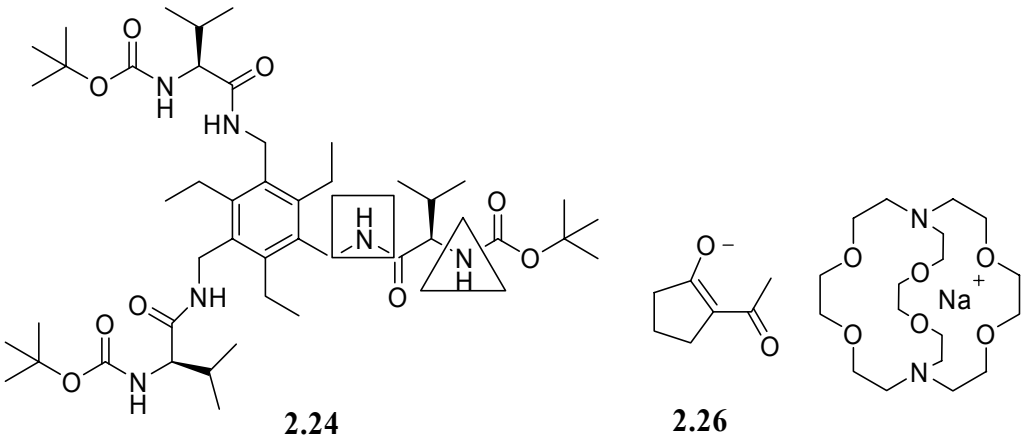

2.24 **2.26**

Figure 2.15 Change in the Amide Chemical Shifts of Host **2.24** with Increasing Concentration of Enolate **2.26** in THF-d_8:CD_3CN. [**2.24**] = 6.4 x 10^{-3} M.

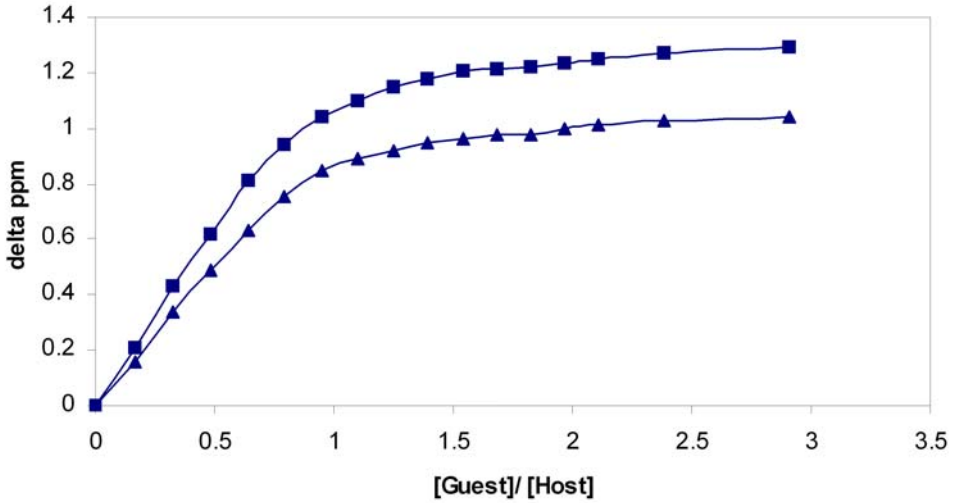

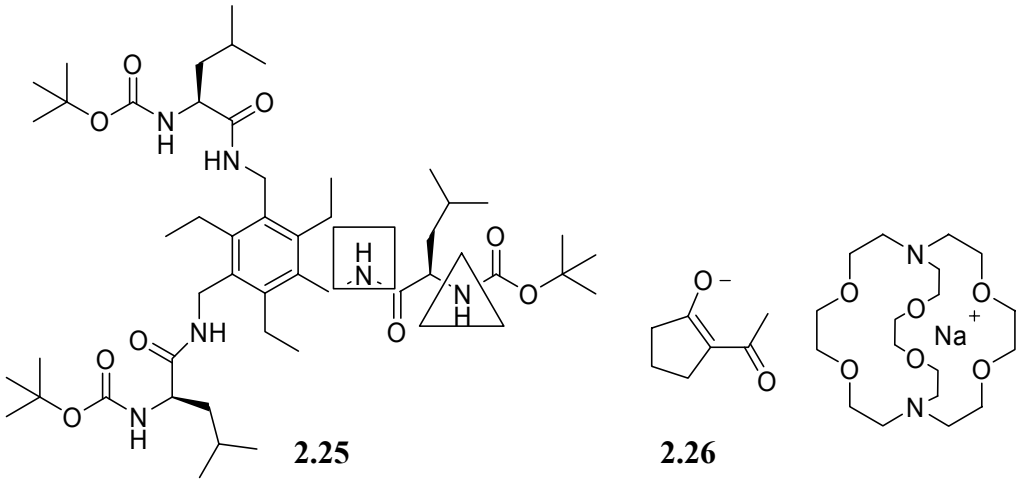

Figure 2.16 Change in the Amide Chemical Shifts of Host **2.25** with Increasing Concentration of Enolate **2.26** in THF-d_8:CD_3CN. [**2.25**] = 4.7 x 10^{-3} M.

The association constants were obtained using the following equation derived from the Rose-Drago equation[41]:

$$\delta_{obs} = \delta_R + \frac{\Delta_0}{2[R^0]}([R^0] + [S^0] + \frac{1}{K} - \sqrt{\{([R^0] + [S^0] + \frac{1}{K})^2 - 4[R^0][S^0]\}})$$

In this equation, δ_{obs} is the observed chemical shift, δ_R is the initial chemical shift of the receptor, δ_{RS} is the shift of the pure complex, $\Delta_0 = \delta_R - \delta_{RS}$, K is the association constant, R_0 is the initial concentration of the receptor, and S_0 is the initial concentration of the substrate. A titration experiment gives a series of data sets including $[R_0]$, $[S_0]$ and δ_{obs}. The unknown parameters in the equation, K and Δ_0, are found using a nonlinear curve fitting method in which the value for K is initially estimated, and δ is calculated for each data point. The process is repeated until convergence of the calculated δ and δ_{obs}.

The observed 1:1 binding stoichiometry for the enolate guest **2.26** and hosts **2.24** and **2.25** supports our proposed host-guest binding mode (Figure 2.17).

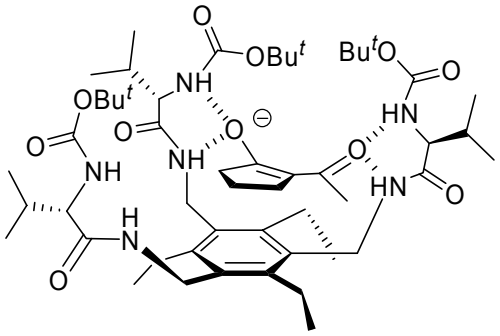

Figure 2.17 Proposed Host-Guest Binding for Enolate **2.26** and Receptor **2.24**.

Additionally, the downfield shift of both amide *NH* resonances indicate they are participating in hydrogen bonding with the guest. Host-enolate binding is also supported by the observation of enhanced nonequivalence of the diastereotopic ArCH_1H_2NH protons in the ^{1}H NMR spectra with increasing enolate concentration. The anisotropy of the diastereotopic protons is indicated by the increasing chemical shift difference between the free ligand and the ligand in the presence of the enolate (Figure 2.18). After a 1:1 binding stoichiometry is reached, a shift of the diastereotopic protons is no longer observed. The observed anisotropy is attributed to the conformational restriction of the amino acid ligands as they are bound by the enolate.[30]

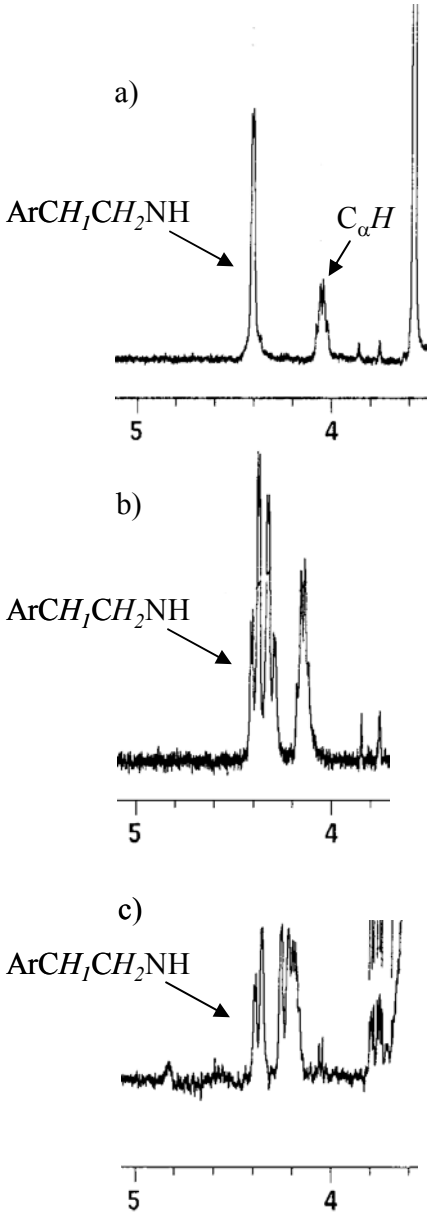

Figure 2.18 ^{1}H NMR Shift of the Diastereotopic ArCH_1H_2NH protons of a) Host **2.25** b) with 0.25 Equivalent of Enolate [2.2.1] cryptand **2.26** c) with 6.5 Equivalents of Enolate-[2.2.1]cryptand **2.26**.

Binding studies between **2.26** and host **2.24** were attempted in chloroform:tetrahydrofuran (5:1). Tetrahydrofuran was added to host **2.24** because of its low solubility in chloroform. Binding saturation could not be reached as amide proton resonances became too broad to measure. This effect is attributed to the "clustering" of nucleophilic enolate anions around the host, resulting in a binding stoichiometry greater than 1:1 in chloroform (Figure 2.19).

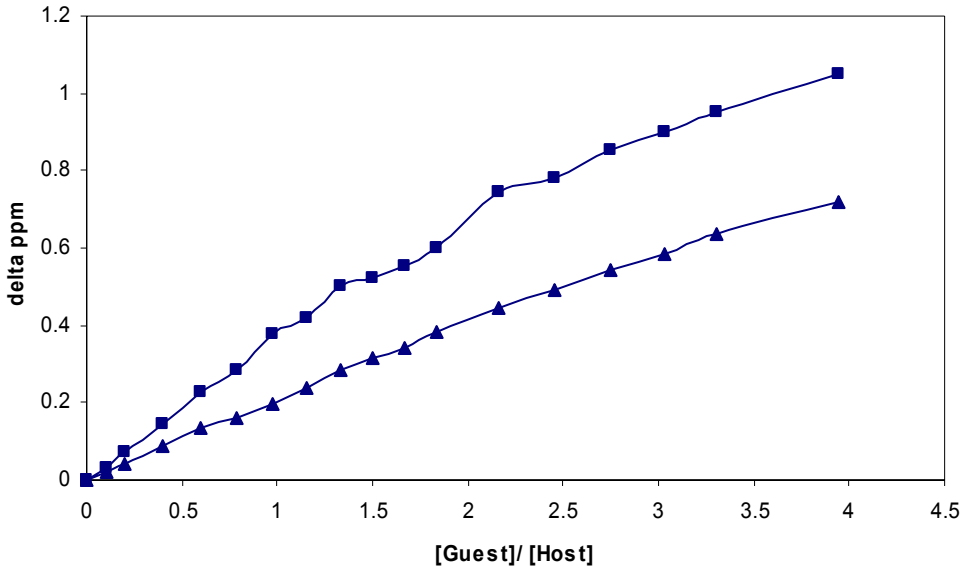

Figure 2.19 Change in the Amide Chemical Shifts of Host **2.24** with Increasing Concentration of Enolate **2.26** in $CDCl_3$:THF-d_8 (5:1), [**2.24**] = 5.0 x 10^{-3} M.

2.7 ENANTIOSELECTIVE ENOLATE ALKYLATION STUDIES

2.7.1 Enolate Alkylation

Having demonstrated 1:1 receptor-enolate binding, alkylation of enolates **2.26**, **2.27** and **2.28** in the presence of hosts **2.18**, **2.22** and **2.25** was performed according to a modified procedure described by Koga *et al.*[13h] The results of the alkylation studies are summarized in Table 2.3. Toluene is the preferred solvent for the reaction because it is aprotic and therefore unlikely to compete with host-enolate hydrogen bonding. However, in most cases tetrahydrofuran was used due to limited host solubility in toluene. Enolate **2.27** was alkylated in the presence of hosts **2.18** and **2.22**, respectively (entries 4 and 5), yielding moderately enantiomerically enriched products. The low enantiomeric excess is proposed to be a result of the limited solubility of the hosts in organic solvents due to intermolecular hydrogen bonding.[30] Alkylation of enolate **2.27** in the presence of host **2.25** in toluene gave a racemic product, however when tetrahydrofuran was used for alkylation, an enantiomeric excess of 42% was obtained, as determined by chiral phase HPLC (Figures 2.20 and 2.21).

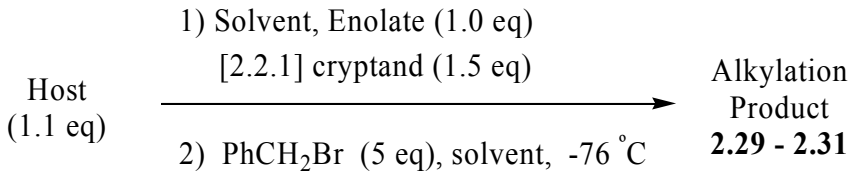

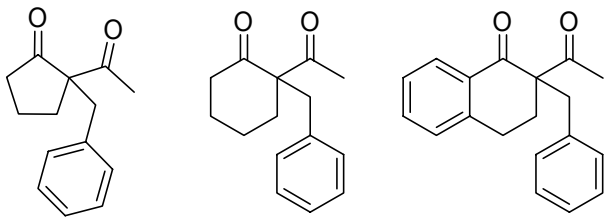

2.29 **2.30** **2.31**

Entry	Host	Enolate	Solvent	Reaction Time	Temp (ºC)	Yield (%)	% ee[a]
1	none	**2.26**	THF	8 hr	-76	54	0
2	none	**2.27**	THF	6 hr	-65	80	0
3	none	**2.28**	THF	12 hr	-76	76	0
4	**2.18**	**2.27**	THF	8 hr	-76	36	20
5	**2.22**	**2.27**	toluene	8 hr	-76	57	10
6	**2.25**	**2.27**	toluene	7 hr	-50	44	< 3
7	**2.25**	**2.27**	THF	8 hr	-65	40	42
8	**2.25**	**2.26**	THF	10 hr	-76	54	< 3
9	**2.25**	**2.28**	THF	12 hr	-76	62	4

[a] Enantiomeric excess was determined by chiral HPLC analysis

Table 2.3 Enantioselective Enolate Alkylation Using Chiral C_3-symmetric Hosts.

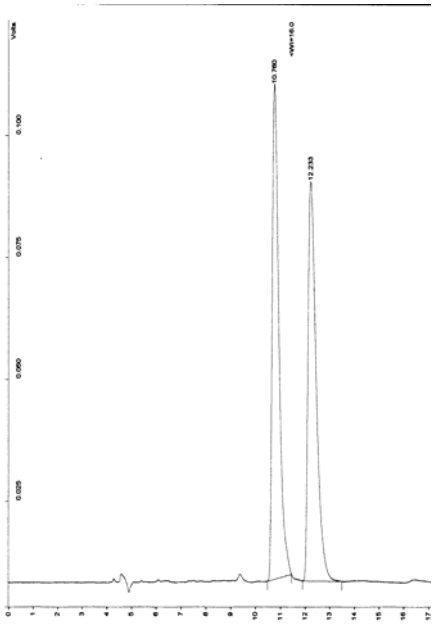

Figure 2.20 HPLC Chromatogram for Entry 2 in Table 2.3.

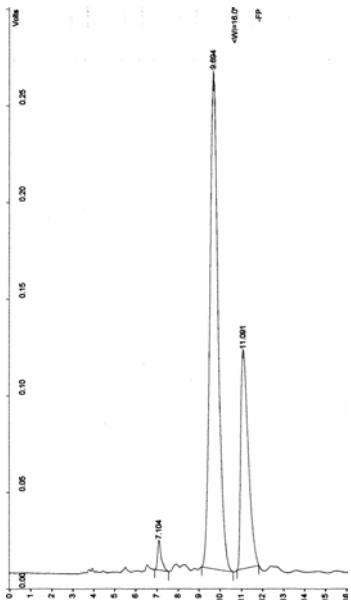

Figure 2.21 HPLC Chromatogram for Entry 7 in Table 2.3.

2.7.2 Alkylation Control Study

In order to demonstrate the necessity of our preorganized host scaffold, the hexasubstituted benzene ring, control compound **2.32** was synthesized from BOC-L-leucine *N*-hydroxysuccinimide ester and benzylamine (Figure 2.22).

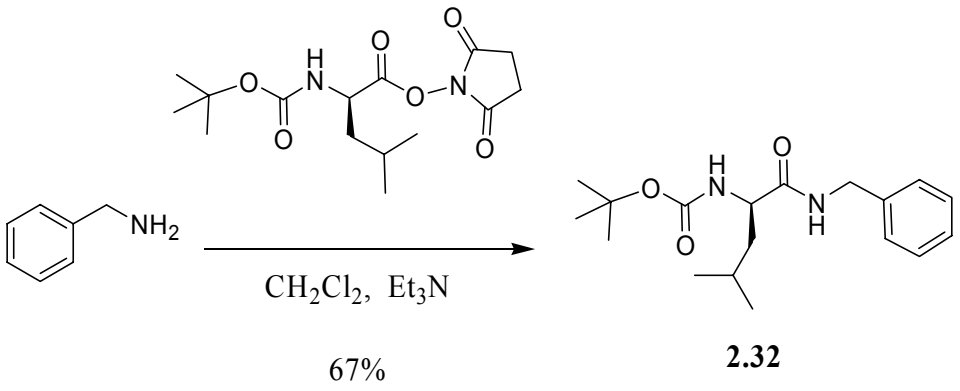

Figure 2.22 Synthesis of Control Host **2.32**.

Compound **2.32** may participate in hydrogen bonding to the enolate, but lacks the ability to form a diastereomeric complex with the enolate *wherein one face of the enolate is protected* from alkylation, as is proposed with our C_3-symmetric receptors (*vide supra*). Benzylation of enolate **2.27** in the presence of 3.1 equivalents of **2.32** resulted in a racemic product (Figure 2.23), supporting that the organization of the coordinating ligands on one face of the hexasubstituted benzene ring is responsible for forming a binding cavity for enolate recognition, thereby directing alkylation enantioselectively.

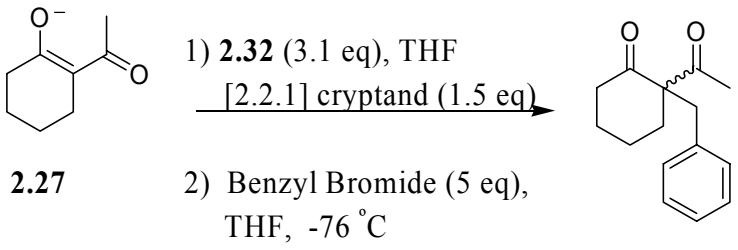

Figure 2.23 Benzylation of Enolate **2.27** in the Presence of Control **2.32**.

2.7.3 Assignment of Stereochemistry

The optical rotation of the benzylation product, 2-acetyl-2-benzyl cyclohexanone, has not previously been reported in the literature.† Therefore, in order to assign the absolute stereochemistry of the major enantiomer of the alkylations in which an enantiomeric excess was observed (Table 2.3, entries 4, 5 and 7) several approaches were considered. First, conversion of 2-acetyl-2-benzyl cyclohexanone to a product with known optical rotation was attempted. The optical rotation of both enantiomers of methyl-1-benzyl-2-oxocyclohexane carboxylate (**2.33**) have been reported.[42] A retrosynthetic analysis of the conversion of 2-acetyl-2-benzyl cyclohexanone to methyl-1-benzyl-2-oxocyclohexane carboxylate is shown in Figure 2.24.

† The synthesis of racemic 2-acetyl-2-benzyl cyclohexanone has been reported. Pei, T.; Widenhoefer, R. A. *J. Am. Chem. Soc.* **2001**, *123*, 11290-11291.

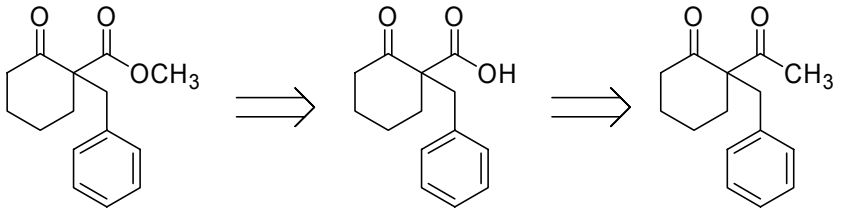

2.33

Figure 2.24 Retrosynthetic Analysis of Methyl-1-benzyl-2-oxocyclohexane carboxylate.

The oxidation of 2-acetyl-2-benzyl cyclohexanone to the carboxylic acid was first attempted using sodium hypochlorite (Iodoform reaction conditions).[43] However, the reaction failed to yield the desired product and starting material was recovered from the reaction. Indeed, upon further search, the conversion of acetyl groups attached to a quaternary carbon to carboxylic acids using iodoform reaction conditions reportedly require harsh reaction conditions (high temperatures and prolonged reaction time).[44] Other reported harsh methods of converting an acetyl moiety α to a quaternary carbon to a carboxylic acid, such as refluxing nitric acid[45], were abandoned because of possible racemization of the stereogenic carbon. Attempted oxidation of 2-acetyl-2-benzyl cyclohexanone using potassium permanganate[46] resulted in the decarboxylation product, **2.35**.

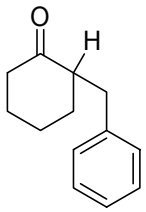

2.35

Other approaches to assigning the stereochemistry of the dominant enantiomer involved the use of hydrazone **2.34**. A pair of diastereomers was obtained from the reaction of 2-acetyl-2-benzyl cyclohexanone (racemic) with (*S*)-(-)-1-amino-2-(methoxymethyl) pyrrolidine (SAMP).[47] After separation of the diastereomers *via* column chromatography, a single enantiomer of 2-acetyl-2-benzyl cyclohexanone was obtained by hydrolysis of one diastereomer of **2.34** using cupric chloride in tetrahydrofuran.[48] Chiral phase HPLC analysis revealed that the fastest eluting diastereomer of **2.34** (silica, 10% ethyl acetate in hexanes) corresponds to the major alkylation product. To assign the stereochemistry of the diastereomers of **2.34**, two approaches were considered: crystal structure formation with **2.34** and picric acid and NOE ^{1}H NMR correlation studies with **2.34**. Crystal formation was unsuccessful, as an oil was obtained with one diastereomer of **2.34** and picric acid. The results of the NOE ^{1}H NMR experiments were inconclusive.

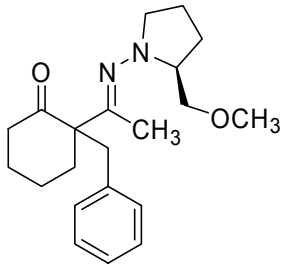

2.34

2.7 SUMMARY AND SUGGESTIONS FOR FURTHER WORK

It has been demonstrated that moderate enantiomeric enrichment of enolate alkylation takes place in the presence of amino acid-based C_3-symmetric hosts. Increasing the enantioselectivity may result from the optimization of the reaction conditions, such as solvent and temperature. Coordinating additives may also prove useful in increasing the enantioselectivities of enolate alkylations, as has lithium bromide with the use of chiral lithium amides as coordinating ligands.[13] Optimization of the C_3-symmetric host may also serve to increase enantioselectivity. The intermolecular hydrogen bonding prevents the use of optimal solvents for the enolate alkylations. Preventing hydrogen bonding may be accomplished by increasing the steric bulk of the host ligands.

In the previous applications, our C_3-symmetric hosts were not used as catalysts for enolate alkylation. It is the ultimate goal of this project to achieve *catalytic enantioselective* alkylation. The catalytic aspect of this project may arise from our studies with polyazacleft **2.9**. The goal of receptor **2.9** was to obtain a reduction in the pK_a of bound carbon acids verses free substrate (Figure 2.25, **c**) such that in the presence of a carefully selected base, deprotonation of only the bound substrate would be possible. Therefore, subsequent alkylation would precede only though the host-substrate complex.

It was found that the acidity of 1,3-cyclohexanedione was reduced by approximately one pK_a unit, however **2.9** was not useful as an alkylation catalyst as was hoped for two main reasons. First, stabilization of the neutral diketone by

the host resulted in a larger energy barrier to deprotonation (Figure 2.25, **a**), thus minimizing the crucial difference in the pK_a between the bound and free substrate. Secondly, stabilization of the enolate resulted in a decreased reactivity towards alkylation (Figure 2.25, **d**). This effect is unavoidable, as anion stabilization is the premise of the host design. Catalytic activity should be the result of minimizing the stabilization of the neutral substrate and maximizing anion stabilization, thus increasing the difference in pK_a between the unbound and bound substrate, such that only the bound substrate may be deprotonated and thus, alkylated.

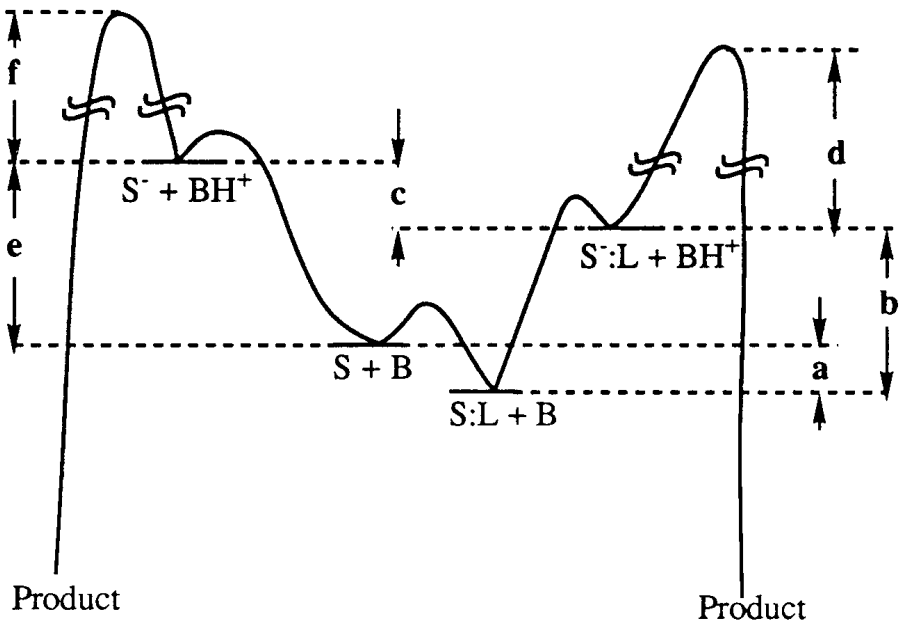

Figure 2.25 Experimentally Determined Energy Diagram for Alkylation of 1,3-Cyclohexanedione in the Presence of Host **2.9**.[24]

Future work on our host design may include modification of the host scaffold to incorporate a transition metal, the benefits of which will be discussed in Chapter 3. The use of transition metal-enolate binding has been demonstrated to reduce the pK_a of carbon acids by approximately 10 pK_a units.[49] Incorporation of transition metals into our host design may prove useful in the selective deprotonation of bound active methylene compounds. Unbound substrates would remain unreactive to alkylation, resulting in a host design capable of catalytic enantioselective enolate alkylation.

2.8 EXPERIMENTAL

2.8.1 Synthesis

General Considerations. ^{1}H and ^{13}C spectra were obtained using a Varian 400 MHz or a Varian Unityplus 300 MHz spectrometer. Chemical shift values in parts per million are referenced to tetramethylsilane as an internal standard. Low-resolution and high-resolution mass spectra were measured with Finnigan TSQ70 and VG Analytical ZAB2-E instruments, respectively. Melting points were obtained on a Thomas Hoover capillary melting point apparatus and are uncorrected.

All glassware, syringes and needles were stored in a drying oven for a minimum of 24 h and purged with argon prior to use. Preparative flash

chromatography was performed on Natland International 200-400 mesh silica gel. Dichloromethane and triethylamine were distilled from calcium hydride. Thionyl chloride was distilled under reduced pressure. Reagents were purchased from Aldrich, Lanscaster or EM Science and used as received unless noted.

1,3,5-Tris(chloromethyl)-2,4,6-triethylbenzene (2.14)

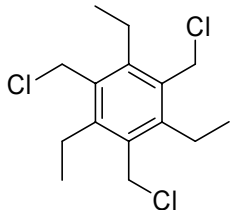

Into a 100 mL round-bottomed flask, fitted with a water condenser and a pressure-equilibrating addition funnel, was placed 1,3,5-triethylbenzene (5.0 g, 16.3 mmol) and 25 mL of carbon disulfide. A glass dispersion tube was placed into the solution and the solution was purged with argon. Tin tetrachloride (24.1 g, 92.0 mol) was added under argon. Chloromethyl methyl ether (22 mL, 277 mmol) was added to the addition funnel and incorporated rapidly, maintaining a controlled reflux. The mixture was stirred for 12 h under argon. The reaction was quenched with saturated aqueous $NaHCO_3$. Carbon disulfide was removed under reduced pressure and the remaining aqueous solution extracted with dichloromethane. The organic layer was washed with saturated aqueous $NaHCO_3$, water, and saturated aqueous sodium chloride, dried over $MgSO_4$, filtered and concentrated under reduced pressure to give a yellow solid. The crude product was purified using flash chromatography (silica, 50%

dichloromethane in hexanes) to yield **2.14** (4.5 g, 48% yield) as a white crystalline solid. Mp. 130-132 °C. ^{1}H NMR (300 MHz, $CDCl_3$) δ (TMS) 4.69 (s, 6H), 2.94 (q, 6H, *J* = 7.5 Hz), 1.31 (t, 9H, *J* = 7.5 Hz); ^{13}C NMR (75 MHz, $CDCl_3$) δ 145.24, 132.86, 40.85, 22.86, 16.32; HRMS (CI^+) calcd for $C_{15}H_{21}Cl_3$: 306.071; found 306.071.

1,3,5-Tris(azidomethyl)-2,4,6-triethylbenzene (2.15)

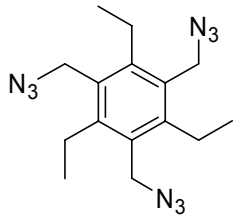

Conversion of 1,3,5-tris(chloromethyl)-2,4,6-triethylbenzene (**2.14**) to 1,3,5-tris(azidomethyl)-2,4,6-triethylbenzene (**2.15**) was accomplished by placing **2.14** (4.0 g, 13 mmol) into a 100 mL round-bottomed flask with 70 mL of *N,N*-dimethylformamide under argon. To this solution was added sodium azide (6.06 g, 93.2 mmol). After the mixture was stirred for 24 hours under argon, the solution was filtered and the *N,N*-dimethylformamide was removed under vacuum. The residue was dissolved in dichloromethane and washed with water followed by saturated aqueous sodium chloride. The organic layer was then dried over $MgSO_4$, filtered and concentrated under reduced pressure to give yellow crystals which were recrystallized from ethylacetate and hexanes to give **2.15** as white crystals (3.40 g, 80% yield). ^{1}H NMR (300 MHz, $CDCl_3$) δ (TMS) 4.49 (s, 6H), 2.85 (q, 6H, *J* = 7.5 Hz), 1.24 (t, 9H, *J* = 7.8 Hz); ^{13}C NMR (75 MHz,

$CDCl_3$) δ 145.10, 130.12, 48.06, 23.30, 15.90. HRMS (CI^+) calcd for $C_{15}H_{21}N_9$: 327.192; found 327.192. FT-IR (deposit from $CDCl_3$ on NaCl) 2972 cm^{-1} (C-H), 2908 cm^{-1} (C-H), 2088 cm^{-1} (N=N=N).

1,3,5-Tris(aminomethyl)-2,4,6-triethylbenzene (2.16)

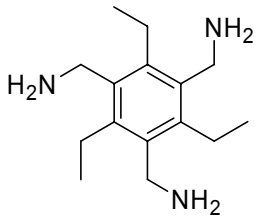

1,3,5-Tris(azidomethyl)-2,4,6-triethylbenzene (**2.15**) (3.0 g, 9.2 mmol) and triphenylphosphine (14.5 g, 55.2 mmol) in tetrahydrofuran-water (10:1) (600 mL) was stirred for 10 h at room temperature. The tetrahydrofuran-water solvent was removed under vacuum. The residue was dissolved in dichloromethane and washed with 1N aqueous HCl. The aqueous phase was then extracted with ethyl acetate. The aqueous phase was made alkaline by adding 3N aqueous sodium hydroxide until the pH was approximately 10 by pH paper and extracted with dichloromethane. The organic layer was dried over anhydrous $MgSO_4$, filtered and concentrated under reduced pressure to give a white solid. The crude product was purified *via* flash chromatography (silica, 1% ammonia saturated methanol in dichloromethane) to give **2.16** as a white solid (1.33 g, 58% yield). Mp. 125-126 °C. ^{1}H NMR (300 MHz, $CDCl_3$) δ (TMS) 3.88 (s, 6H), 2.83 (q, 6H, J = 7.8 Hz), 1.32 (bs, 6H), 1.24 (t, 9H, J = 7.5 Hz); ^{13}C NMR (75 MHz, $CDCl_3$) δ 140.61,

137.66, 39.90, 22.84, 17.07; FT-IR (deposit from $CDCl_3$ on NaCl) 3353 cm^{-1}, 3272 cm^{-1} (N-H); HRMS (CI^+) calcd for $C_{15}H_{26}N_3$: 248.212; found 248.212.

(1-Chlorocarbonyl-2-phenyl-ethyl)- carbamic acid 9H-fluoren-9-ylmethyl ester (2.17 a)

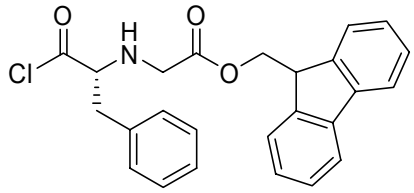

Into a 100 mL round-bottomed flask equipped with a pressure equilibrating addition funnel was placed *N*-(9-fluorenylmethoxycarbonyl)-L-phenylalanine (1.06 g, 2.75 mmol) and 30 mL of anhydrous dichloromethane. To this solution was added an excess of thionyl chloride (2.5 mL, 34.3 mmol). The solution was allowed to reflux for 1 h under argon and excess thionyl chloride and dichloromethane were removed under reduced pressure. The resulting residue was recrystallized from dichloromethane and hexanes to give **2.17 a** as a white solid (0.92 g, 82 % yield). Mp. 118-122 °C. ^{1}H NMR (300 MHz, CD_2Cl_2) δ 7.78 (d, 2H, *J* = 7.5 Hz), 7.54 (d, 2H, *J* = 7.5 Hz), 7.44-7.21 (m, 9H), 5.25 (m, 1H), 4.79 (m, 1H), 4.42 (d, 2H, *J* = 7.2 Hz), 4.21 (t, 2H), 3.22 (m, 2H); ^{13}C NMR (75 MHz, CD_2Cl_2) δ 155.59, 143.53, 141.53, 134.76, 129.44, 129.18, 127.98, 127.90, 127.32, 125.19, 120.21, 67.43, 64.11, 47.32, 37.00; FT-IR (deposit from CD_2Cl_2, on NaCl) 3317 cm^{-1} (N-H), 3025 cm^{-1} (C-H), 1825 cm^{-1} (C=O, acid chloride), 1686 cm^{-1} (C=O, amide).

(1-Chlorocarbonyl-2-methyl-propyl)- carbamic acid 9H-fluoren-9-ylmethyl ester (2.17 b)

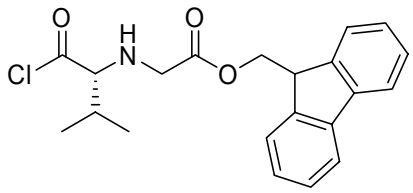

Into a 100 mL round-bottomed flask equipped with a condenser and a pressure equilibrating addition funnel was placed *N*-(9-fluorenylmethoxycarbonyl)-L-valine (0.93 g, 2.75 mmol) and 30 mL of anhydrous dichloromethane under argon. To this solution was added an excess of thionyl chloride (2.2 mL, 29.5 mmol). The solution was allowed to reflux for 1 h under argon. The dichloromethane and thionyl chloride were removed under reduced pressure and the resulting residue recrystallized from dichloromethane and hexanes to give **2.17 b** as a white solid (0.35 g, 35 % yield). Mp. 113-115 °C. ^{1}H NMR (300 MHz, CD_2Cl_2) δ 7.80 (d, 2H), 7.33 (d, 2H), 7.45-7.25 (m, 4H), 4.40 (m, 4H), 2.30 (m, 1H), 1.10 (m, 6H); ^{13}C NMR (75 MHz, CD_2Cl_2) δ 143.89, 141.52, 134.76, 121.91, 127.31, 125.27, 120.18, 47.40, 30.04; FT-IR (deposit from CD_2Cl_2 on NaCl) 3409 cm^{-1} (N-H), 3343 cm^{-1} (N-H), 3067 cm^{-1} (C-H), 2967 cm^{-1} (C-H), 1825 cm^{-1} (C=O, acid chloride), 1713 cm^{-1} (C=O, amide).

(1-Chlorocarbonyl-2-methyl-isobutyl)- carbamic acid 9H-fluoren-9-ylmethyl ester (2.17 c)

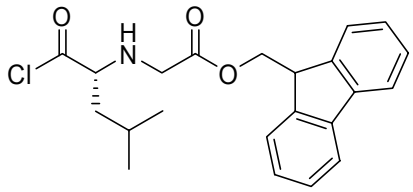

Into a 100 mL round-bottomed flask equipped with a condenser and a pressure equilibrating addition funnel was placed *N*-(9-fluorenylmethoxycarbonyl-L- leucine (1.50 g, 4.24 mmol) and 20 mL of anhydrous dichloromethane under argon. To this solution was added an excess of thionyl chloride (6.53 g, 55 mmol). The solution was heated to reflux for 1.5 h under argon. The dichloromethane and thionyl chloride were removed under reduced pressure and the resulting residue recrystallized from dichloromethane and hexanes to give **2.17 c** as a white solid (0.84 g, 53 % yield). Mp. 80-85 °C. ^{1}H NMR (300 MHz, CD_2Cl_2) δ 7.78 (d, 2H, *J* = 7.5 Hz), 7.61 (d, 2H, *J* = 5.7 Hz), 7.43-7.29 (m, 4H), 5.19 (d, 1H, *J* = 8.7 Hz), 4.43-4.36 (m, 3H), 4.23 (t, 1H, *J* = 6.3 Hz), 1.71-1.54 (m, 3H), 0.953 (s, 6H); ^{13}C NMR (75 MHz, CD_2Cl_2) δ 178.1, 156.4, 144.2, 144.0, 141.5, 127.9, 127.3, 125.3, 120.2, 67.1, 47.4, 41.3, 25.0, 22.9, 21.6.

1,3,5-[*N*-(9-Fluorenylmethylcarbonyl)-L-phenyl alanyl aminomethyl]- 2,4,6-triethylbenzene (2.13 a)

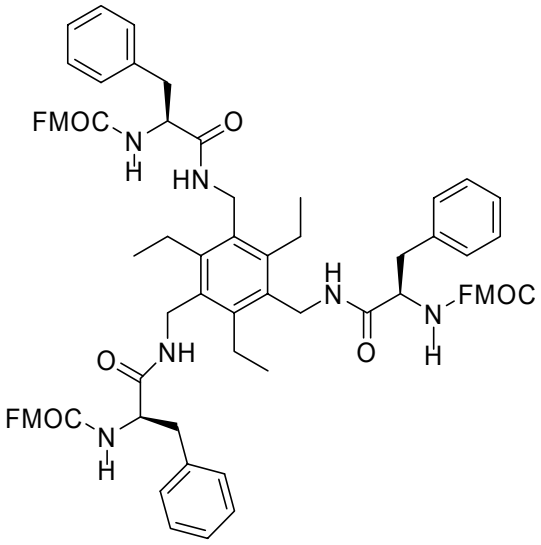

Into a 100 mL round-bottomed flask equipped with a pressure equilibrating addition funnel was placed **2.16** (0.16 g, 0.66 mol) and 30 mL of anhydrous dichloromethane. To this solution was added triethylamine (0.4 mL, 2.89 mmol) under argon. A solution of **2.17 a** (0.92 g, 2.27 mmol), dissolved in 30 mL of dichloromethane, was added dropwise *via* the addition funnel. The solution was allowed to stir for 2 h and the precipitate recovered by filtration leaving a white solid. The crude product was washed with dichloromethane to give **2.13 a** as a white solid (0.72 g, 80 % yield). Mp. 238 °C. ^{1}H NMR (300 MHz, DMSO-d_6) δ 7.95 (m, 3H), 7.86 (d, 6H, J = 7.5 Hz), 7.61 (m, 6H), 7.26 (m, 24H), 4.30 (m, 6H), 4.12 (m, 9H), 2.83 (m, 6H), 2.63 (m, 6H), 1.07 (t, 9H); ^{13}C NMR (75 MHz, DMSO-d_6) δ 172.02, 156.43, 144.44, 141.36, 138.76, 132.60,

129.94, 128.67, 128.31, 127.74, 125.94, 120.79, 66.27, 56.63, 47.24, 16.80; HRMS (CI^+) calcd for $C_{87}H_{85}N_6O_9$: 1357.6378; found 1357.6379.

1,3,5-[*N*-(9-Fluorenylmethoxycarbonyl)-L-valyl aminomethyl]-2,4,6-triethylbenzene (2.13 b)

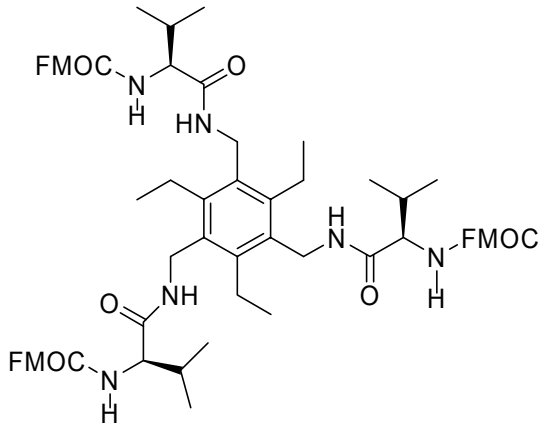

Into a 100 mL round-bottomed flask equipped with a pressure equilibrating addition funnel was placed **2.16** (0.068 g, 0.27 mol) and 30 mL of anhydrous dichloromethane. To this solution was added triethylamine (0.3 mL, 2.14 mmol) under argon. A solution of **2.17 b** (0.35 g, 0.97 mmol), dissolved in 20 mL of dichloromethane, was added slowly. The solution was allowed to stir for 2 h and the precipitate recovered by filtration leaving a white solid. The crude product was washed with dichloromethane to give **2.13 b** as a white solid (0.11 g, 33 % yield). Mp. 220 °C. ^{1}H NMR (300 MHz, DMSO-d_6) δ 7.79 (m, 15H), 7.35 (m, 15H), 4.25 (m, 15H), 3.90 (m, 3H), 2.62 (m, 6H), 1.91 (m, 3H), 1.05 (m, 9H), 0.82 (m, 18H); ^{13}C NMR (75 MHz, DMSO-d_6) δ 182.87, 154.06, 144.20, 128.33,

128.01, 120.75, 108.00, 93.58, 92.18, 89.41, 59.23, 19.94, 11.89; HRMS (CI^+) calcd for $C_{75}H_{85}N_6O_9$: 1213.6378; found 1213.6378.

1,3,5-[*N*-(9-Fluorenylmethoxycarbonyl)-L-leucylaminomethyl]-2,4,6-triethylbenzene (2.13 c)

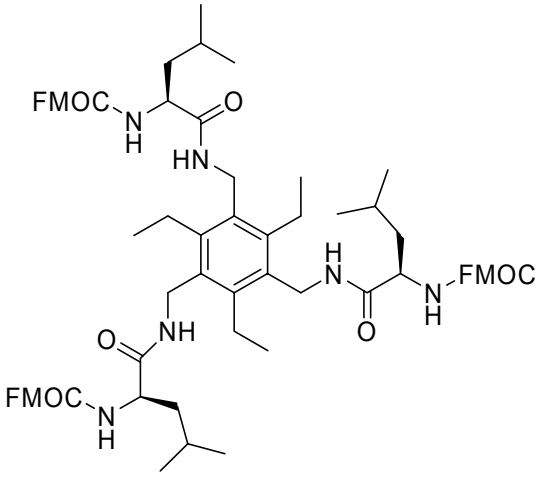

Into a 100 mL round-bottomed flask equipped with a pressure equilibrating addition funnel was added **2.16** (0.10 g, 0.41 mmol) under argon. Anhydrous dichloromethane, 10 mL, was then added with triethylamine (0.4 mL, 0.28 mmol). A solution of **2.17 c** in 15 mL dichloromethane was then added dropwise *via* the addition funnel. The solution was allowed to stir for 4 h. The precipitate was recovered by filtration leaving a white solid. The crude product was washed with ethyl acetate to yield **2.13 c** as a white solid (0.43 g, 83%). ^{1}H NMR (300 MHz, DMSO-d_6) δ 7.87 (d, 6H, J = 7.5 Hz), 7.71 (bs. 3H), 7.69 (d, 6H Hz, J = 7.2 Hz), 7.43-7.30 (m, 12H), 4.27-4.02 (m, 21H), 2.64 (m, 6H), 1.49 (m, 6H), 1.33 (m, 3H), 1.03 (m, 9H), 0.823 (dd, 18H, J_1 = 6.6 Hz, J_2 = 10.8 Hz); ^{13}C

NMR (75 MHz, DMSO-d_6) δ 172.8, 156.4, 144.4, 141.4, 140.6, 137.7, 128.3, 127.7, 125.0, 120.8, 67.1, 47.4, 41.0, 39.4, 25.0, 23.8, 22.0, 16.7, 14.8; HRMS (CI^+) calcd for $C_{78}H_{91}N_6O_9$: 1255.6848; found 1255.6847.

1,3,5-[Phenyl alanyl aminomethyl]-2,4,6-triethylbenzene (2.13 d)

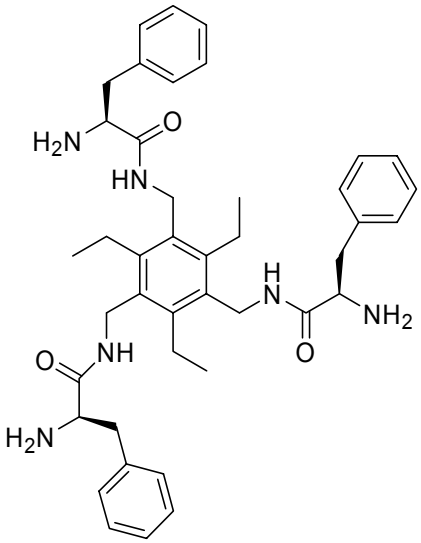

Into a 100 mL round-bottomed flask was added **2.13 a** (0.59 g, 0.48 mmol) and 5 mL of anhydrous *N*,*N*-dimethylformamide and piperidine (1.5 mL, 20.5 mmol) under argon. The solution was allowed to stir for two hours. The *N*,*N*-dimethylformamide was removed under vacuum to give a yellow residue. The residue was purified *via* column chromatography (silica, gradient elution with dichloromethane, followed by 10% ammonia saturated methanol in dichloromethane). The purified product, **2.13 d**, was obtained as a white solid (0.163 g, 61%). ^{1}H NMR (300 MHz, $CDCl_3$) δ 7.33-7.20 (m, 15 H), 7.08 (bs, 3H), 4.44 (d, 6H, J = 3.3 Hz), 3.64 (dd, 3H, J_1 = 9 Hz, J_2 = 4.2 Hz), 3.28 (dd, 3H,

J_1 = 13.8 Hz, J_2 = 4.2 Hz), 2.75 (dd, 3H, J_1 = 13.5 Hz, J_2 = 9.0 Hz), 2.59 (q, 6H, J_1 = 6.9 Hz), 1.39 (bs, 6H), 1.171 (t, 9H, J_1 = 7.5Hz); ^{13}C NMR (75 MHz, $CDCl_3$) δ 174.0, 144.3, 137.0, 132.3, 129.6, 129.0, 127.1, 56.6, 41.2, 37.0, 32.2, 16.7; HRMS (CI^+) calcd for $C_{42}H_{54}N_6O_3$: 691.4336; found 691.4336.

1,3,5-[Valyl aminomethyl]-2,4,6-triethylbenzene (2.13 e)

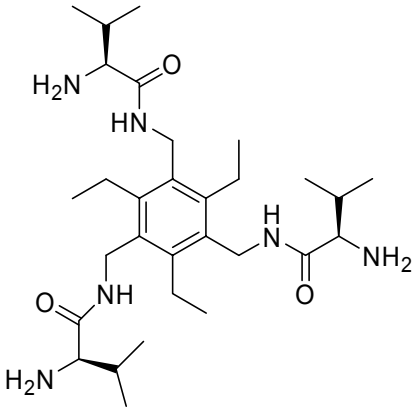

Into a 100 mL round-bottomed flask was added **2.13 b** (0.59 g, 0.48 mmol) and 5 mL of anhydrous *N*,*N*-dimethylformamide and piperidine (1.5 mL, 20.5 mmol) under argon. The solution was allowed to stir for two hours. The *N*,*N*-dimethylformamide was removed under vacuum to give a yellow residue. The residue was purified *via* column chromatography (silica gel, gradient elution with dichloromethane, followed by 10% ammonia saturated methanol in dichloromethane). The purified product, **2.13 e**, was obtained as a white solid (0.163 g, 61%). ^{1}H NMR (300 MHz, $CDCl_3$) δ 7.155 (bs, 3H), 4.47 (t, 6H, J = 4.8 Hz), 3.26 (d, 3H, J = 3.6 Hz), 2.69 (q, 6H, J = 9 Hz), 2.40-2.34 (m, 3H), 1.21 (t, 15H, J = 7.8 Hz), 0.99 (d, 9H, J = 6.9 Hz), 0.83 (d, 9H, J = 6.9 Hz); ^{13}C NMR (75

MHz, $CDCl_3$) δ 174.3, 144.3, 132.5, 60.4, 34.0, 31.0, 23.3, 20.0, 16.7, 16.3; HRMS (CI^+) calcd for $C_{30}H_{55}N_6O_3$: 547.4335; found 547.4330.

1,3,5-[Leucyl aminomethyl]-2,4,6-triethylbenzene (2.13 f)

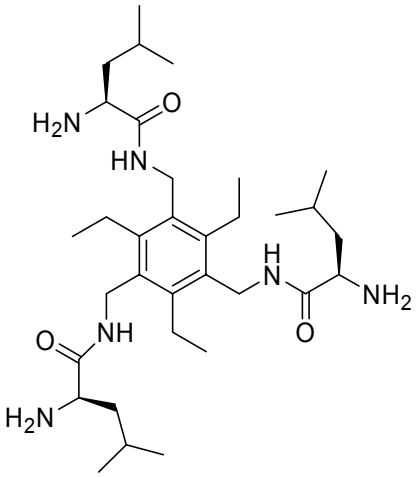

Into a 100 mL round-bottomed flask was added **2.13 c** (1.1 g, 0.87 mmol) with 5 mL of anhydrous *N*,*N*-dimethylformamide. Piperidine (2.0 mL, 20 mmol) was then added and the solution stirred for 12 h. The solvent was removed under vacuum and the residue purified by column chromatography (silica, gradient elution with dichloromethane, followed by 10% ammonia saturated methanol in dichloromethane). The purified product, **2.13 f**, was obtained as a white solid (0.39 g, 76%). ^{1}H NMR (300 MHz, $CDCl_3$) δ (TMS) 7.10 (bs, 3H), 4.46 (m, 6H), 3.43 (m, 3H), 2.69 (m, 6H), 1.75 (m, 12H), 1.36-1.12 (m, 12H), 0.955 (dd, 12H, J_1 = 6.0 Hz, J_2 = 9.3 Hz); ^{13}C NMR (75 MHz, $CDCl_3$) δ 183.0, 144.3, 132.4, 53.7, 44.1, 38.0, 25.1, 23.6, 23.3, 21.7, 19.5, 16.7.

1,3,5-[*N*-Acetyl phenyl alanyl aminomethyl]-2,4,6-triethylbenzene (2.18)

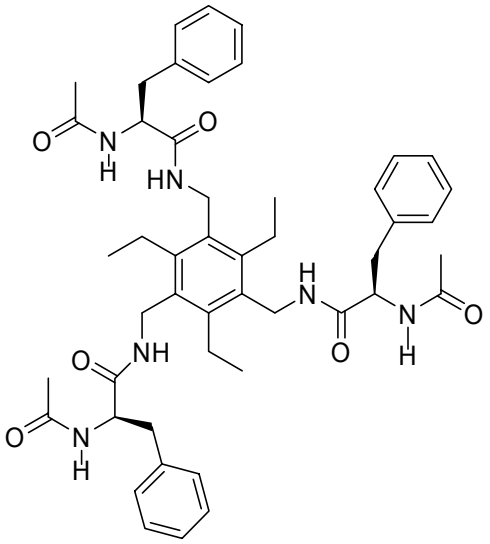

Into a 100 mL round-bottomed flask equipped with a pressure equilibrating addition funnel was placed 0.36 g (0.53 mmol) of **2.13 d** and 20 mL of anhydrous dichloromethane under argon. To this solution was added triethylamine (0.3 mL, 2.15 mmol). Acetyl chloride (0.20 mL, 2.82 mmol) was added slowly and the solution was allowed to stir for 12 h under argon. The solution was washed with water, followed by saturated aqueous sodium chloride. The organic phase was isolated, dried, filtered and concentrated under reduced pressure to give **2.18** as a yellow solid (0.34 g, 79%). Decomposes at 250-255 °C. ^{1}H NMR (300 MHz, DMSO-d_6) δ 8.12 (d, 3H, J = 8.7 Hz), 7.90 (m, 3H), 7.23 (m, 15H), 4.55 (sextet, 3H, J = 5.1 Hz), 4.26 (m, 6H), 2.93 (m, 3H), 2.74 (m, 3H), 2.58 (m, 6H), 1.72 (s, 9H), 1.05 (t, 9H, J = 7.8 Hz); ^{13}C NMR (75 MHz, DMSO-d_6) δ 171.81, 169.63, 164.54, 144.16, 138.65, 132.48, 129.84, 128.65,

54.38, 23.13, 16.75; HRMS (CI^+) calcd for $C_{48}H_{61}N_6O_6$: 817.465; found 817.464.

1,3,5-[*N*-Valeryl phenyl alanyl aminomethyl]-2,4,6-triethylbenzene (2.19)

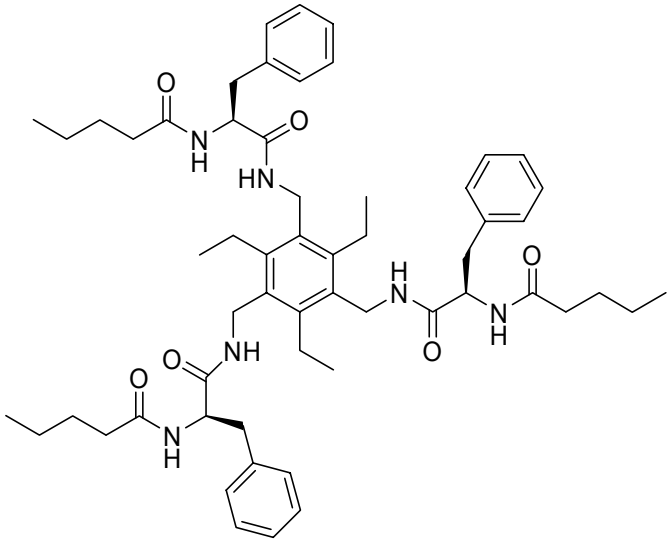

Into a 100 mL, round-bottomed flask under argon was added **2.13 d** (0.152 g, 0.220 mmol). Anhydrous acetonitrile, 10 mL was added with triethylamine, (0.10 mL, 0.99 mmol). Valeryl chloride (0.117 mL, 0.99 mmol), diluted in 8 mL of acetonitrile, was added dropwise by an addition funnel and the solution stirred for 4 h. The precipitate was filtered and the solid washed with dichloromethane. The product, **2.19**, was recovered as a white solid (0.21 g, 15%). ^{1}H NMR (300 MHz, DMSO-d_6) δ 8.01 (d, 3H, J = 8.7 Hz), 7.87 (bs, 3H), 7.226-7.167 (m, 15 H), 4.57 (m, 3H), 4.27 (m, 6H), 2.85-2.65 (m, 6H), 2.58 (m, 6H), 1.98 (t, 6H, J = 7.5 Hz), 1.29 (m, 6H), 1.06 (m, 15 H), 0.747 (t, 9H, J = 7.2 Hz); ^{13}C NMR (125 MHz, DMSO-d_6) δ 172.0, 171.2, 143.5, 138.0, 131.8, 129.2, 127.9, 126.2, 118.1,

72.3, 60.3, 53.6, 48.6, 45.7, 37.8, 37.2, 35.2, 30.6, 24.9, 22.4, 21.9, 16.0, 13.8, 8.6; HRMS (CI^+) calcd for $C_{60}H_{85}N_6O_6$: 985.6531; found 985.6505.

1,3,5-[*N*-Hexanoyl phenyl alanyl aminomethyl]-2,4,6-triethylbenzene (2.20)

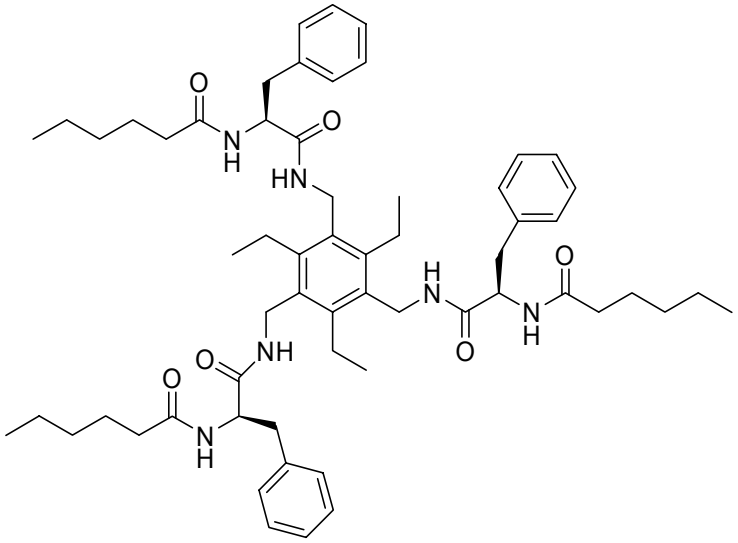

Into a 50 mL, three-necked flask equipped with an addition funnel was added **2.13 d** (0.022g, 0.032 mmol) under argon. Dichloromethane, 8 mL was added with triethylamine (0.4 mL, 2.8 mmol). Hexanoyl chloride (0.015 mL, 0.107 mmol), diluted in 6 mL of dichloromethane, was then added dropwise. The solution was allowed to stir for 4 h under argon. The solution was filtered and the precipitate washed with dichloromethane, giving **2.20** as a white solid (0.030 g, 94%). ^{1}H NMR (300 MHz, DMSO-d_6) δ 8.02 (d, 3H, J = 9.6 Hz), 7.87 (bs, 3H), 7.23-7.15 (m, 15 H), 4.57 (m, 3H), 4.29 (m, 6H), 2.95-2.70 (m, 6H), 2.60 (m, 6H), 1.97 (t, 6H, J = 6.6 Hz), 1.33-1.00 (m, 27H), 0.782 (t, 9H, J = 7.5 Hz); ^{13}C NMR (125 MHz, DMSO-d_6) δ 172.1, 171.2, 143.5, 137.9, 131.9, 129.2, 127.9, 126.2,

118.1, 79.17, 79.0, 78.7, 72.3, 60.3, 53.6, 48.6, 37.9, 37.21, 34.9, 27.4, 22.4, 21.5, 16.0, 13.7; HRMS (CI^+) calcd for $C_{57}H_{79}N_6O_6$: 943.6061; found 943.6077.

1,3,5-[*N*-(3,5-(bis(trifluoromethyl) benzyl) carbonyl phenyl alanyl aminomethyl]-2,4,6-triethylbenzene (2.21)

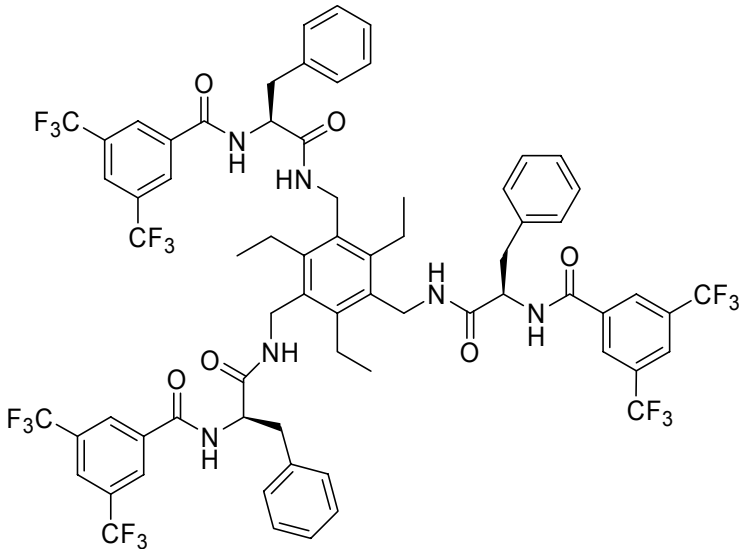

Into a 100 mL round-bottomed flask equipped with a pressure equilibrating addition funnel was placed **2.13 d** (0.13 g, 0.185 mmol) and 10 mL of anhydrous dichloromethane under argon. To this solution was added triethylamine (0.20 mL, 1.43 mmol). 3,5-Bis(trifluoromethyl)benzyl chloride (0.40 mL, 2.21 mmol), dissolved in 7 mL dichloromethane, was added slowly *via* addition funnel and the solution was allowed to stir for 4 h under argon. The solution was filtered and the filtrate washed with dichloromethane to give **2.21** as a white solid (0.24 g, 91%). ^{1}H NMR (300 MHz, DMSO-d_6) δ 9.22 (d, 3H, J = 9.0 Hz), 8.35 (dd, 9H, J_1 = 13.8 Hz, J_2 = 35.4 Hz), 7.33-7.13 (m, 15), 4.87 (m,

3H), 4.37 (m, 6H), 3.11-2.94 (m, 6H), 2.68 (m, 6H), 1.09 (t, 9H, J = 7.2 Hz); HRMS (CI^+) calcd for $C_{69}H_{61}N_6O_6F_{18}$: 1411.4375; found 1411.4365.

1,3,5-[*N*-tert-butoxy carbonyl phenyl alanyl aminomethyl]-2,4,6-triethylbenzene (2.22)

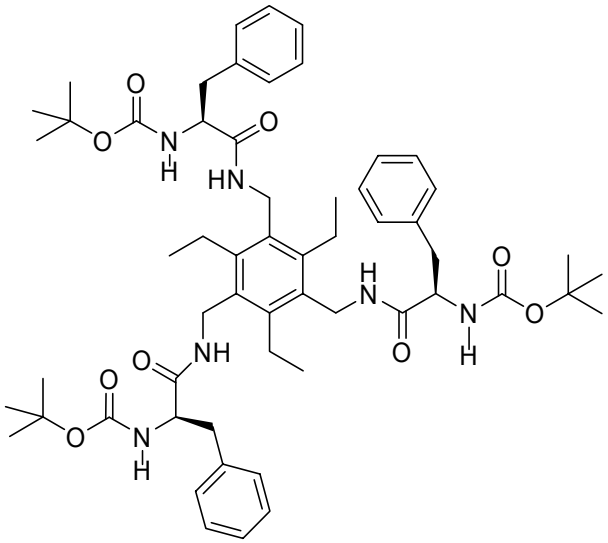

Into a 100 ml, three-necked round bottomed flask equipped with an addition funnel was added **2.13 d** (0.115 g, 0.166 mmol) with 20 mL of dichloromethane. Di-*tert*-butyl dicarbonate (0.15 g, 0.687 mol), dissolved in 7 mL of dichloromethane was then added dropwise. The solution was allowed to stir for 3 h. Dichloromethane, 100 mL, was then added to dissolve the precipitate. The organic phase was washed with 1.5 M aqueous sodium hydroxide (100 mL), water (100 mL) and saturated aqueous sodium chloride (50 mL). The organic phase was isolated, dried over Na_2SO_4, filtered and the solvent removed under vacuum to yield **2.22** as a white solid (0.123 g, 75%). ^{1}H NMR (300 MHz,

DMSO-d_6) δ 7.76 (bs, 3H), 7.30-7.18 (m, 15H), 6.92 (d, 3H, J = 8.1 Hz), 4.30-4.21 (m, 9H), 2.94-2.64 (m, 12H), 1.27 (s, 27H), 1.09 (t, 9H, J = 7.2 Hz); ^{13}C NMR (125 MHz, DMSO-d_6) δ 171.4, 155.1, 143.5, 138.0, 131.9, 129.1, 127.9, 126.1, 118.0, 78.0, 55.5, 48.6, 37.7, 37.2, 28.0, 27.7, 22.4, 16.0; HRMS (CI^+) calcd for $C_{57}H_{79}N_6O_9$: 991.5909; found 991.5932.

1,3,5-[*N*-(3,5-(bis(trifluoromethyl) benzyl) carbonyl valyl aminomethyl]-2,4,6-triethylbenzene (2.23)

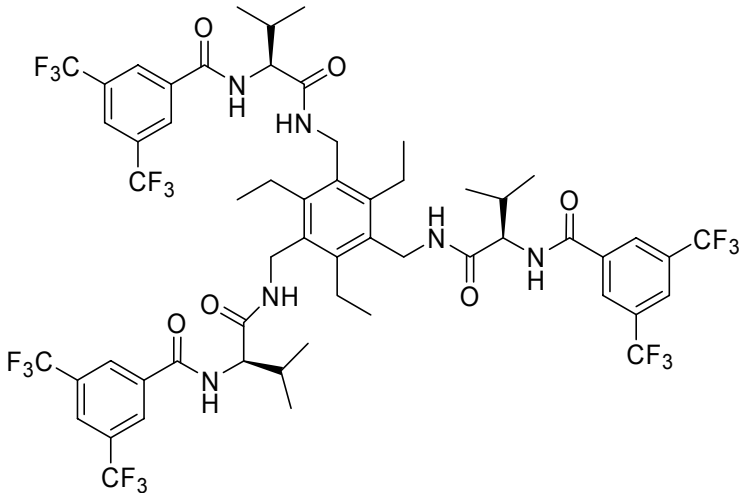

Into a 100 mL, three-necked flask under argon was added **2.13 e** (0.10 g, 0.185 mmol) with 10 mL anhydrous dichloromethane. Triethylamine (0.2 mL, 1.43 mmol) was then added with stirring. 3,5-Bis(trifluoromethyl)benzyl chloride (0.40 mL, 2.21 mmol), dissolved in 7 mL of dichloromethane, was added dropwise. The solution was allowed to stir for 4 h. The precipitate was filtered and washed with dichloromethane to give **2.23** as a white solid (0.225 g, 96%). ^{1}H NMR (300 MHz, DMSO-d_6) δ 9.01 (d, 3H, J = 8.1 Hz), 8.49 (d, 15H, J = 22.5

Hz), 8.25 (bs, 3H), 4.44-4.28 (m, 9H), 2.68 (m, 6H), 2.10 (m, 3H), 1.18 (t, 9H, J = 7.5 Hz), 0.88 (d, 18H, J = 6.6 Hz); HRMS (CI^+) calcd for $C_{57}H_{61}N_6O_6F_{18}$: 1267.4365; found 1267.4378.

1,3,5-[*N*-tert-butoxy carbonyl valyl aminomethyl]-2,4,6-triethylbenzene (2.24)

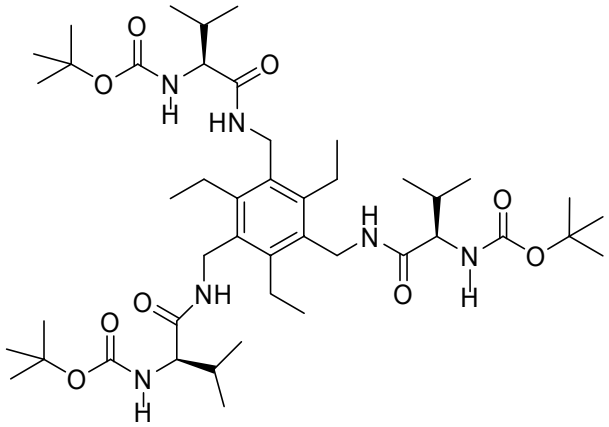

Into a 100 mL, three-necked flask equipped with an addition funnel was added **2.13 e** (0.155 g, 0.283 mmol) with 10 mL anhydrous dichloromethane under argon. Di-*tert*-butyl dicarbonate (0.223 g, 1.02 mmol), dissolved in 5 mL of dichloromethane, was added dropwise. The solution was allowed to stir for 4 h. The reaction was diluted with an additional 50 mL of dichloromethane and washed with water, 3M aqueous sodium hydroxide, and saturated aqueous sodium chloride. The organic phase was isolated, dried over $MgSO_4$, filtered and the solvent removed under vacuum to leave **2.24** as a white solid (0.14 g, 59%). ^{1}H NMR (300 MHz, $CDCl_3$) δ 5.76 (bs, 3H), 5.00 (bs, 3H), 4.45 (m, 6H), 3.82 (t, 3H, J = 8.1 Hz), 2.62 (q, 6H, J = 7.8 Hz), 2.11 (m, 3H), 1.38 (s, 27H), 1.12 (t, 9H, J =

7.2 Hz), 0.916 (dd, 18H, J_1 = 6.6 Hz, J_2 = 14.4 Hz); ^{13}C NMR (125 MHz, DMSO-d_6) δ 171.3, 155.4, 143.5, 131.9, 118.0, 78.1, 59.6, 48.6, 37.2, 30.5, 28.1, 22.4, 19.3, 18.1, 16.0; HRMS (CI^+) calcd for $C_{45}H_{79}N_6O_9$: 847.5909; found 847.5901.

1,3,5-[*N*-tert-butoxy carbonyl leucyl aminomethyl]-2,4,6-triethylbenzene (2.25)

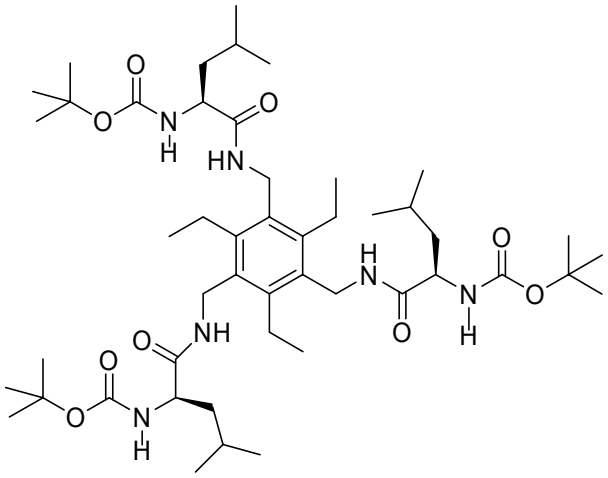

To a solution of **2.13 f** (0.39 g, 0.66 mmol) in anhydrous dichloromethane (15 mL) was added di-*tert*-butyl dicarbonate (0.62 g, 2.86 mmol) dissolved in 10 mL of dichloromethane. The solution was allowed to stir for 12 h. To the solution was then added an additional 30 mL of dichloromethane and the solution was extracted with 20 % aqueous acetic acid (50 mL), washed with water (2 x 50 mL) and washed with saturated aqueous sodium chloride (50 mL). The organic phase was isolated, dried over $MgSO_4$, filtered and the solvent removed *in vacuo* to yield the crude product as a white solid. The solid was purified by a short path column (silica, 5 % ammonia saturated methanol in dichloromethane) affording

2.25 as a white solid (0.438 g, 74%). ^{1}H NMR (300 MHz, $CDCl_3$) δ (TMS) 6.04 (bs, 3H), 4.89 (bs, 3H), 4.45 (dq, 6H, J_1 = 24 Hz, J_2 = 3 Hz), 4.06 (m, 3H), 2.66 (q, 6H, J = 6.6 Hz), 1.68-1.60 (m, 6H), 1.53-1.42 (m, 3H), 1.39 (s, 27H), 1.17 (t, 9H, J = 6 Hz), 0.93 (dd, 18H, J_1 = 6.3 Hz, J_2 = 2.1 Hz); ^{13}C NMR (75 MHz, DMSO-d_6) δ 172.5, 163.2, 144.4, 141.1, 41.2, 38.3, 34.2, 28.5, 25.3, 24.9, 23.2, 22.2, 16.7; HRMS (CI^+) calcd for $C_{48}H_{84}N_6O_9$: 889.6378; found 889.6392.

***N*-tert-butoxy carbonyl-L-leucine benzylamide (2.32)**

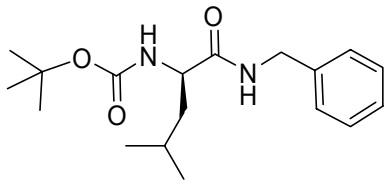

BOC-L-leucine-*N*-hydroxysuccinimide ester (2.0 g, 6.0 mmol) was dissolved in 40 mL of anhydrous dichloromethane under argon. Benzyl amine (0.85 mL, 7.8 mmol) was dissolved in 20 mL dichloromethane and added dropwise *via* an addition funnel. Triethylamine (1.0 mL, 7.2 mmol) was added and the solution stirred under argon for 12 h. The mixture was diluted with 50 mL dichloromethane and washed with 20% aqueous acetic acid (100 mL), water (4 x 100 mL) and saturated aqueous sodium chloride (100 mL). The organic layer was isolated, dried over $MgSO_4$, filtered and the solvent removed *in vacuo*. The resulting white solid was purified by short-path column (10 % ammonia saturated methanol in dichloromethane) to yield **2.32** as a white solid (1.3 g, 67%). ^{1}H NMR (300 MHz, DMSO-d_6) δ (TMS) 7.34-7.24 (m 5H), 6.49 (bs, 1H), 4.87 (bs, 1H), 4.44 (d, 1H, J = 5.4 Hz), 4.11 (m, 1H), 1.73-1.65 (m, 2H), 1.52-1.44 (m,

1H), 1.41 (s, 9H), 0.94 (dd, 6H, J_1 = 6.3 Hz, J_2 = 6.3 Hz); ^{13}C (75 MHz, $CDCl_3$) δ (TMS) 155.8, 138.1, 128.9, 127.9, 127.3, 80.0, 53.2, 43.7, 43.3, 41.3, 28.5, 25.0, 23.2, 22.0; HRMS (CI^+) calcd for $C_{18}H_{28}N_2O_3$: 321.2178; found 321.2182.

General Procedure for Enolate Synthesis.

Sodium enolates **2.26**-**2.28** were synthesized from sodium ethoxide in ethanol. One equivalent of freshly cut sodium metal (from mineral oil) was placed into a tared, three-neck round-bottomed flask under argon. The mineral oil was removed by washing with 1.0 mL portions of petroleum ether and decanting the solvent under argon after each wash. After washing, the metal was dried under a stream of argon and the weight obtained by difference. The flask was cooled in an ice-water bath and ethanol was added dropwise from an addition funnel under argon. After the metal dissolved, one equivalent of β-diketone was added as a solution in ethanol. Subsequent removal of the ethanol under vacuum produced the enolate as a solid. To remove any unreacted starting material, the resulting solid was washed with anhydrous acetonitrile in a glovebox under nitrogen. The purified solid was stored in a glovebox under nitrogen.

2.8.2 General Procedure for ^{1}H NMR Binding Studies

General Considerations. The ^{1}H NMR binding studies were carried out on a Varian Unityplus -300 NMR spectrometer. All Hamilton gas-tight syringes and volumetric flasks were dried in a vacuum dessicator for 24 hours prior to use. Septa and argon balloons were used to exclude water outside of the dry box. The sodium enolates were stored in a dry box under nitrogen. The enolate-[2.2.1]cryptand solutions and host solutions were freshly prepared prior to each titration.

Procedure. For a typical experiment, a stock solution of enolate-[2.2.1]cryptand was prepared in by dissolving one equivalent of a sodium enolate and one equivalent of [2.2.1]cryptand in anhydrous acetonitrile under argon. The solvent was then removed under vacuum and the resulting solid washed with anhydrous acetonitrile in a glovebox under nitrogen. The solid was then weighed into a tared 2 mL volumetric flask and diluted with acetonitrile-d_3. A stock solution of host was prepared by weighing the solid into a 2 mL volumetric flask and diluting with deuterated solvent (either chloroform-d_3 or tetrahydrofuran-d_8). The titrand was prepared by combining 1 mL of host stock solution to 1 mL of enolate-[2.2.1]cryptand stock solution. The initial ^{1}H NMR sample was prepared by diluting 0.40 mL of the host stock solution with 0.40 mL of deuterated solvent in an ^{1}H NMR tube in a glovebox under nitrogen. The ^{1}H NMR tube was then sealed with a rubber septum. The titrand was added in 5 μL additions *via* syringe to the initial sample of host and the ^{1}H NMR spectrum recorded after each addition.

Calculation of Association Constants by ^{1}H NMR Chemical Shifts

The equilibrium constant (*K*) for the formation of a 1:1 complex (*RS*) between a receptor (*R*) and a substrate (*S*) (Equation 1.1) may be found from Equation 1.2.

$$R+S \rightleftharpoons RS$$

Equation 1.1

$$K = \frac{[RS]}{[R][S]}$$

Equation 1.2

If the separate observation of chemical shifts for *R* and *RS* is not possible, the observed chemical shift (δ_{obs}) can be expressed as a mole fraction weighted shift of *R* and *RS* (Equation 1.3) where δ_R is the shift of the free receptor, δ_{RS} is the shift of the complex and N_R and N_{RS} are the mole fractions of the receptor and complex, respectively ($N_R + N_{RS} = 1$).

$$\delta_{obs} = N_R\delta_R + N_{RS}\delta_{RS}$$

Equation 1.3

The mole fractions of *R* and *RS* are defined by Equations 1.4 and 1.5.

$$N_R = \frac{[RS]}{[R]+[RS]}$$

Equation 1.4

$$N_{RS} = \frac{[R]}{[R]+[RS]}$$

Equation 1.5

Using Equations 1.4 and 1.5, δ_{obs} (Equation 1.3) may be expressed as Equation 1.6.

$$\delta_{obs} = \delta_R + \frac{[RS]}{[R]+[RS]}(\delta_{RS} - \delta_R)$$

Equation 1.6

Since the equilibrium concentrations of [RS] and [R] are not known, the concentrations of *R*, *S* and *RS* may be expressed in terms of the initial concentrations in Equations 1.7 and 1.8.

$$[R^0] = [R] + [RS]$$

Equation 1.7

$$[S^0] = [S] + [RS]$$

Equation 1.8

Equation 1.2 can then be written in terms of $[R^0]$ and $[S^0]$ (Equation 1.9).

$$K = \frac{[RS]}{([R^0]-[RS])([S^0]-[RS])}$$

Equation 1.9

The expansion of Equation 1.9 gives Equation 1.10.

$$K = \frac{[RS]}{[R^0][S^0]-[RS]([R^0]+[S^0])+[RS]^2}$$

Equation 1.10

Rearrangement of Equation 1.10 gives Equation 1.11.

$$[RS]^2 - ([R^0] + [S^0] + \frac{1}{K})\,[RS] + [R^0][S^0] = 0$$

Equation 1.11

Equation 1.11 is a quadratic equation and the root is shown in Equation 1.12.

$$[RS] = 0.5([R^0] + [S^0] + \frac{1}{K} - \sqrt{\{([R^0] + [S^0] + \frac{1}{K})^2 - 4[R^0][S^0]\}})$$

Equation 1.12

An expression for δ_{obs} may then be found by substituting Equation 1.12 into Equation 1.6 to yield Equation 1.13.[41]

$$\delta_{obs} = \delta_R + \frac{\Delta_0}{2[R^0]}([R^0] + [S^0] + \frac{1}{K} - \sqrt{\{([R^0] + [S^0] + \frac{1}{K})^2 - 4[R^0][S^0]\}})$$

Equation 1.13

In this equation, δ_{obs} is the observed chemical shift, δ_R is the initial chemical shift of the receptor, δ_{RS} is the shift of the pure complex, $\Delta_0 = \delta_R - \delta_{RS}$, K is the association constant, R_0 is the initial concentration of the receptor, and S_0 is the initial concentration of the substrate. A titration experiment gives a series of data sets including $[R_0]$, $[S_0]$ and δ_{obs}. The unknown parameters in the equation, K and Δ_0, are found using a nonlinear curve fitting method in which the value for K is initially estimated, and δ is calculated for each data point. The process is repeated until convergence of the calculated δ and δ_{obs}.

2.8.4 General Procedure for Enolate Alkylation.

In a drybox under nitrogen, one equivalent of sodium enolate was added to 1.5 equivalents of [2.2.1]cryptand in a 100 mL, three-neck, round-bottomed flask. The host (1.1 equivalents) was then added under an argon atmosphere followed by anhydrous THF (40 mL). The solution was then stirred for 30 minutes and cooled to -78ºC in an acetone-dry ice bath. Benzyl bromide (5 equivalents) in

THF (10 mL) was added dropwise *via* an addition funnel and the solution stirred for 8 hours at -78ºC. The reaction was quenched with water (1 mL) and the THF was removed in vacuo. The residue was dissolved in dichloromethane and washed with water (1 x 30 mL), saturated aqueous $NaHCO_3$ (1 x 30 mL) and brine, and dried with $MgSO_4$. After filtration, the filtrate was concentrated *in vacuo* to give a yellow oil. This crude product was purified by flash chromatography (silica, hexanes/ ethyl acetate (90:10)) to give the desired product. Enantiomeric excess of the product was determined by chiral phase HPLC. For entries 1, 3, 8 and 9, a Chiralcel AD column (hexane/ 2-propanol (30/1), 1.0 mL/min, 260 nm UV detection) was used. For entries 2 and 4-7, a Chiralcel OJ-H column (hexane/ 2-propanol (49/1), 1.0 mL/min, 260 nm UV detection) was used.

2.8.4.1 Characterization of Alkylation Products

2-Acetyl-2-benzyl cyclopentanone (2.29)

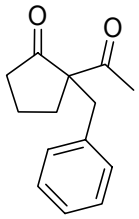

^{1}H NMR (300 MHz, $CDCl_3$) δ (TMS) 7.263-7.214 (m, 3H), 7.076 (dd, 2H, J_1 = 9.6 Hz, J_2 = 2.1 Hz), 3.164 (dd, 2H, J_1 = 59.1 Hz, J_2 = 13.8 Hz), 2.585 (m, 1 H), 2.288 (m, 4H), 2.039 (m, 1H), 1.701 (m, 3H); ^{13}C (75 MHz, $CDCl_3$) δ (TMS)

216.354, 204.184, 136.672, 129.958, 128.778, 127.205, 70.013, 40.466, 39.112, 30.270, 26.651, 19.579; HRMS (CI^+) calcd for $C_{14}H_{16}O_2$: 217.1228; found 217.1226.

2-Acetyl-2-benzyl cyclohexanone (2.30)

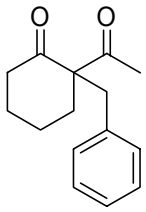

^{1}H NMR (300 MHz, $CDCl_3$) δ (TMS) 7.264-7.200 (m, 3H), 7.065 (dd, 2H, J_1 = 6.0 Hz, J_2 = 1.5 Hz), 3.164 (dd, 2H, J_1 = 24.9 Hz, J_2 = 10.5 Hz), 2.516 (ddt, 1 H, J_1 = 10.5 Hz, J_2 = 3.9 Hz, , J_3 = 1.2 Hz), 2.361 (dq, 1H, J_1 = 10.5 Hz, , J_2 = 2.4 Hz), 2.286-2.204 (m, 1H), 2.097 (s, 3H), 1.966 (m, 1H), 1.733-1.581 (m, 3H), 1.463-1.387 (m, 1H); ^{13}C (75 MHz, $CDCl_3$) δ (TMS) 209.697, 205.990, 136.403, 130.518, 128.435, 127.023, 68.949, 42.309, 40.219, 34.166, 27.248, 27.102, 22.441; HRMS (CI^+) calcd for $C_{15}H_{18}O_2$: 231.1385; found 231.1394.

2-Acetyl-2-benzyl-1-tetralone (2.31)

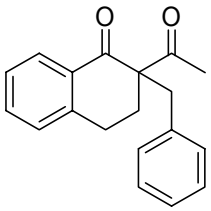

^{1}H NMR (300 MHz, $CDCl_3$) δ (TMS) 8.084 (dd, 1H, J_1 = 8.10 Hz, J_2 = 1.2 Hz), 7.473-7.135 (m, 8H), 3.304 (dd, 2H, J_1 = 134.1 Hz, J_2 = 13.5 Hz), 3.103-2.950 (m, 1H), 2.820-2.704 (m, 1H), 2.521-2.448 (m, 1H), 2.180 (s, 3H), 1.944-1.843 (m, 1H); ^{13}C (75 MHz, $CDCl_3$) δ (TMS) 205.5, 197.4, 144.1, 136.5, 134.1, 132.5, 130.8, 129.2, 128.4, 128.2, 127.1, 126.9, 65.5, 40.7, 29.4, 2.6, 26.1; HRMS (CI^+) calcd for $C_{19}H_{18}O_2$: 279.1385; found 279.1389.

2.8.5 Assignment of Stereochemistry: Characterization of Products

2-Benzyl cyclohexanone (2.35)

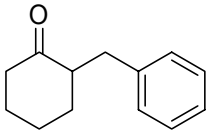

^{1}H NMR (400 MHz, $CDCl_3$) δ (TMS) 7.29-7.26 (m, 2H), 7.21-7.14 (m, 3H), 3.23 (dd, 1H, J_1 = 10.5 Hz, J_2 = 3.6 Hz), 2.59-2.51 (m, 1H), 2.47-2.29 (m, 3H), 2.10-1.99 (m, 2H), 1.86-1.52 (m, 3H), 1.43-1.30 (m, 1H); ^{13}C (100 MHz, $CDCl_3$) δ (TMS) 212.9, 140.6, 129.4, 128.5, 126.2, 52.7, 42.4, 35.7, 33.6, 28.3, 25.3; HRMS (CI) m/z (rel. intensity, %) 171 (14), 189 (100), 190 (11), 217 (13), 219 (18).

2-Acetyl-2-benzyl cyclohexanone (2.30)

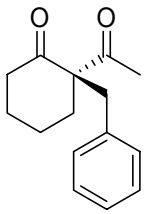

Into a 100 mL flask was added sodium (0.23g, 10.2 mmol) in mineral oil under argon. The metal was washed with petroleum ether (3 x 25 mL) to remove the mineral oil. Ethanol was added dropwise via an addition funnel at 0 ºC for 2 h. 2-Acetylcyclohexanone (1.3 mL, 10.0 mmol) in 20 mL of ethanol was added dropwise at 0 ºC and the solution stirred for 30 min. Benzyl bromide (1.2 mL, 10.1 mmol) in 20 mL of ethanol was added dropwise at 0 ºC and the solution stirred for 8 h under argon. The solvent was removed under vacuum, leaving a yellow oil. The oil was dissolved in dichloromethane and the solution washed with 1.0 M HCl, followed by water and then saturated aqueous NaCl. The organic phase was isolated, dried over $MgSO_4$, filtered and the solvent removed under vacuum to yield a yellow oil. The crude product was purified via column chromatography (silica, 10% ethyl acetate in hexanes), leaving **2.30** as a yellow oil (1.22g, 53%). ^{1}H NMR (400 MHz, $CDCl_3$) δ (TMS) 7.264-7.200 (m, 3H), 7.065 (dd, 2H, J_1 = 6.0 Hz, J_2 = 1.5 Hz), 3.164 (dd, 2H, J_1 = 24.9 Hz, J_2 = 10.5 Hz), 2.516 (ddt, 1 H, J_1 = 10.5 Hz, J_2 = 3.9 Hz, , J_3 = 1.2 Hz), 2.361 (dq, 1H, , J_1 = 10.5 Hz, J_2 = 2.4 Hz), 2.286-2.204 (m, 1H), 2.097 (s, 3H), 1.966 (m, 1H),

1.733-1.581 (m, 3H), 1.463-1.387 (m, 1H); ^{13}C (100 MHz, $CDCl_3$) δ (TMS) 209.697, 205.990, 136.403, 130.518, 128.435, 127.023, 68.949, 42.309, 40.219, 34.166, 27.248, 27.102, 22.441; HRMS (CI^+) calcd for $C_{15}H_{18}O_2$: 231.1385; found 231.1394.

2-[(2-methoxymethyl-pyrrolidin-1-yl)-(1-methyl-methylidene amine)-2-benzyl cyclohexanone (2.34 a and b)

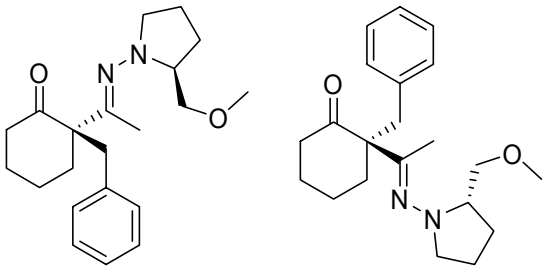

a **b**

Into a 100 mL flask was added 2-acetyl-2-benzyl cyclohexanone (0.52g, 2.3 mmol) under argon. (S)-(-)-1-amino-2-(methoxy methyl) pyrrolidine (0.30 mL, 2.2 mmol) was added neat. The mixture was heated at 60 ºC for 20 h under argon. The crude product was purified by column chromatography (silica, 10% ethyl acetate in hexanes) to give diastereomers **2.34 a** and **b** as yellow oils (0.53g, 68%). **2.34 a**: ^1H NMR (400 MHz, $CDCl_3$) δ (TMS) 7.24-7.09 (m, 5H), 3.47 (dd, 2H, J_1 = 4, J_2 = 9.6), 3.38 (s, 3H), 3.35-3.09 (m, 5H), 2.56 (q, 1H J = 8.4), 2.19 (dt, 2H, J_1 = 3.2, J_2 = 13.2), 2.14 (s, 3H), 2.06-1.99 (m, 1H), 1.89-1.81 (m, 2H), 1.74-1.26 (m, 6H); ^{13}C (100 MHz, $CDCl_3$) δ (TMS) 208.9, 166.8, 137.8, 130.8, 128.0, 126.5, 75.9, 66.7, 61.7, 59.5, 54.2, 40.9, 33.4, 29.1, 26.8, 26.6, 26.2, 22.4, 21.4; HRMS (CI^+) calcd for $C_{21}H_{30}O_2N_2$: 343.2386; found 343.2391. **2.34 b**: ^1H

NMR (400 MHz, $CDCl_3$) δ (TMS) 7.23-7.10 (m, 5H), 3.49 (m, 2H), 3.36 (s, 3H), 3.33-3.05 (m, 5H), 2.70 (m, 1H), 2.27-1.25 (m, 14H); ^{13}C (100 MHz, $CDCl_3$) δ 208.9, 165.5, 137.9, 130.9, 128.0, 126.5, 75.9, 66.8, 61.8, 59.5, 55.3, 41.0, 33.3, 31.2, 29.2, 27.0, 26.7, 26.1, 22.6, 22.2; HRMS (CI^+) calcd for $C_{21}H_{30}O_2N_2$: 343.2386; found 343.2391.

2.9 REFERENCES AND NOTES

[1] Caine, D. In *Comprehensive Organic Synthesis*, Vol. 3; Trost, B. M., Fleming, I., Eds. Pergamon Press: Oxford, 1991; Chapter 11.

[2] Caine, D. In *Carbon-Carbon Bond Formation*, Vol. 1; Augustine, R. L. Ed. Marcel Dekker: New York, 1979; Chapter 2.

[3] a) Mulzer, J. In *Comprehensive Asymmetric Catalysis*, Vol. I; Jacobsen, E. N., Pfaltz, A., Yamamoto, H. Eds. Springer: Berlin, 1999; pp. 66-74. b) Evans, D. A. In *Asymmetric Synthesis,* Vol. 3; Morrison, J. D. Ed. Academic Press: New York, 1984; pp 1- 110. c) Arya, P; Qin, H. *Tetrahedron* **2000**, 917-947.

[4] Meyers, A. I.; Williams, D. R.; Druelinger, M. *J. Am. Chem. Soc.* **1976**, *98*, 3032-3033.

[5] For a review, see Bergbreiter, D. E.; Newcomb, M. In *Asymmetric Synthesis*, Vol. 2; Morrison, J. D. Ed. Academic Press: New York, 1983; Chapter 9.

[6] Meyers, A. I.; Williams, D. R.; Erickson, G. W.; White, S.; Druelinger, M. *J. Am. Chem. Soc.* **1981**, *103*, 3081-3087.

[7] Meyers, A. I.; Knaus, C.; Kamata, K.; Ford, M. F. *J. Am. Chem. Soc.* **1976**, *98*, 567-576.

[8] Evans, D. A.; Takacs, J. M. *Tetrahedron Lett.* **1980**, *21*, 4233-4236.

[9] Enders, D.; Eichenauer, H. *Angew. Chem. Int. Ed., Engl.* **1976**, *15*, 549. b) Enders, D.; Eichenauer, H.; Baus, U.; Schubert, H.; Kremer, K. A. M. *Tetrahedron* **1984**, *40*, 1345-1359. c) Enders, D.; Kipphardt, H.; Fey, P. *Org. Syn.* **1987**, *65*, 183.

[10] Tomioka, K.; Ando, K.; Takemasa, Y.; Koga, K. *J. Am. Chem. Soc.* **1984**, *106*, 2718-2719.

[11] Whitesell, J. K.; Felman, S. W. *J. Org. Chem.* **1977**, *42*, 1663-1664.

[12] a) Evans, D. A.; Takacs, J. M.; McGee, L. R.; Ennis, M. D.; Mathre, D. J.; Bartroli, J. *Pure Appl. Chem.* **1981**, *53*, 1109-1127. b) Evans, D. A.; Ennis, M. D.; Mathre, D. J. *J. Am. Chem. Soc.* **1982**, *104*, 1737-1739. c) Cowden, C. J.; Paterson, I. In *Organic Reactions,* Vol. 51; Paquette, L. A., Ed. Wiley: New York, 1997; Chapter 1. d) Franklin, A. S.; Paterson, I. *Contemp. Org. Syn.* **1994**, *1*, 317-338. e) Ager, D. J.; Prakash, I.; Schaad, D. R. *Aldrichim. Acta* **1997**, *30*, 3-12.

[13] a) Murakata, M.; Nakajima, M.; Koga, K. *J. Chem. Soc., Chem. Commun.* **1990**, 1657-1658. b) Yasukata, T.; Koga, K. *Tetrahedron Asym.* **1993**, *4*, 35-38. c) Imai, M.; Hagihara, A.; Kawasaki, H.; Manabe, K.; Koga, K. *J. Am. Chem. Soc.* **1994**, *116*, 8829-8830. d) Yasukata, K.; Shindo, M.; Koga, K. *Tetrahedron Lett.* **1996**, *37*, 6343-6346. e) Riviere, P.; Koga, K. *Tetrahedron Lett.* **1997**, *38*, 7589-7592. f) Murakata, M.; Yasukata, T.; Aoki, T.; Nakajima, M.; Koga, K. *Tetrahedron* **1998**, *54*, 2449-2458. g) Matsuo, J.-I.; Kobayashi, S.; Koga, K. *Tetrahedron Lett.* **1998**, *39*, 9723-9726. h) Yamashita, Y.; Odashima, K.; Koga, K. *Tetrahedron Lett.* **1999**, *40*, 2803-2806.

[14] Matsuo, J.; Odashima, K.; Kobayashi, S. *Org. Lett.* **1999**, *1*, 345-347.

[15] Brun, E.; Gil, S.; Parra, M. *Tetrahedron Asym.* **2001**, *12*, 915-921.

[16] Flinois, K.; Bastide, C.; Harrison-Marchand, A.; Maddaluno, J. *Tetrahedron* **2002**, *58*, 4707-4716.

[17] Kawabata, T.; Yahiro, K.; Fuji, K. *J. Am. Chem. Soc.* **1991**, *113*, 9694-9696.

[18] a) Dolling, U.-H.; Davis, P.; Grabowski, E. J. J. *J. Am.Chem. Soc.* **1984**, *106*, 446-447. b) O'Donnell, M. J.; Bennett, W. D.; Wu, S. *J. Am. Chem. Soc.* **1989**, *111*, 2353-2355. c) O'Donnell, M. J.; Wu, S.; Huffman, J. C. *Tetrahedron* **1994**, *50*, 4507-4518. d) O'Donnell, W. J.; Wu, S.; Esikova, I.; Mi, A. U.S. Patent, 1996, 5,554,753. e) Lipkowitz, K. B.; Cavanaugh, M. W.; Baker, B.; O'Donnell, M. J. *J. Org. Chem.* **1991**, *56*, 5181-5192. f) Corey, E. J.; Xu, F.; Noe, M. C. *J. Am. Chem. Soc.* **1997**, *119*, 12414-12415. g) Lygo, B.; Wainwright, P. G. *Tetrahedron Lett.* **1997**, *38*, 8595-8598. h) Corey, E. J.; Noe, M. C.; Xu, F.

Tetrahedron Lett. **1998**, *39*, 5347-5350. i) Corey, E. J.; Yunxin, B.; Busch-Petersen, J. *J. Am. Chem. Soc.* **1998**, *120*, 13000-13001. j) O'Donnell, M. J.; Delgado, F.; Hostettler, C.; Schwesinger, R. *Tetrahedron Lett.* **1998**, *39*, 8775-8778. k) Lygo, B.; Crosby, J.; Peterson, J. A. *Tetrahedron Lett.*, **1999**, *40*, 1385-1389. l) Lygo, B. *Tetrahedron Lett.* **1999**, *40*, 1389. m) Lygo, B.; Crosby, J.; Peterson, J. A. *Tetrahedron Lett.* **1999**, *40*, 8671.

[19] Park, H.; Jeong, B.; Yoo, M.; Park, M.; Huh, H.; Jew, S. *Tetrahedron Lett.* **2001**, *42*, 4645-4648.

[20] Ooi, T.; Takeuchi, M.; Kameda, M.; Maruoka, K. *J. Am. Chem. Soc.* **2000**, *122*, 5228-5229.

[21] Trost, B. M.; Radinov, R.; Grenzer, E. M. *J. Am. Chem. Soc.* **1997**, *119*, 7879-7880.

[22] Kelly-Rowley, A. M.; Lynch, V. M.; Anslyn, E. V. *J. Am. Chem. Soc.* **1995**, *117*, 3438-3447.

[23] a) Snowden, T. S.; Bisson, A. P.; Anslyn, E. V. *J. Am. Chem. Soc.* **1999**, *121*, 624-6325. b) Snowden, T. S.; Bisson, A. P.; Anslyn, E. V. *Bio. Med. Chem.* **2001**, *9*, 2467-2478.

[24] Kelly-Rowley, A. Ph.D. Dissertation, The University of Texas at Austin, August 1994.

[25] a) Iverson, D. J.; Hunter, G.; Blount, J. F.; Damewood, J. R., Jr.; Mislow, K. *J. Am. Chem. Soc.* **1981**, *103*, 6073-6083. b) Kilway, K. V.; Siegel, J. S. *J. Am. Chem. Soc.* **1992**, *114*, 255-261. c) Hunter, G.; MacKay, R. L.; Kremminger, P.; Weissensteiner, W. *J. Chem. Soc. Dalton Trans.* **1991**, 3349-3358.

[26] Moberg, C. *Angew. Chem. Int. Ed.* **1998**, *37*, 248-268.

[27] Zhang, X. X.; Bradshaw, J. S.; Izah, R. M. *Chem. Rev.* **1997**, *97*, 3313-3361.

[28] Kim, S.-G.; Ahn, K. H. *Tetrahedron Lett.* **2001**, *42*, 4175-4177.

[29] Hennrich, G.; Anslyn, E. V. *Chem. Eur. J.* **2002**, *8*, 2218-2224.

[30] Tor, Y.; Libman, J.; Shanzer, A.; Felder, C.; Lifson, S. *J. Am. Chem. Soc.* **1992**, *114*, 6653-6661.

[31] Hanes, R. E., Jr.; Lavigne, J. J.; Anslyn, E. V.; Kilway, K. V.; Siegel, J. *Org. Syn.* **2003**, In preparation.

[32] Scriven, E. F. V.; Turnbull, K. *Chem. Rev.* **1988**, *88*, 297-388.

[33] Vaultier, M.; Knouzi, N.; Carrie, R. *Tetrahedron Lett.* **1983**, *24*, 763.

[34] Carpino, L. A.; Cohen, B. J.; Stephens, K. E., Jr.; Sadat-Aalee, S. Y.; Tien, J.; Langridge, D. L. *J. Org. Chem.* **1986**, *51*, 3732-3734.

[35] Jencks, W. P. *Proc. Natl. Acad. Sci., U.S.A.* **1981**, *78*, 4046-4050.

[36] Serjeant, E. P.; Dempsey, B. In *Ionization Constants of Organic Acids in Aqueous Solution*; Pergamon Press: Oxford, 1979.

[37] Jackman, L. M.; Lange, B. C. *Tetrahedron* **1977**, *33*, 2737-2769.

[38] Bernasconi, C. F.; Kanavarioti, A. *J. Am. Chem. Soc.* **1986**, *108*, 7744-7751.

[39] Mathieu, F.; Metz, B.; Moras, D.; Weiss, R. *J. Am. Chem. Soc.* **1978**, *100*, 4412.

[40] Brunet, E.; Poveda, A. M.; Rabasco, D.; Oreja, E.; Font, L. M.; Batra, M. S.; Rodríguez-Ubis, J. C. *Tetrahedron Asym.* **1994**, *5*, 935-948.

[41] Tsukube, H.; Furuta, H.; Odani, A.; Takeda, Y.; Kudo, Y.; Inoue, Y.; Liu, Y.; Sakamoto, H.; Kimura, K. In *Comprehensive Supramolecular Chemistry*, Vol. 8; Davies, J. E. D.; Ripmeester, J. A., Eds. Pergamon Press: Oxford, 1996; Chapter 10.

[42] Tomioka, K.; Ando, K.; Takemara, Y.; Koga, K. *J. Am. Chem. Soc.* **1984**, *106*, 2718-2719.

[43] Katoh, T.; Nishide, K.; Node, M.; Ogura, H. *Heterocycles* **1999**, *50*, 833-841.

[44] Beggs, J. J.; Meyers, M. B. *J. Chem. Soc. (B)* **1970**, 930-934.

[45] Howlett, K. E. *J. Chem. Soc.* **1955**, 1781-1784.

[46] Bowman, R. E.; Campbell, A.; Tanner, E. M. *J. Chem. Soc.* **1959**, 444-447.

[47] Enders, D.; Eichenauer, H.; Baus, U.; Schubert, H.; Kremer, K. A. M. *Tetrahedron* **1984**, *40*, 1345-1359.

[48] Corey, E. J.; Knapp, S. *Tetrahedron Lett.* **1976**, 4687-4690.

[49] Kimura, E.; Gotoh, T.; Koike, T.; Shiro, M. *J. Am. Chem. Soc.* **1999**, *121*, 1267-1274.

Chapter 3: Synthetic Receptor for Shifting the pK_a of Carbon Acids

3.1 Introduction

The creation of carbon-carbon bonds in natural systems often involves the formation of an enolate intermediate in the active site of an enzyme. One principle of enzymatic enolate formation is clear: at physiological pH (6-8), enolates formed from typical carbon acids (pK_a 11-20) require a reduction in pK_a, achieved by stabilization of developing charge in the transition state. To accomplish this, enzymes utilize charge-pairing, hydrogen bonding, and/ or metal-ion electrostatic interactions. Artificial enolase mimics, employing one or more of these interactions, have been designed to study electrophilic catalysis observed in natural systems. The following examples illustrate synthetic systems which incorporate transition metals for anion binding, a key element in the function of several types of enzymes.

3.2 Transition Metal Complexes for Anion Recognition

Macrocycles that contain three or four amine groups can bind a variety of transition metal ions while leaving vacant binding sites on the metal for anionic

species. Early examples of enzyme models involve the use of cyclodextrins bearing pendant functional groups, such as amine ligands, for metal coordination. β-Cyclodextrins (Figure 3.1) are often used in biomimetic chemistry because these cyclic glucose oligomers form a hydrophobic cavity that is able to encapsulate organic molecules in aqueous systems.[1] β-Cyclodextrin is composed of seven glucose units arranged such that the hydroxyl substituents are oriented away from the center of the ring, leaving a relatively hydrophobic cavity. The hydroxyl groups are not only responsible for the solubility of the macrocycle in aqueous media, but also act as handles, so that functional groups may be appended to the macrocycle. Hence, cyclodextrin is a versatile scaffold for the construction of enzyme mimics.

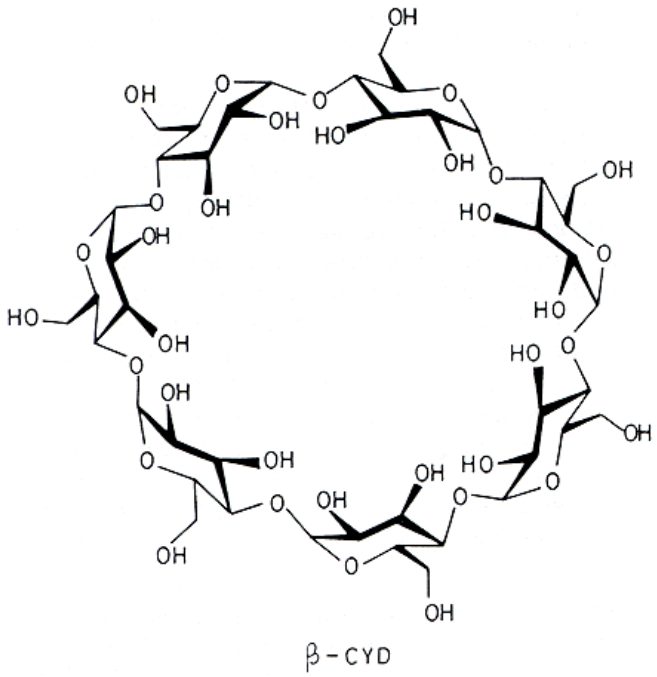

Figure 3.1 Diagram of β-cyclodextrin.

Examples of receptors incorporating metal centers bound to cyclodextrin by polyamine ligands have been described by Tabushi *et al.*[2] to model the cooperative binding found in metalloenzymes. Tabushi *et al.* found that the metallocyclodextrins bind anions more strongly than either the parent or polyamine functionalized cyclodextrin. The binding of adamantan-2-one-1 carboxylate by metallocyclodextrin **3.1** is 330 times greater than the binding of the anion by the parent cyclodextrin (borate buffer, pH 10.0). This large enhancement in substrate binding is attributed to the additive hydrophobic and electrostatic interactions between the guest and the host. Metal-anion coordination within a hydrophobic binding pocket is thought to be fundamental to enzymatic function.

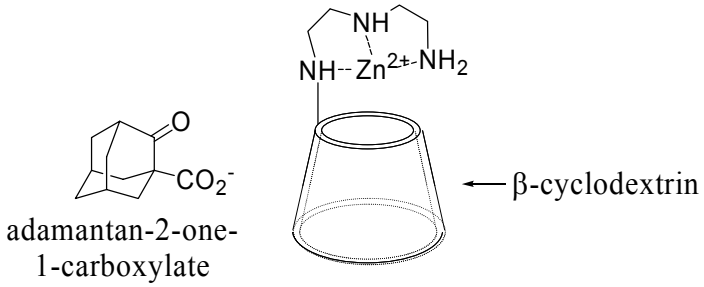

3.1

Figure 3.2 Polyamine Functionalized Cyclodextrin Used to Bind Adamantan-2-one-1-carboxylate.

The first compound referred to as an "artificial enzyme" in the literature was a β-cyclodextrin with a carboxylate ligand for binding copper (II) (Figure 3.3).[3] This complex was found to catalyze the hydrolysis of substrates bound

within the cyclodextrin cavity which were not normally hydrolyzed by copper complexes. When coupled with a nickel oximate ligand, host **3.3** also catalytically hydrolyzed *para*-nitrophenyl acetate.[4] The mechanism of hydrolysis occurs first through the acylation of the oxime oxyanion by the bound *para*-nitrophenyl acetate substrate. Subsequent hydrolysis of the acetate regenerates the catalyst. It was shown that host **3.3** is over four times more reactive toward

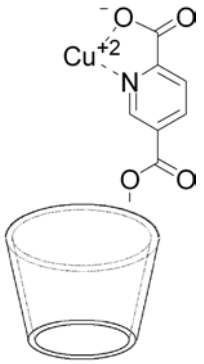

3.2

Figure 3.3 The First Reported Artificial Enzyme.

the hydrolysis of *para*-nitrophenyl acetate than an equivalent amount of the nickel-pyridine carboxaldoxime The observed increase in reactivity is proposed to result from the binding of the substrate within the hydrophobic cavity, thus bringing it into close proximity to the reactive site. This is consistent with the observation that the hydrolysis of *para*-nitrophenyl acetate by **3.3** is inhibited by the addition of cyclohexanol, while the rate of the hydrolysis of the substrate with nickel- pyridine carboxaldoxime is unaffected by the addition of cyclohexanol.

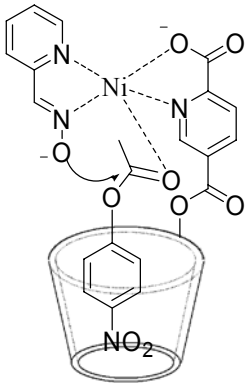

3.3

Figure 3.4 Metallocyclodextrin Host for Catalytic Ester Hydrolysis.

Less complex designs for anion receptors involve the use of polyaza macrocycles for metal coordination.[5] Binding sites that contain three to four amino groups bind a variety of metals while leaving binding sites accessible on the metal ion (Figure 3.5).

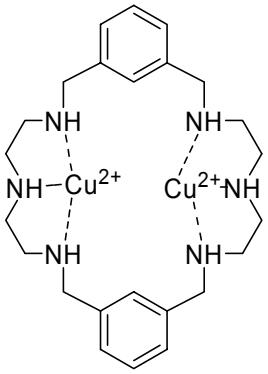

3.4

Figure 3.5 Polyaza Macrocyle Designed for Anion Recognition.

Anion recognition using metal complex **3.4** relies on coordinative bonds. The binding of amino acids was studied with the dinuclear copper (II) species of

macrocycle **3.4**.[5d] Among the amino acids alanine, valine, leucine, norleucine, norvaline and serine, norleucine was found to have the largest affinity for the dinuclear copper (II) complex. Steric effects are thought to contribute to the higher binding of norleucine.

The cooperativity of metal coordination with steric effects has also been investigated in the enantioselective recognition of anions. Kim *et al*.[6] illustrated enantioselective binding of natural amino acids through the use of tetradentate chiral cobalt complex **3.5 b**. As shown in Figure 3.6, the carboxylate of the alanine guest prefers to bind *trans* to the carboxylate of the ligand, as was demonstrated previously for square planar *bis*-glycine complexes of Ni(II), Cu(II) and Zn(II).[7] This preferential binding geometry by the metal center establishes regioselective binding of the amino acid. Stereospecific binding is controlled by the unfavorable steric interaction between the α-proton of alanine and the methyl group of the ligand. The preferential formation of one diastereomeric complex was found with the D-amino acid by X-ray crystallography and ^{1}H NMR, as the model in Figure 3.6 predicts.

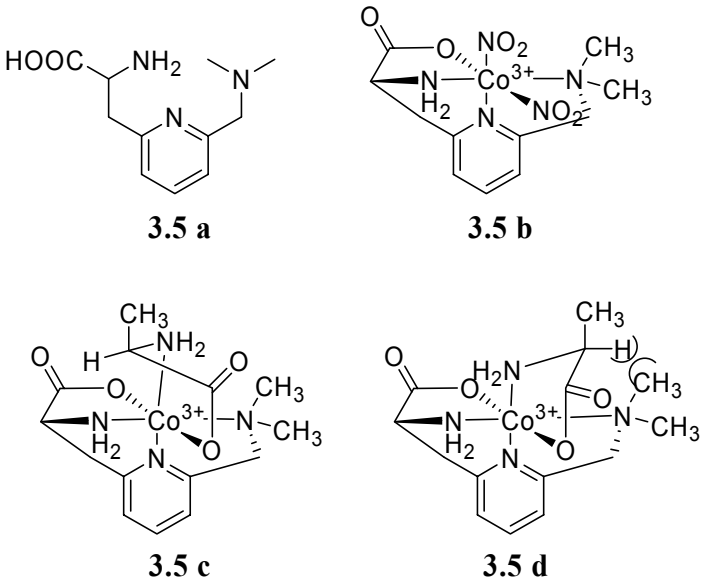

Figure 3.6 Chiral Cobalt(III) Ligand for Enantioselective Amino Acid Recognition.

Cooperativity between metal coordination and hydrogen bonding has also been explored by Kim *et al.* using a cadmium coordinating ligand for the recognition of cytidine in polar, protic solvents (Figure 3.7).[8] The combination of metal coordination and hydrogen bonding results in a substantial increase in the complexation between the receptor and cytidine (K = 117 M^{-1}) when compared to ligand free cadmium, $CdCl_2$ (K = 7.2 M^{-1}) in dimethyl sulfoxide. Free cadmium should be expected to bind cytidine more strongly than in the presence of the ligand because chelation to the ligand reduces the Lewis acidity of the metal. Although not a formal negative charge, the carbonyl of cytidine bears a partial negative charge and the nitrogen bears a partial positive charge. This

complimentary charge-pairing may contribute to the larger association constants in dimethyl sulfoxide compared to the free ligand.

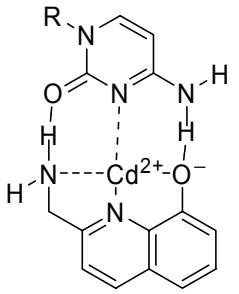

3.6

Figure 3.7 Artificial Receptor for Binding Cytidine Through the Cooperative Interaction of Metal Coordination and Hydrogen Bonding.

An advantage of polyaza macrocycles as enzyme mimics is manifest in an example from Albelda *et al.*[9] in which a polyaza[*n*]paracyclophane-zinc complex promotes proton exchange of acetonitrile. In a ^{1}H NMR experiment designed to study the different protonation states of polyaza[*n*]paracyclophane-zinc complex **3.7**, it was fortuitously discovered that the zinc complex facilitates deuterium-proton exchange of the solvent, acetonitrile-d_3. The mechanism of proton exchange relies on two factors; first, the activation of acetonitrile through coordination with zinc and secondly, proton abstraction by the proximal noncoordinated nitrogen atom, as illustrated in Figure 3.8

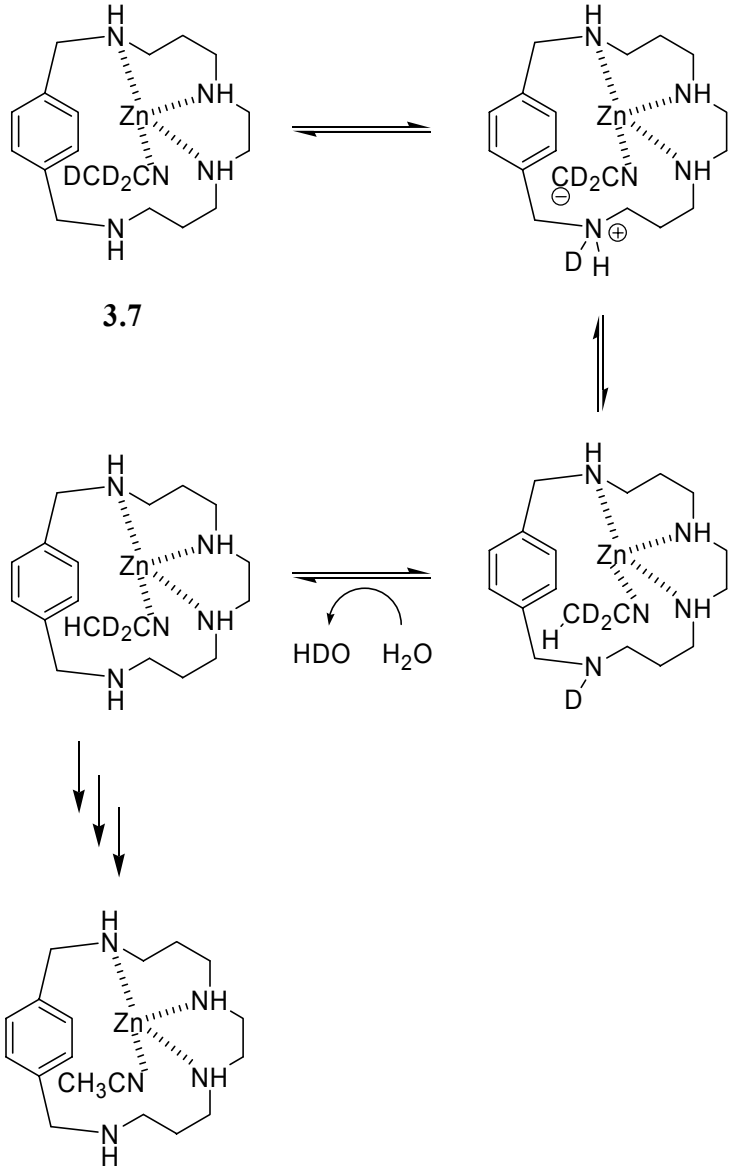

Figure 3.8 Proposed Mechanism for H-D Exchange in Acetonitrile Catalyzed by Polyaza[*n*]paracyclophane **3.7**.

Complex **3.7** may be considered an artificial enzyme, consisting of a metal with vacant coordination sites and an amine which provides nucleophilic assistance for proton abstraction through general acid-base catalysis.

Zinc complexes of multidentate nitrogen ligands have been utilized to catalyze aldol reactions through substrate activation. Darbre *et al.* found that zinc complexes of polyaza ligands **3.8 a** and **3.8 b** catalyzed the aldol condensation between benzaldehyde and 2-hydroxyacetophenone.[10]

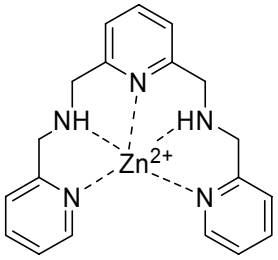

3.8 a

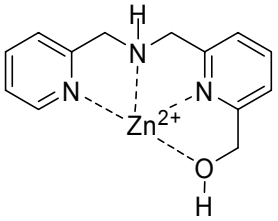

3.8 b

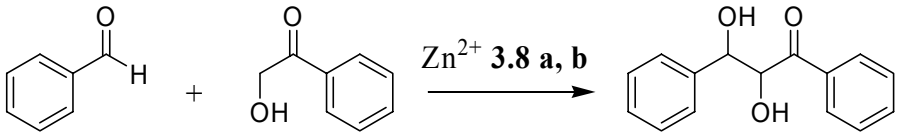

benzaldehyde 2-hydroxyacetophenone

Figure 3.9 Zinc Complexes of Mulitdentate Nitrogen Ligands for Catalysis of Aldol Reactions.

Yields of approximately 20% to 60% were obtained for the aldol condensations in the presence of the zinc complex of the ligands, whereas no reaction was observed in the presence of the ligands alone. Although lacking the hydrophobic binding

ability of the cyclodextrin complexes, these hosts offer an advantage in the simplicity of their design. Although no mechanism was proposed for the observed catalysis, it may be assumed that these ligands activate the α-proton of 2-hydroxyacetophenone towards deprotonation in the presence of relatively weak bases, mimicking the function of certain enzymes, such as class II aldolases.

3.3 ARTIFICIAL RECEPTORS USED IN pK_A SHIFT STUDIES

The catalytic function of enzymes relies on the preferential stabilization of a transition state compared to a substrate. Preferential stabilization of an enolate intermediate results in the depression of the pK_a of a carbon acid substrate. Several enzymatic studies have focused on determining the mechanism through which enolate stabilization is achieved in enolases[11], racemases[12] and aldolases[13]. These enzymes share a common feature: the use of a transition metal ion in the active site to stabilize negative charge on the transition state during substrate deprotonation.

It was proposed that the stabilization of the intermediates by zinc in the previously described receptors **3.7**, **3.8 a** and **3.8 b** is related to the stabilization of an enolate intermediate by class II aldolases. Reversible aldol condensations are catalyzed in the active site of class II aldolases, which contains a zinc atom ligated by the imidazole groups of three histidines.[14] In these enzymes, zinc functions as a Lewis acid, activating methylene groups α to a carbonyl towards

deprotonation by withdrawing negative charge from the carbonyl oxygen in the transition state. As illustrated in Figure 3.10, aldol condensation of dihydroxyacetone phosphate (DHAP) and D-glyceraldehyde 3-phosphate (G3P) to form D-fructose 1,6-bis(phosphate) occurs in the active site of fructose 1,6-bis(phosphate) aldolase (FBP-aldolase), containing a zinc ion.

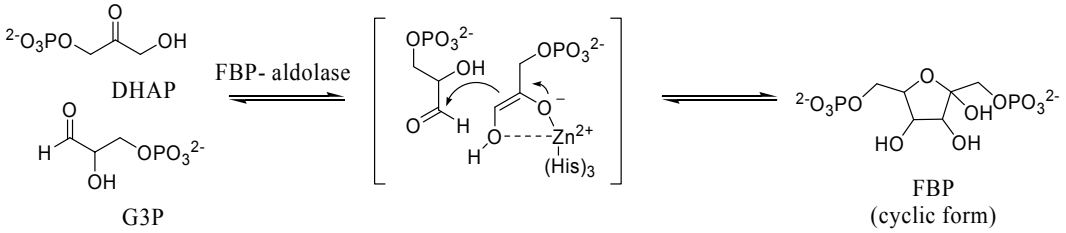

Figure 3.10 Reversible Aldol Condensation of DHAP and G3P by FBP-aldolase.

Another class II aldolase, fuculose 1-phosphate aldolase (FucA) catalyzes a similar aldol condensation between L-lactaldehyde and dihydroxyacetone phosphate.[15] The mechanism of FucA for the reversible aldol condensation of dihydroxyacetone (DHAP) and L-lactaldehyde to form L-fuculose 1-phosphate (Fuc1P) (Figure 3.11) was elucidated by the crystal structure of FucA ligated with

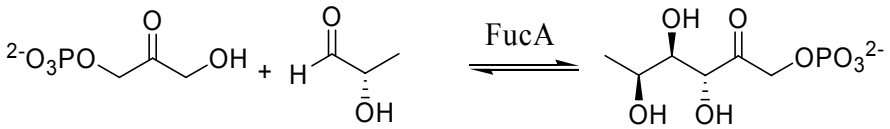

Figure 3.11 Reversible Aldol Condensation of DHAP and L-lactaldehyde Catalyzed by L-Fuculose 1-phosphate Aldolase.

inhibitor phosphoglycolohydroxamate (PGH). It is proposed that Glu73 deprotonates DHAP, producing an enediolate stabilized by complexation with zinc. Complexation with zinc reduces the pK_a of the methylene hydrogen, thus allowing the relatively weak base, Glu73, to form this intermediate. Formation of the product is completed by nucleophilic attack of the aldehyde by the enediolate intermediate, followed by protonation (Figure 3.12).

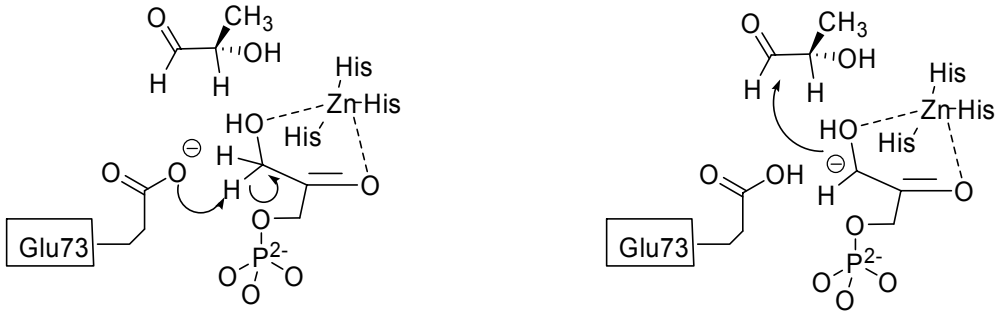

Figure 3.12 a) Deprotonation by Glu73 and Stabilization of the Enediolate Intermediate by Zinc in FucA and b) Aldol Condensation Between the Enediolate of DHAP and L-lactaldehyde.

Based on the study of several mutants of the enzyme, it was determined that the general acid for protonation of the substrate after carbon-carbon bond formation is Glu73. Thus, Glu73 acts as a general base and a general acid during catalysis.

Kimura *et al.* proposed a model system for class II aldolases to study how much the acidity of the hydrogen adjacent to the carbonyl of the substrate may be increased through the coordination of the zinc(II) center to the carbonyl in the intermediate.[16] The model system specifically sought to determine how the

formation of the enediolate by a relatively weak base (glutamic carboxylate) at physiological pH is possible in the enzyme active site. The model system, 4-bromophenacyl-pendant zinc cyclen (**3.9**), is illustrated in Figure 3.13.

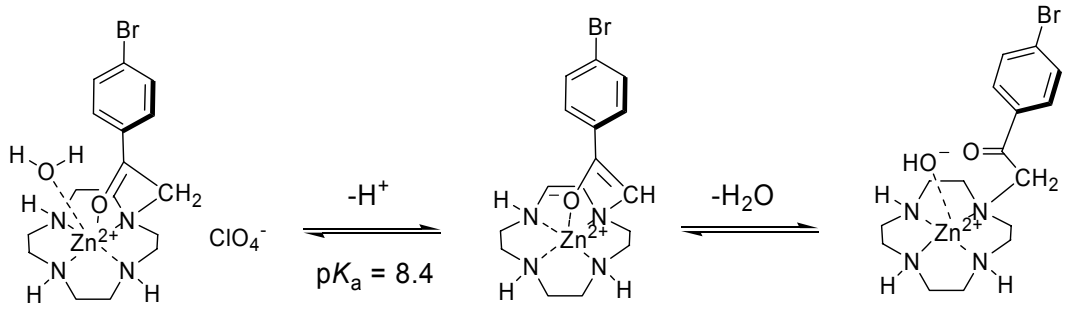

3.9 **3.9a** **3.9b**

Figure 3.13 Class II Aldolase Mimic, 4-Bromophenacyl-pendant Zinc Cyclen.

The α-methylene hydrogen of complex **3.9** was found to have a pK_a of 8.41, almost 10 units lower than the bromoacetophenone methyl group (pK_a = 19). Activation of the α-methylene hydrogen is also supported by rapid exchange with deuterium , k_{obs} = 2.8 x 10^{-2} min^{-1} (10% (v/v) CD_3CN / D_2O, pD 7.0 MOPS buffer (20 mM)), in comparison to proton exchange by the diprotonated cyclen without the Zn^{2+} ion, which is approximately 100 times slower. Two complexes were identified in the potentiometric titration of the carbonyl-bound Zn^{2+} complex. The first, **3.9 b**, is thought to be important in catalyzing the reverse aldol reaction, as the zinc-bound hydroxide acts as the base to neutralize the alcohol, fructose 1,6-bis(phosphate). Second, the enolate-bound zinc complex was isolated from acetonitrile (**3.9 a**) and characterized, providing evidence for the role of zinc in

the mechanism through which enolates may be formed at physiological pH in enzymatic systems.

Examples of enzyme mimics that do not contain transition metals have also been reported. Anslyn *et al.* have studied how hydrogen bond formation may contribute to a reduction of the pK_a of certain carbon acids. Two possible hydrogen bond orientations were postulated to be responsible for stabilization of the developing charge on an enolate in an enzyme active site. The first reported example utilizes a polyazacleft (**3.10**) capable of forming hydrogen bonds directed toward the oxygen lone pairs of carbon acids (Figure 3.14).[17] The premise of this model study was supported by the stabilization of anionic intermediates by amide hydrogen bonds in chymotrypsin.[18]

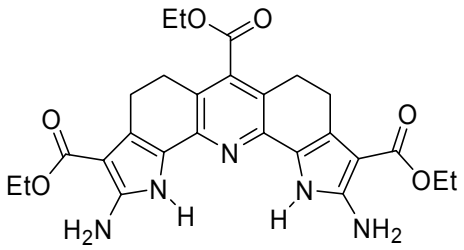

3.10

Figure 3.14 Polyazacleft Designed to Study the Effect of Hydrogen Bonding on Anion Stabilization.

Also, the acyl-CoA dehydrogenase class of enzymes is proposed to activate carbon acids for proton removal through hydrogen bonding, as the active site is free of any transition metals.[19] A series of carbon acids were studied for binding to receptor **3.10** and 1,3-cyclohexanedione was found to have the largest

association constant with the receptor (1.35 x 10^4 M^{-1} in acetonitrile) as determined by ^{1}H NMR. Even though two pairs of hydrogen bonds are proposed in the binding mode of 1,3-cyclohexanedione and receptor **3.10**, the observed pK_a shift of the substrate was only one pK_a unit.

Anslyn *et al.* designed a second generation receptor (**3.11**), capable of forming hydrogen bonds to the π-system of an enolate (Figure 3.15) rather than to the oxygen lone pairs, as shown in the previous example.[20]

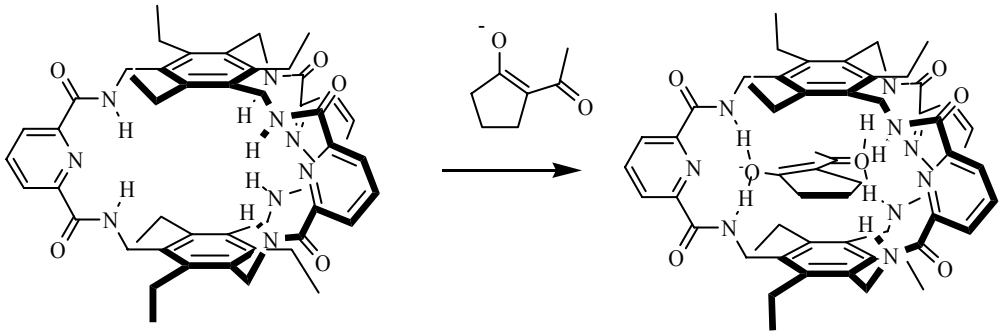

3.11

Figure 3.15 Proposed Binding of the Enolate of 2-Acetylcyclopentanone and a Bicyclic Cyclophane Receptor (**3.11**).

It was proposed that receptor **3.11** would be more effective in stabilizing an enolate (and consequently, produce a larger pK_a depression in the carbon acid) because negative charge delocalization occurs mainly in the π-system of an enolate. This proposal is supported by a crystal structure of the enzyme 4-chlorobenzoyl-CoA dehalogenase, an enzyme which catalyzes nucleophilic aromatic substitution of an aryl halogen through a Meisenheimer intermediate (Figure 3.16).

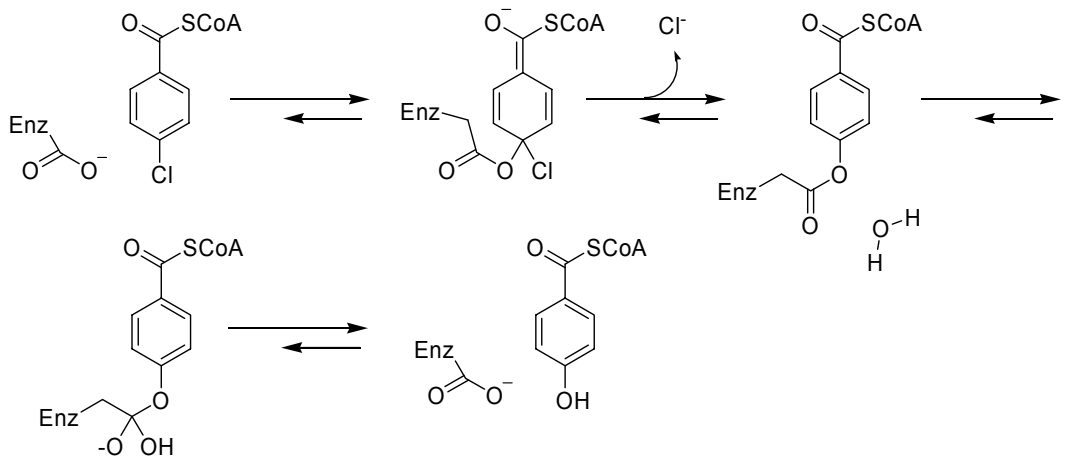

Figure 3.16 Mechanism of 4-Chlorobenzoyl-CoA-dehalogenase *via* a Meisenheimer Intermediate Stabilized by Amide Hydrogen Bonding in the Active Site.

The active site contains a pair of amide hydrogen bonds from Phe 64 and Gly 114 oriented toward the π-system of the intermediate.[21] Additionally, this proposal is supported by molecular modeling of the complex formed between receptor **3.11** and the enolate of 2-acetylcyclopentanone. As illustrated in Figure 3.15, the confined space of the cyclophane (7.0 Å) forces the enolate to lie parallel between the aromatic rings, placing the amide hydrogen bonds perpendicular to the enolate π-system. A reduction of the pK_a of 2.9 pK_a units of 2-acetylcyclopentanone was found by spectrophotometric titration of 2-acetylcyclopentanone in the presence of receptor **3.11**. This finding exhibits a significant increase in anion stabilization over receptor **3.10**, which stabilizes the developing charge of an enolate through forming hydrogen bonds to the lone pair electrons. It may be concluded from these studies that hydrogen bond geometry plays a significant role in enolate

stabilization by synthetic systems and this may also be the case within enzyme active sites.

3.4 Design and Evaluation of a Cyclophane for Shifting the pK_A of Active Methylene Compounds

The previous examples illustrate synthetic systems that show promise for anion stabilization and inducing pK_a shifts of carbon acids through the use of transition metal coordination and hydrogen bonding. For a third generation anion receptor designed to reduce the pK_a of carbon acids, we propose a bicyclic host that may bind an anionic guest through charge-pairing with two bound divalent metal centers and hydrogen bonding, with the two binding interactions behaving cooperatively to induce large pK_a shifts. Host **3.12** is proposed to encapsulate an active methylene enolate inside the cavity and potentially bind to the guest though hydrogen bonding to the enolate π-system and through electrostatic interactions with bound metal ions. Our host design **3.12** is modeled from C_3-symmetric bicyclic cyclophane **3.11**. Host **3.11** is an appealing design template because a direct comparison of the pK_a shift obtained with 2-acetylcyclopentanone and **3.11** can be compared with results obtained from **3.12**, as the basic designs are structurally very similar. Therefore, two of the diamido pyridine moieties of host **3.11** were replaced by aminomethyl pyridine groups in host **3.12**. Aminomethyl pyridine groups are known to bind metal ions, such as copper(I), copper(II) and zinc(II).[22] Copper(II) is proposed for use in our host design because if it adopts a

trigonal bipyramidal geometry inside host **3.12**, an enolate will be bound in the equatorial position on the metal and, therefore, lie parallel to the host aromatic rings.

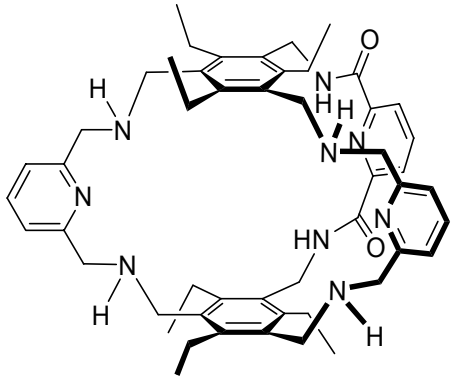

3.12

Although receptor **3.11** was previously shown to form hydrogen bonds directed toward the π-system of anionic guests (Section 3.3 and additional references[23]), it is likely that our proposed host will not achieve simultaneous hydrogen bonding and metal-ion coordination with an active methylene enolate because of the relatively weak strength of hydrogen bonds compared to strong electrostatic interactions of the metal ions and steric crowding inside the cavity. However, the acetyl portion of 2-acetylcyclopentanone may fit inside the cavity, and because of the electrophilic environment of the interior of the cavity, stabilization of the enolate may be achieved with the negative charge residing on only one carbonyl moiety. Primarily, the intention of this design is to demonstrate the effect of electrostatic interactions in stabilizing enolate anions, thereby effecting a reduction in pK_a, as observed in enzymatic reactions.

Our receptor (**3.12**) is designed to bind two metal ions, either copper or zinc, through the use of two amine bonds and the lone pair of pyridine. The

aromatic rings of receptor **3.12** are proposed to provide a rigid binding site for an enolate guest in which the guest is parallel to both rings. If the enolate fits inside **3.12**, this arrangement will position the active methylene enolate guest such that the other enolate oxygen may participate in binding with the other metal or the hydrogen bond donating amides.

3.2.1 Synthesis

The synthesis of compound **3.12** is accomplished by joining two hexasubstituted benzene rings, 1,3,5-tris(aminomethyl)-2,4,6-triethylbenzene (**3.15**) with 2,6-pyridine dicarbonyl dichloride (Figure 3.17). A hexasubstituted benzene ring is used to arrange the functional groups on the 1, 3 and 5 positions to one face of the benzene ring.[24] Compound **3.13** is synthesized from 1,3,5-triethylbenzene using chloromethyl methyl ether and tin tetrachloride.[25] Reaction with sodium azide yields 1,3,5-tris(azidomethyl)-2,4,6-triethylbenzene (**3.14**). Staudinger reduction of **3.14** yields **3.15**.[26] Prior to the coupling reaction, the primary amines on **3.15** were protected with di-*tert*-butyldicarbonate (1.5 equivalents) and **3.16** isolated by column chromatography. Two equivalents of **3.16** were coupled by reaction with 2,6-pyridine dicarbonyl dichloride. Removal of the Boc protecting groups with trifluoroacetic acid followed by ion exchange chromatography yields cleft **3.17**. The synthesis of macrocycle (**3.12**) is completed by nucleophilic substitution of the primary amines of the cleft to two

equivalents of 2,6-pyridine dicarboxaldehyde followed by reductive amination in which the imine groups are converted to secondary amines. The reaction is carried out in toluene at high dilution. The use of toluene as the reaction solvent is attributed to the usually high yield (approximately 75%) obtained from the cyclization reaction.

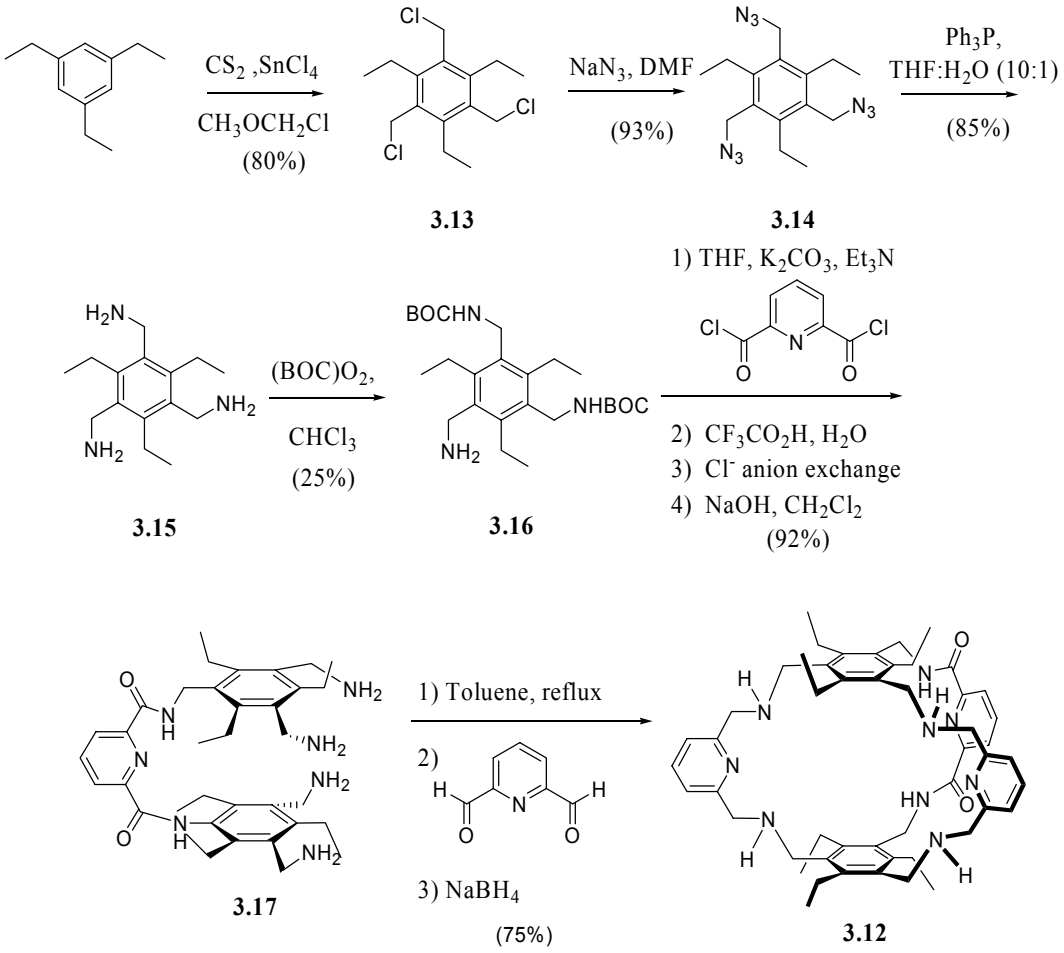

Figure 3.17 Synthesis of Receptor **3.12**.

3.4.2 Spectrophotometric Binding Studies

3.4.2.1 Metal-Host Binding

To initiate our study with host **3.12**, it was necessary to determine the binding stoichiometry between the host and metal ions. Several attempts were made, utilizing various metal ions, including silver(I) and copper(I), to determine a binding stoichiometry. Attempts at crystallization using silver(I) from *N*,*N*'-dimethyl formamide were not successful. ^{1}H NMR binding studies with copper(I) gave inconclusive results, however suggested 1:2 host-metal binding.

Copper (II) chloride has been used in similar macrocyclic receptors and the binding stoichiometry determined by spectroscopic methods. For example, copper(II), when bound to a pyridine-2,6-imine ligand (Figure 3.18), has an

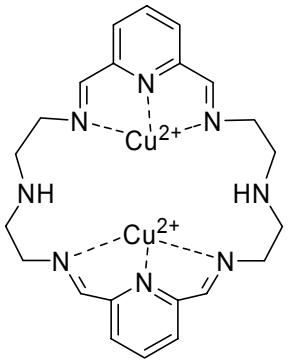

Figure 3.18 Dinuclear Copper(II) Complex Utilizing Pyridine-2,6-imine Ligands.

absorbance in the visible region at approximately 620 nm indicative of copper(II) in a trigonal bipyramidal environment.[22] Optical absorption spectroscopy, particularly UV, is a convenient method to study binding[27] in our system because neither the free host **3.12** or the copper(II) chloride titrant absorbs in the visible region. Therefore, the binding stoichiometry of host **3.12** with copper(II) chloride was determined by following the absorbance increase at approximately 600 nm *via* spectrophotometric titration. The first titrations were carried out in water and methanol (3:1) with 0.18 M Trizma buffer (tris[hydroxymethyl]aminomethane hydrochloride) and 5.0 mM **3.12** as the titrand and 5.0 mM **3.12** with 50.2 mM $CuCl_2$ titrant in water and methanol (3:1) with 0.18 M Trizma buffer. Maintaining a constant pH during spectrophotometric titrations is important because the change in the absorbance should not mistakenly be attributed to a change in the protonation state of the host. However, the copper(II) chloride was found to bind to both the receptor **3.12** and the buffer (Figure 3.19, a). A blank titration with Trizma buffer and copper(II) chloride was obtained (Figure 3.19, b) and the difference plotted against the ratio of $CuCl_2$ and **3.12** (Figure 3.20). Figure 3.20 reveals a 1:2 host-guest binding curve.

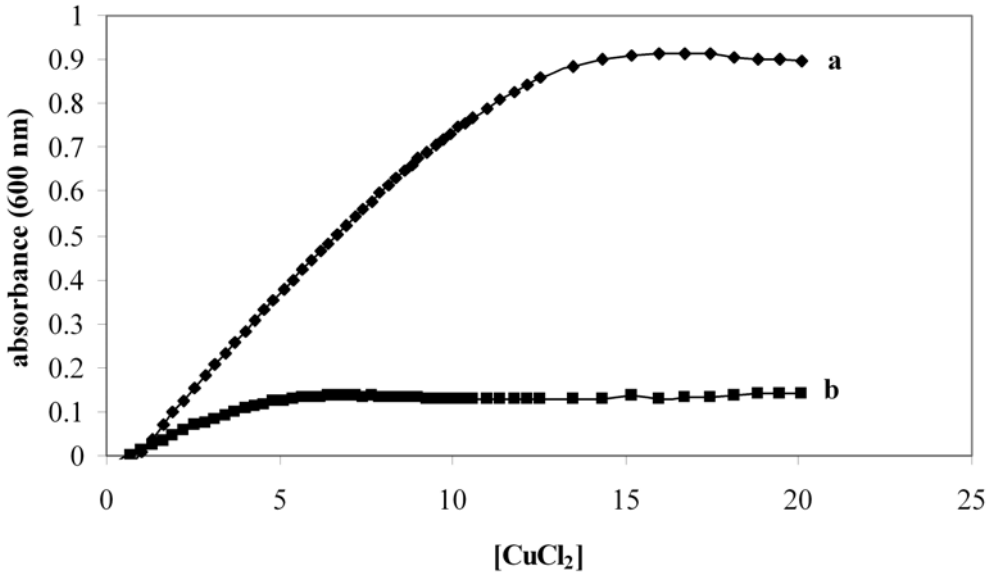

Figure 3.19 Titration of a) **3.12** (5.0 mM) with $CuCl_2$ in Methanol:H_2O (3:1) with 0.18 M Trizma Buffer and b) $CuCl_2$ in Methanol:H_2O (3:1) with 0.18 M Trizma Buffer.

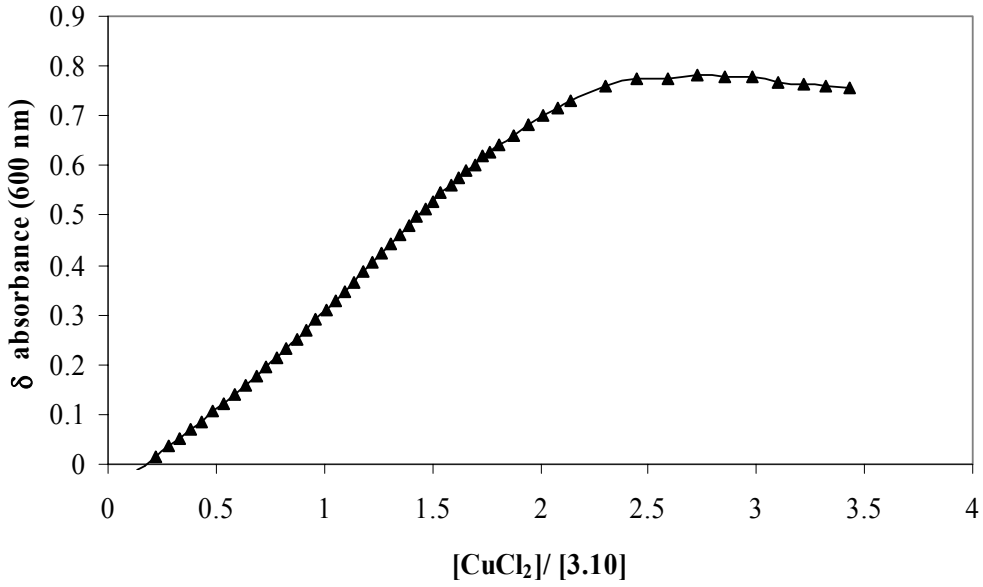

Figure 3.20 Corrected Binding Curve for Receptor **3.12** and $CuCl_2$ in Trizma Buffer.

The binding curve in Figure 3.20 shows weak binding between **3.12** and $CuCl_2$. In order to increase the slope for the binding curve such that a sharp break is obtained at two equivalents of copper(II) to one equivalent of **3.12**, the concentration of the receptor **3.12** should be increased. However, the absorbance of the titration at 5.0 mM **3.12** approaches an absorbance of unity. Therefore, the titration was repeated under different conditions using HEPES ([4-(2-hydroxyethyl)-1-piperazine ethane sulfonic acid)]) buffer to maintain a constant pH instead of Trizma. Titration of a concentrated solution of copper(II) chloride in water (0.22 M) into a host solution (2.22 mM in 16.3 mM HEPES, 1:1

methanol:H_2O) resulted in a binding curve with a 1:2 binding stoichiometry for the host and copper(II) chloride (Figure 3.21).

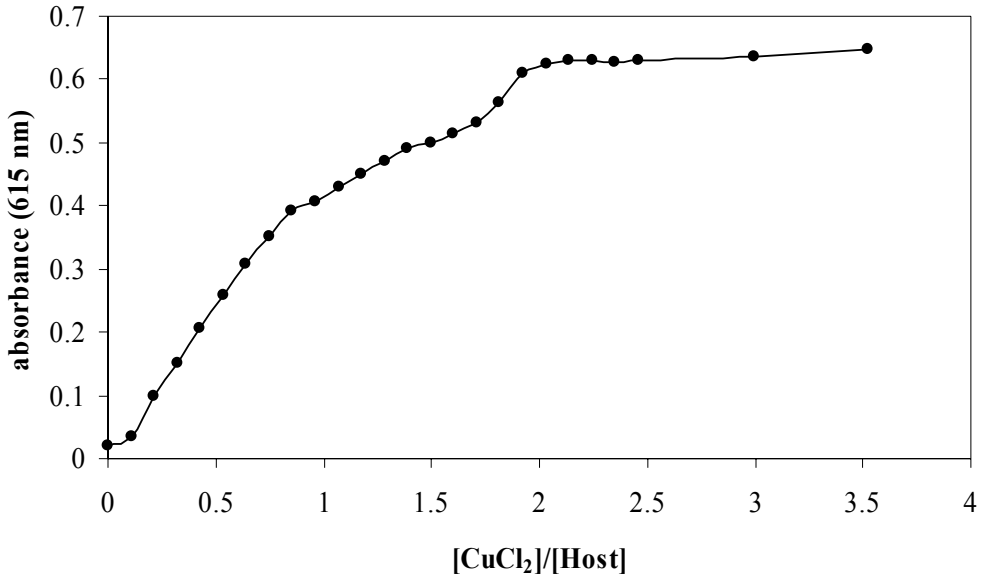

Figure 3.21 Titration Curve for Receptor **3.12** and $CuCl_2$ in 16.3 mM HEPES Buffer.

The titration curve in Figure 3.21 also shows a change in the slope after one equivalent of $CuCl_2$ had been added to the receptor. This indicates that the binding of one ion of copper(II) chloride is relatively facile and the second ion binds less readily. After obtaining the anticipated binding stoichiometry of two copper(II) ions to one host, the molar ratio of host to copper(II) obtained from the titration shown in Figure 3.21 was used in enolate binding studies to ensure that

two copper(II) ions are bound to the host throughout the titration of the anionic guests.

3.4.2.2 Enolate Binding Studies

Enolates of active methyene compounds (**3.18**-**3.20**) were selected for binding studies in order to compare the results of pK_a shift experiments obtained with host **3.12** with results obtained using receptor **3.11**. The sodium-[2.2.1]cryptand was selected as the counterion over the 15-crown-5 ether used in previous experiments because it is known to saturate the coordination sites on the sodium ion, leaving the "free" enolate.[28] Hence, stronger host-guest binding is expected with this counterion.

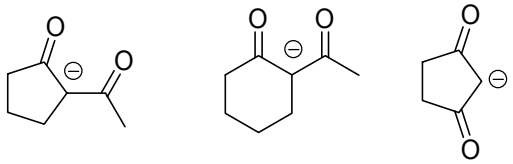

3.18 **3.19** **3.20**

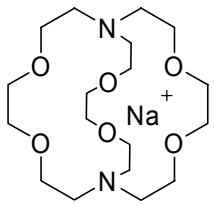

sodium-[2.2.1] cryptand counterion

^{1}H-NMR titrations were used with receptor **3.11** to determine binding stoichiometry and binding constants for a variety of enolate guests by following the downfield shift of the amide *NH* resonances.[20] However, the use of copper(II) precludes the use of ^{1}H NMR for determining the binding of $(Cu_2$:**3.12**$)^{4+}$and enolate guests, as copper(II) is paramagnetic. Therefore, UV spectroscopic titrations were employed to study the binding mode of enolates **3.18**-**3.20** with $(Cu_2$:**3.12**$)^{4+}$. Attempts to perform aqueous titrations of **3.18**-[2.2.1]cryptand enolate in HEPES and Trizma buffers were unsuccessful, as no change was observed in the absorbance spectra of $(Cu_2$:**3.12**$)^{4+}$ during the titrations. The preferential solvation of the enolate in water presumably prevents binding to the host complex. Although an aqueous medium is optimal for the titrations, acetonitrile is also an acceptable solvent because its dielectric constant (37.5) is proposed to mimic the interior of an enzyme the active site.[17] Additionally, a direct comparison may be made between the results of pK_a shift experiments with receptors **3.10** and **3.11**, also preformed in acetonitrile. A two to one binding stoichiometry was found from a decrease in absorbance of receptor $(Cu_2$:**3.12**$)^{4+}$ (2.33 mM) at 460 nm upon titration of **3.18**-[2.2.1]cryptand (0.24 M) in acetonitrile, as shown in Figure 3.22.

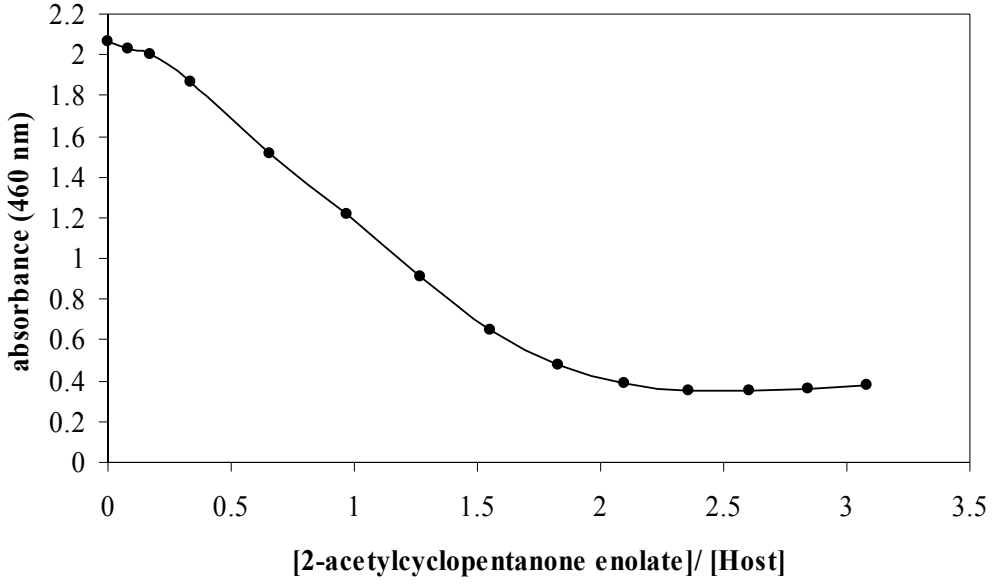

Figure 3.22 Titration Curve for Receptor $(Cu_2$:**3.12**$)^{4+}$ (2.33 mM) and **3.18**-[2.2.1]cryptand in Acetonitrile.

Titration of a solution of the sodium [2.2.1]cryptand enolate of 2-acetylcyclohexanone (**3.19**) (27 mM in acetonitrile) to $(Cu_2$:**3.12**$)^{4+}$ produced a similar binding curve, showing two to one enolate binding with the receptor (Figure 3.23). The binding stoichiometry indeed points to coordination of the enolates to the copper(II) ions outside of the host, as anticipated.

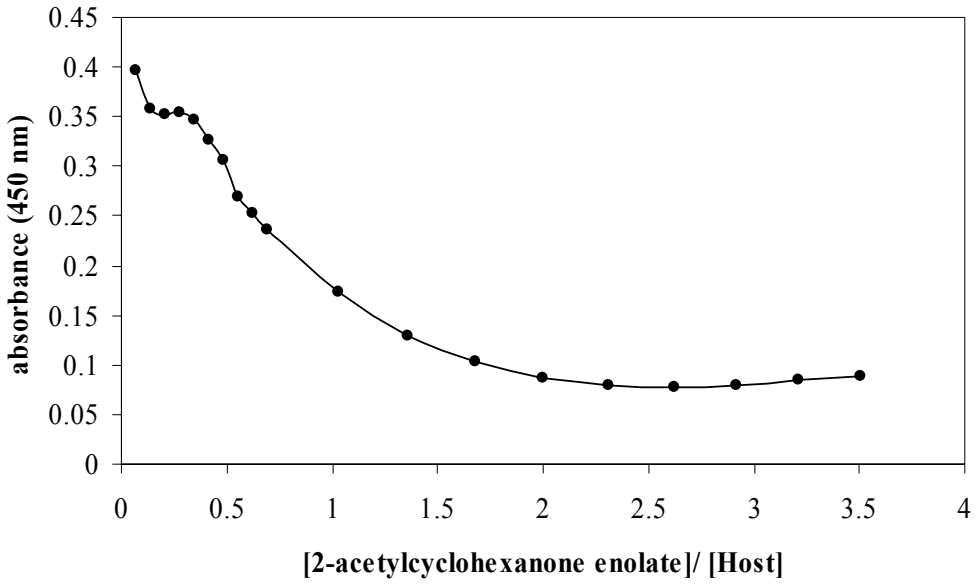

Figure 3.23 Titration Curve for Receptor $(Cu_2$:**3.10**$)^{4+}$ (0.76 mM) and **3.19**-[2.2.1] cryptand in Acetonitrile.

The fluxional conformation of enolates **3.18** and **3.19** was thought to contribute to the observed two to one binding in that both oxygens of each enolate are able to coordinate to a copper(II) ion by assuming the *Z*,*Z* conformation. However, the titration of the conformationally restricted sodium [2.2.1]cryptand enolate of 1,3 cyclopentane dione (**3.20**) also resulted in a two to one binding stoichiometry (Figure 3.24).

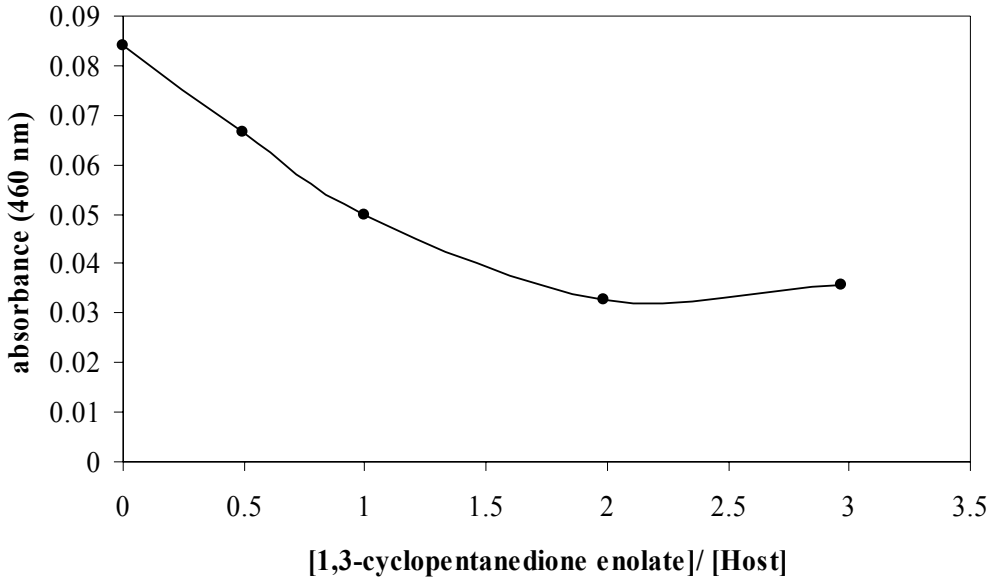

Figure 3.24 Titration Curve for Receptor (Cu_2:**3.12**)$^{4+}$ (0.07 mM) and **3.20**-[2.2.1] cryptand in Acetonitrile.

3.4.2.3 Deprotonation Studies

A key step in enzyme catalysis is the deprotonation of carbon acid substrates using peptide bases with much lower conjugate acid pK_as than the substrate. It was shown in experiments with receptors **3.10** and **3.11** that bases with lower conjugate acid pK_a values than active methylene compounds 1,3-cyclohexanedione and 2-acetylcyclopentanone, respectively, could be used to deprotonate the carbon acids in the presence of the receptors and induce complex

formation. For hosts **3.10** and **3.11**, the complexation of the enolate and receptor was followed by ^{1}H NMR shifts of the amide *NH* protons of the hosts. UV spectroscopy was used with receptor $(Cu_2$:**3.12**$)^{4+}$ to determine the extent of deprotonation of 2-acetylcyclopentanone in the presence of systematically selected bases.

The strategy for selective deprotonation of the parent active methylene compound in the presence of the receptor is to optimize the base such that the pK_a of the conjugate acid of the base is lower than the carbon acid, but close to the pK_a of the carbon acid-receptor complex. The aqueous pK_a of the conjugate acid fo 5-fluoro-2-nitrophenoxide is 6.07, lower than the aqueous pK_a of 2-acetylcyclopentanone (7.8), but close enough to the assumed pK_a of the host-guest complex to allow deprotonation.‡ The titration of 5-fluoro-2-nitrophenoxide-[2.2.1]cryptand (48 mM, 1.02 mM $(Cu_2$:**3.12**$)^{4+}$, 2.02 mM 2-acetylcyclopentanone in acetonitrile) into a solution of $(Cu_2$:**3.12**$)^{4+}$ (1.02 mM) and 2-acetylcyclopentanone (2.02 mM) initially resulted in a decrease in the absorbance of the host complex at 460 nm (Figure 3.25), as previously observed in the titration of the enolate of 2-acetylcyclopentanone into $(Cu_2$:**3.12**$)^{4+}$.

‡ The selective deprotonation of 2-acetylcyclopentanone in the presence of receptor **3.11** was accomplished with 2,4,6-trichlorophenoxide (pK_a of the conjugate acid is 21.2 in acetonitrile). The aqueous pK_a of the conjugate acid of 2,4,6-trichlorophenoxide is 6.23, therefore the pK_a of the conjugate acid of 5-fluoro-2-nitrophenoxide in acetonitrile should be close to 21.2.

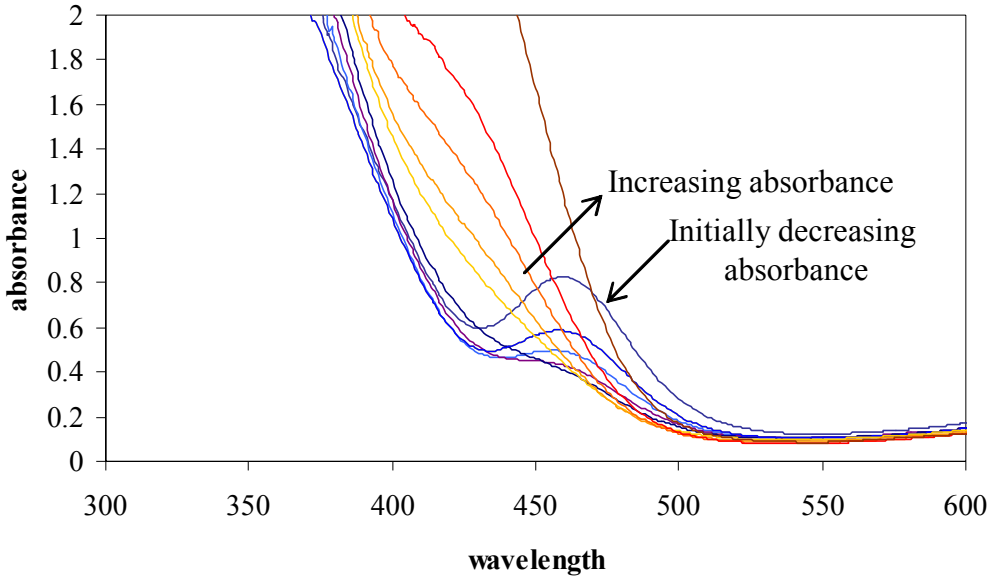

Figure 3.25 Absorbance Spectra of $(Cu_2$:**3.12**$)^{4+}$ in the Presence of 2-Acetylcyclopentanone with Increasing Concentration of 5-Fluoro-2-nitrophenoxide-[2.2.1]cryptand.

However, as the titration progressed, the absorbance of the phenoxide base (Figure 3.26) began to grow in (Figure 3.25). A comparison with the absorbance spectrum of the phenol (Figure 3.27) shows no overlap at 460 nm with the host complex. The titration suggests that initially, the phenoxide deprotonates 2-acetylcyclopentanone and the resulting enolate binds to the receptor. As the concentration of the phenoxide increases and the enolate is no longer deprotonated, an overlap in the spectra is observed.

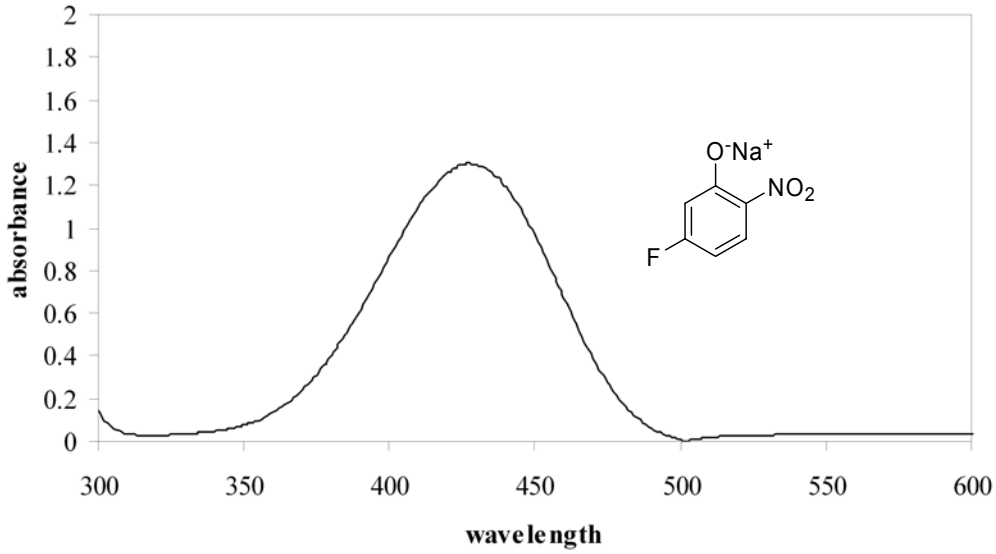

Figure 3.26 Absorbance Spectrum of 5-Fluoro-2-nitrophenoxide-[2.2.1]cryptand (0.19 mM) in Acetonitrile.

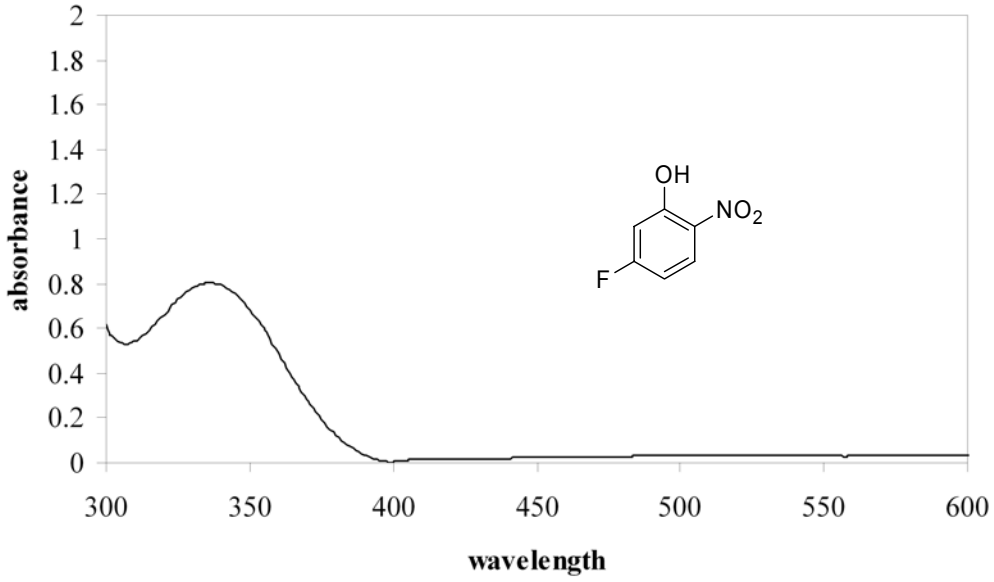

Figure 3.27 Absorbance Spectrum of 5-Fluoro-2-nitrophenoxide-[2.2.1]cryptand (0.22 mM) in Acetonitrile.

As a result of the overlapping absorbance of the phenoxide with the host complex at 460 nm, the use of phenoxide bases was abandoned. Sterically hindered amine bases, whose conjugate acid pK_as in acetonitrile have been previously reported, were used instead. Table 3.1 lists amine bases used in the titrations with their conjugate acid pK_as in acetonitrile.

Amine Base	Number	pK_a *
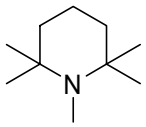	**3.21**	18.2[a]
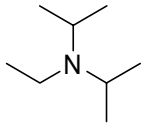	**3.22**	18.1[a]
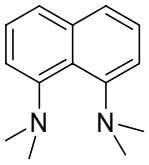	**3.23**	17.8[a]
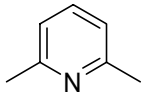	**3.24**	14.2[b]
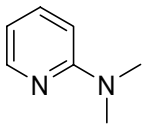	**3.25**	13.4[a]

* pK_a of the conjugate acid in acetonitrile

Table 3. 1 List of Amine Bases used to Deprotonate 2-Acetycyclopentanone in the Presence of Host Complex (Cu_2:**3.12**)$^{4+}$ and Conjugate Acid pK_as in Acetonitrile, a[17] and b.[29]

The pK_a of the conjugate acid of 5-fluoro-2-nitrophenoxide in acetonitrile may be estimated at approximately 21 using the known aqueous conjugate acid pK_a value (6.07)[30] and the conjugate acid pK_a values of 2,4,6-trichlorophenoxide in acetonitrile (21.2) and water (6.23). Amine bases, *N*,*N*-diisopropylethylamine (**3.22**) and 1,2,2,6,6-pentamethylpiperidine (**3.21**) were selected for spectrophotometric titration of the host complex in the presence of 2-acetylcyclopentanone because their conjugate acid pK_as are approximately 18 (Table 3.1). Figures 3.28 and 3.29 illustrate a decrease in absorbance (λ_{max} 460 nm) with increasing concentration of base, similar to the decrease obtained in the titration of the enolate of 2-acetylcyclopentanone (Figure 3.22). At one equivalent of base, the enolate is completely deprotonated and complexed with the host for both **3.22** (Figure 3.32, ■)and **3.21** (Figure 3.32, ◊) Titration of the host complex with 2-(dimethylamino) pyridine (**3.25**) shows a very small decrease in the absorbance at 460 nm (Figure 3.30) and little $(Cu_2$:**3.12**$)^{4+}$-enolate complex formation (Figure 3.32, ▲). However, titration of the host complex and 2-acetylcyclopentanone with 2,6-lutidine (**3.24**) indicates an intermediate decrease in absorbance (Figure 3.31) such that with 3 equivalents of base, the enolate is 45 % deprotonated (Figure 3.32, ●).

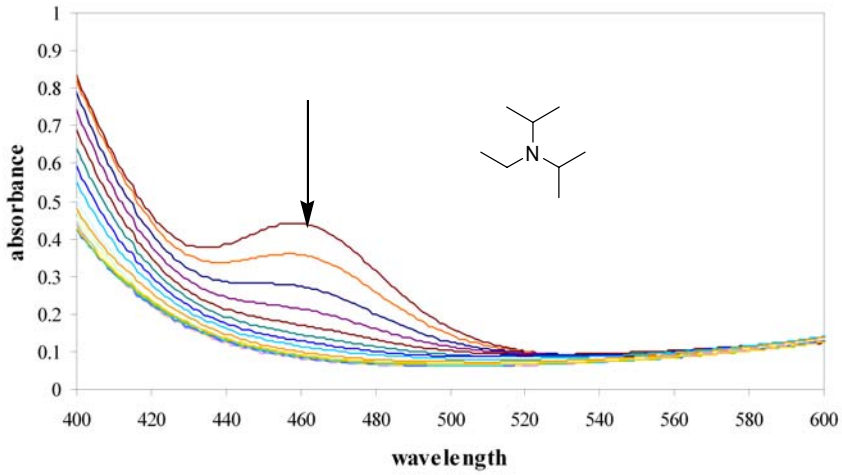

Figure 3.28 Decrease in the Absorbance of $(Cu_2$:**3.12**$)^{4+}$ with 2-Acetylcyclopentanone (2.1 eq.) upon Titration of **3.22**.

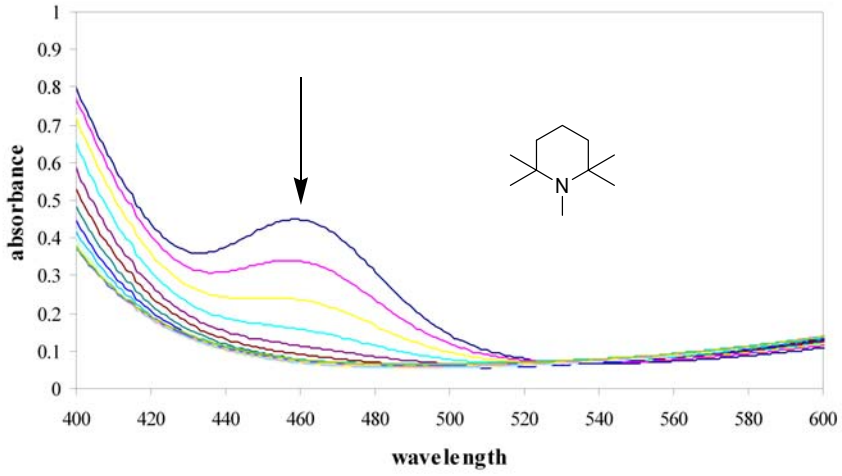

Figure 3.29 Decrease in the Absorbance of $(Cu_2$:**3.12**$)^{4+}$ with 2-Acetylcyclopentanone (2.1 eq.) upon Titration of **3.21**.

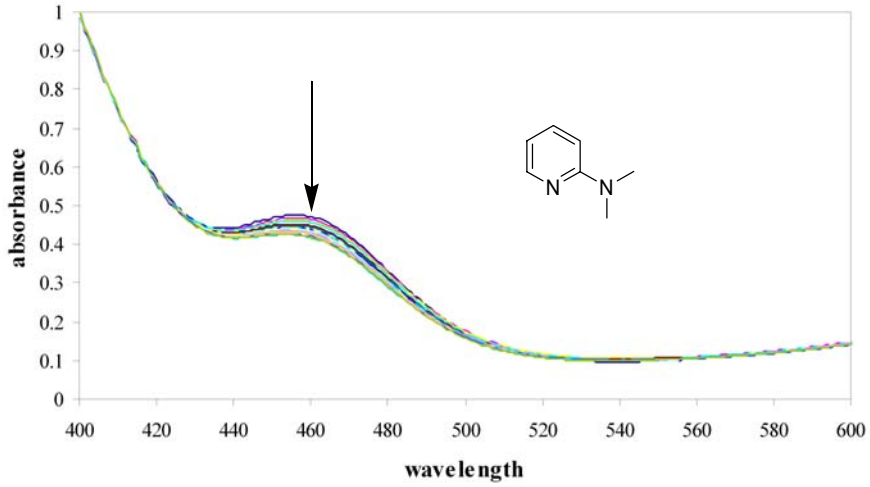

Figure 3.30 Decrease in the Absorbance of $(Cu_2$:**3.12**$)^{4+}$ with 2-Acetylcyclopentanone (2.1 eq.) upon Titration of **3.25**.

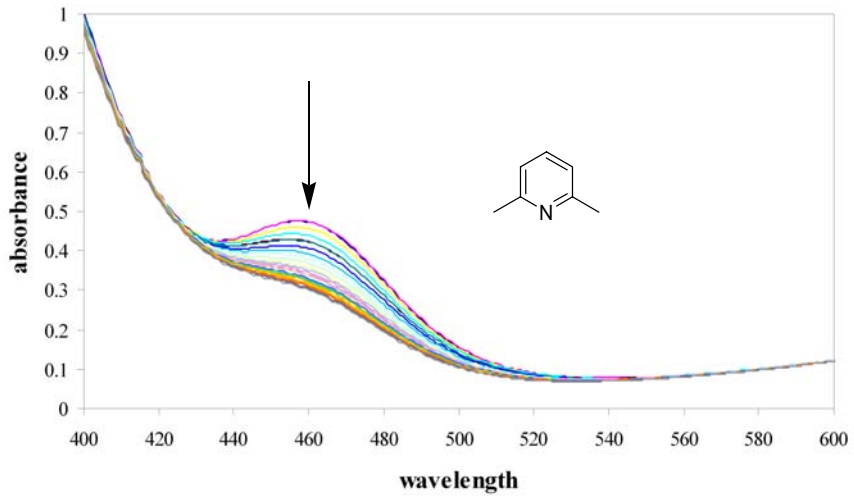

Figure 3.31 Decrease in the Absorbance of $(Cu_2$:**3.12**$)^{4+}$ with 2-Acetylcyclopentanone (2.1 eq.) upon Titration of **3.24**.

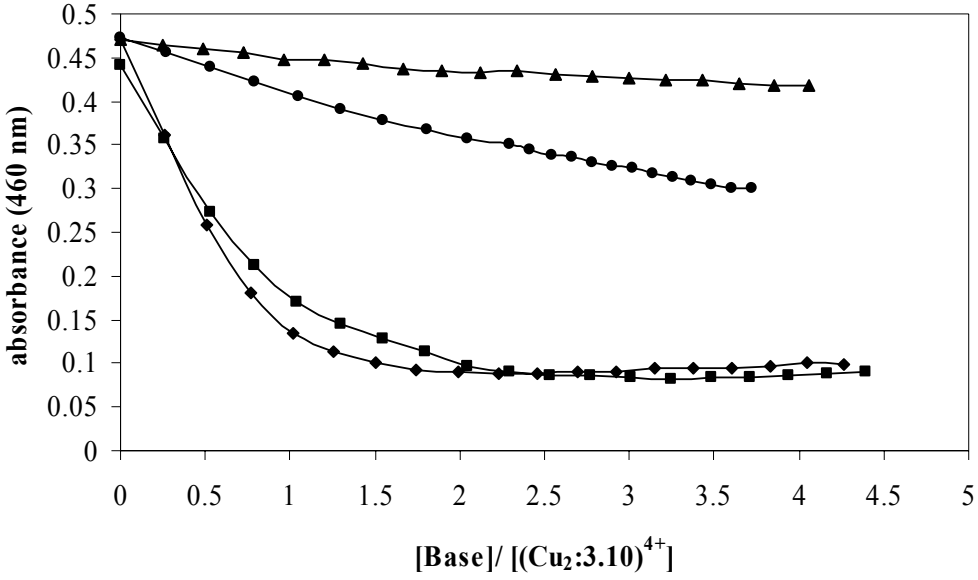

Figure 3.32 Decrease in the Absorbance of 0.97 mM (Cu_2:**3.12**)$^{4+}$ at 460 nm in the Presence of 2-Acetylcyclopentanone (2.1 equivalents) with Increasing Concentration of **3.21** (◊), **3.22** (■), **3.24** (▲), and **3.25** (●).

3.4.3 Results and Discussion

Qualitatively, Figure 3.32 indicates that 2,6-lutidine (**3.24**), with a conjugate acid pK_a of 14.2 in acetonitrile (Table 3.1) is capable of deprotonating 2-acetylcyclopentanone with a pK_a of 25.4 in acetonitrile.[20] From the information presented in Figure 3.32 the pK_a shift of 2-acetylcyclopentanone may be

calculated from the equilibrium expression between the carbon acid (HA) and the amine base (BH) as follows:

$$K_{eq} = ([A^-][BH^+])/ ([AH][B]) = K_{aAH}/K_{aBH^+}$$

The initial concentration of 2-acetylcyclopentanone for the titrations represented in Figure 3.32 is 0.00214 M. Upon the addition of 3 equivalents of 2,6-lutidine (B), the initial concentration of the carbon acid (AH) was 45% deprotonated, as indicated by the decrease in the absorbance of $(Cu_2$:**3.10**$)^{4+}$. The equilibrium expression becomes:

$$K_{eq} = ((0.45)\ [0.00214\ M]\ (0.45)\ [0.00214\ M])\ /\ ((0.55)\ [0.00214\ M])((3\ equivs. - 0.45)\ [0.00214\ M]) = 0.144$$

The conjugate acid pK_a of 2,6-lutidine in acetonitrile is 14.2 (Table 3.1). The pK_a shift may then be calculated from the equilibrium expression as follows:

$$K_{aAH} = (K_{aBH^+})(K_{eq}) = (6.30 \times 10^{-15})(0.144) = 9.07 \times 10^{-16}$$

The calculated pK_a for 2-acetylcyclopentanone in the presence of the $(Cu_2$:**3.12**$)^{4+}$ is 15.0. The shift in the pK_a is thus 10.4 pK_a units, as the pK_a of the carbon acid in acetonitrile is 25.4.

The 10 unit shift in the pK_a of 2-acetylcyclopentanone in the presence of $(Cu_2$:**3.12**$)^{4+}$ may be attributed to strong charge-pairing interactions between the enolate anion and metal center. A 10 unit shift is in good agreement with the 10 unit pK_a shift found by Kimura *et al.* with receptor **3.6** which similarly utilizes a zinc moiety to activate a carbonyl and subsequently reduce the pK_a of the α methylene proton.[16] These results suggest that the use of metal ions to reduce the pK_a of carbon acids is more effective than traditional hydrogen bonding (as used in receptors **3.10** and **3.11**).

In order to achieve such a dramatic shift in the pK_a, the binding of the anionic substrate must be significantly stronger than the binding of the neutral substrate. This relationship can be illustrated by the thermodynamic cycle of host-substrate binding (Figure 3.33) in which two routes to anion binding are shown. The first path, K_1- K_2, represents deprotonation of the substrate before binding to the host. In the second path, K_4- K_3, host-substrate binding occurs prior to deprotonation.

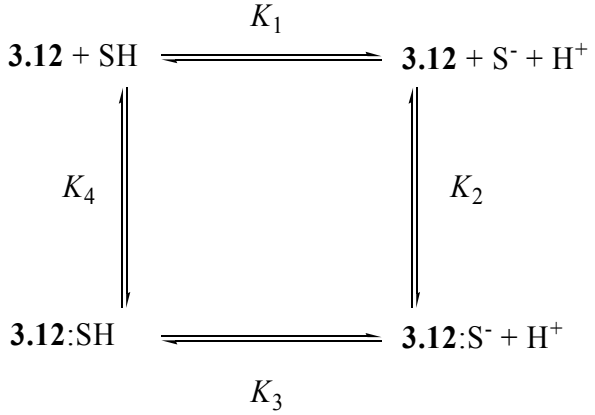

Figure 3.33 Thermodynamic Cycle for Substrate (S) Association and Substrate Deprotonation with **3.12**.

The ratio of the acid disassociation constants, K_1 and K_3, is equal to the ratio of the binding constants, K_2 and K_4 because $K_1K_2 = K_3K_4$. For cationic host complex $(Cu_2$:**3.12**$)^{4+}$, the value of K_2 should be large compared to K_4. Therefore, K_3 should be much greater than K_1. Since the ratio of K_3 and K_1 is the pK_a shift, a substantial pK_a shift is expected with the complex.

The stabilization of enolate anions by complex $(Cu_2$:**3.12**$)^{4+}$ is reminiscent of the use of the zinc(II) ion in the active site of class II aldolases. It is proposed that electrostatic interactions between the zinc(II) ion and carbon acid substrates increase the acidity of the substrates, such that the relatively weak base, glutamic carboxylate, in the enzyme active site of the enzyme FucA effects substrate deprotonation.[15]

3.4.4 Summary

The use of receptor **3.12** incorporating metal ions, specifically copper(II), has been shown to reduce the pK_a of 2-acetylcyclopentanone in acetonitrile by approximately 10 pK_a units. The relatively large pK_a reduction achieved by the complex is attributed to the electrostatic interaction between the anionic π-system of the enolate and the copper(II) ions. As in the active site of class II aldolases, electrostatic induction is more effective in stabilizing highly reactive

intermediates and inducing pK_a shifts of carbon acids than traditional hydrogen bonds.

3.4.5 Experimental

3.4.5.1 Synthesis

General Considerations. ^{1}H and ^{13}C spectra were obtained using an Oxford 400 MHz, Bruker AC-250 or a Varian 300 MHz spectrometer. Chemical shift values in parts per million are referenced to tetramethylsilane as an internal standard. Low-resolution and high-resolution mass spectra were measured with Finnigan TSQ70 and VG Analytical ZAB2-E instruments respectively.

All volumetric flasks and syringes were stored in a vacuum desiccator for 24 hours prior to use. Preparative flash chromatography was performed on Natland International 200-400 mesh silica gel. Dichloromethane and triethylamine were distilled from calcium hydride. Thionyl chloride was distilled under reduced pressure. Reagents were purchased from Aldrich, Lanscaster or EM Science and used as received unless noted.

1,3,5-Tris(chloromethyl)-2,4,6-triethylbenzene (3.13)

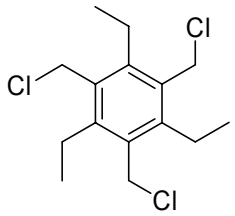

Into a 100 mL round-bottomed flask, fitted with a water condenser and a pressure-equilibrating addition funnel, was placed 1,3,5-triethylbenzene (5.0 g, 16.3 mmol) and 25 mL of carbon disulfide. A glass dispersion tube was placed into the solution and the solution was purged with argon. Tin tetrachloride (24.1 g, 92.0 mol) was added under argon. Chloromethyl methyl ether (22 mL, 277 mmol) was added to the addition funnel and incorporated rapidly, maintaining a controlled reflux. The mixture was stirred for 12 h under argon. The reaction was quenched with saturated aqueous $NaHCO_3$. Carbon disulfide was removed under reduced pressure and the remaining aqueous solution extracted with dichloromethane. The organic layer was washed with saturated aqueous $NaHCO_3$, water, and saturated aqueous sodium chloride, dried over $MgSO_4$, filtered and concentrated under reduced pressure to give a yellow solid. The crude product was purified using flash chromatography (silica, 50% dichloromethane in hexanes) to yield **3.13** (4.5 g, 48% yield) as a white crystalline solid. Mp. 130-132 °C. ^{1}H NMR (300 MHz, $CDCl_3$) δ (TMS) 4.69 (s, 6H), 2.94 (q, 6H, J = 7.5 Hz), 1.31 (t, 9H, J = 7.5 Hz); ^{13}C NMR (75 MHz, $CDCl_3$) δ 145.24, 132.86, 40.85, 22.86, 16.32; HRMS (CI^+) calcd for $C_{15}H_{21}Cl_3$: 306.071; found 306.071.

1,3,5-Tris(azidomethyl)-2,4,6-triethylbenzene (3.14)

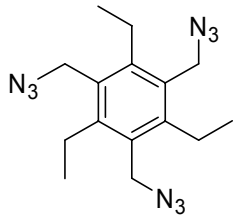

Conversion of 1,3,5-tris(chloromethyl)-2,4,6-triethylbenzene (**3.13**) to 1,3,5-tris(azidomethyl)-2,4,6-triethylbenzene (**3.14**) was accomplished by placing **3.13** (4.0 g, 13 mmol) into a 100 mL round-bottomed flask with 70 mL of *N,N*-dimethylformamide under argon. To this solution was added sodium azide (6.06 g, 93.2 mmol). After the mixture was stirred for 24 hours under argon, the solution was filtered and the *N,N*-dimethylformamide was removed under vacuum. The residue was dissolved in dichloromethane and washed with water followed by saturated aqueous sodium chloride. The organic layer was then dried over $MgSO_4$, filtered and concentrated under reduced pressure to give yellow crystals which were recrystallized from ethylacetate and hexanes to give **3.14** as white crystals (3.40 g, 80% yield). ^{1}H NMR (300 MHz, $CDCl_3$) δ (TMS) 4.49 (s, 6H), 2.85 (q, 6H, J = 7.5 Hz), 1.24 (t, 9H, J = 7.8 Hz); ^{13}C NMR (75 MHz, $CDCl_3$) δ 145.10, 130.12, 48.06, 23.30, 15.90; HRMS (CI^+) calcd for $C_{15}H_{21}N_9$: 327.192; found 327.192. FT-IR (deposit from $CDCl_3$ on NaCl) 2972 cm^{-1} (C-H), 2908 cm^{-1} (C-H), 2088 cm^{-1} (N=N=N).

1,3,5-Tris(aminomethyl)-2,4,6-triethylbenzene (3.15)

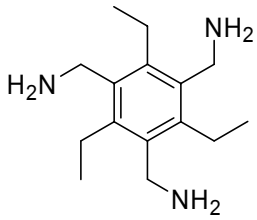

1,3,5-Tris(azidomethyl)-2,4,6-triethylbenzene (**3.14**) (3.0 g, 9.2 mmol) and triphenylphosphine (14.5 g, 55.2 mmol) in tetrahydrofuran-water (10:1) (600 mL) was stirred for 10 h at room temperature. The tetrahydrofuran-water solvent was removed under vacuum. The residue was dissolved in dichloromethane and washed with 1N aqueous HCl. The aqueous phase was then extracted with ethyl acetate. The aqueous phase was made alkaline by adding 3N aqueous sodium hydroxide until the pH was approximately 10 by pH paper and extracted with dichloromethane. The organic layer was dried over anhydrous $MgSO_4$, filtered and concentrated under reduced pressure to give a white solid. The crude product was purified *via* flash chromatography (silica, 1% ammonia saturated methanol in dichloromethane) to give **3.15** as a white solid (1.33 g, 58% yield). Mp. 125-126 °C. ^{1}H NMR (300 MHz, $CDCl_3$) δ (TMS) 3.88 (s, 6H), 2.83 (q, 6H, J = 7.8 Hz), 1.32 (bs, 6H), 1.24 (t, 9H, J = 7.5 Hz); ^{13}C NMR (75 MHz, $CDCl_3$) δ 140.61, 137.66, 39.90, 22.84, 17.07; FT-IR (deposit from $CDCl_3$ on NaCl) 3353 cm^{-1}, 3272 cm^{-1} (N-H); HRMS (CI^+) calcd for $C_{15}H_{26}N_3$: 248.212; found 248.212.

[3-aminomethyl-5(*tert*-butoxycarbonylamino-methyl)-2,4,6-triethyl-benzyl]-carbamic acid *tert*-butyl ester (3.16)

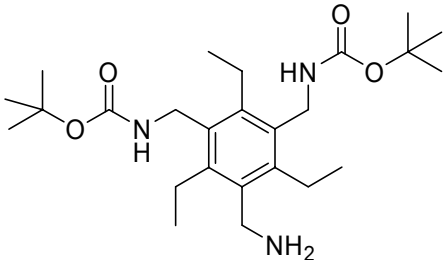

To a solution of 1,3,5-Tris(aminomethyl)-2,4,6-triethylbenzene (**3.15**) (0.5 g, 2.0 mmol) in chloroform was added di-*tert*-butyldicarbonate (0.65 g, 3.0 mmol). The solution was stirred for 3 hours. The solution was then filtered and the filtrand washed with 1N aqueous NaOH, water and saturated brine. The organic phase was isolated, dried over $MgSO_4$, filtered and the solvent removed under vacuum. Purification and isolation of the desired product was accomplished *via* column chromatographic purification (silica, 5% ammonia saturated methanol in dichloromethane, gradient elution to 30%) to yield **3.16** as a white solid (0.23 g, 25%). ^{1}H NMR (300 MHz, $CDCl_3$) δ (TMS) 4.35 (bs, 2H), 4.32 (m, 4H), 3.86 (s, 2H), 2.79-2.65 (m, 6H), 1.65 (bs, 2H), 1.42 (s, 18H), 1.21-1.15 (m, 9H); ^{13}C (100 MHz, $CDCl_3$) δ 181.1, 155.7, 144.0, 143.0, 141.6, 78.0, 39.0, 37.6, 28.6, 23.0, 16.9.

2,6-Pyridine dicarbonyl dichloride

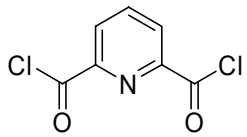

To a round bottomed flask equipped with a condenser, an addition funnel and a Dean-Stark trap was added pyridine dicarboxylic acid (10 g, 0.06 mol) with

100 mL of toluene. The solution was then refluxed to azeotropically remove water. Oxalyl chloride (23 g, 0.18 mol) was added via the addition funnel to the refluxing solution. A calcium hydride drying tube was placed on the condenser. The reaction was stirred at reflux until a clear, yellow solution was obtained. The solvent was then removed under vacuum and the residue recrystallized to yield **2,6-pyridine dicarbonyl dichloride** as a white crystalline solid (8.5 g,70%). ^{1}H NMR (250 MHz, $CDCl_3$) δ (TMS) 8.37 (d, 2H, J = 8.0 Hz), 8.17 (t, 1H, J = 8.0 Hz); ^{13}C (62.5 MHz, $CDCl_3$) δ 171.36, 151.24, 141.95, 131.56; FT-IR (deposit from $CDCl_3$ on NaCl) 1752 cm^{-1} (C=O).

Pyridine-2,6-dicarboxylic acid 2-(3,5-bis-aminomethyl-2,4,6-triethyl-benzylamide) 6-[(3,5-bis-aminomethyl-2,4,6-triethyl-phenyl)-amide] (3.17)

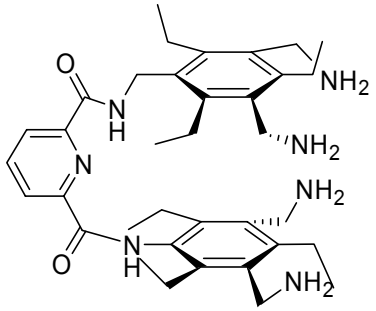

To a round-bottomed flask equipped with an addition funnel, condenser and a Dean Stark trap was added **3.16** (3.04 g, 6.76 mmol) in benzene. The solution was refluxed and water removed. The benzene was then removed in vacuo and the residue dissolved in 50 mL of anhydrous THF (previously distilled over sodium and benzophenone ketyl) and triethylamine (3.42 g, 33.8 mmol, previously distilled from calcium hydride). Anhydrous potassium carbonate was

then added (1.38 g, 10 mmol). 2,6-Pyridine dicarbonyl dichloride (0.69 g, 3.38 mmol) was added dropwise in 25 mL anhydrous THF. The reaction was monitored by thin layer chromatography. The solution was vacuum filtered and the solvent was removed under vacuum. The residue was purified by column chromatography (silica, ethyl acetate). The Boc protecting groups were removed in 100 mL of an aqueous solution of trifluoroacetic acid (1:1 v/v) and 20 mL of dichloromethane. The reaction was stirred at room temperature for two hours. The solvent was removed under vacuum and the residue was dissolved in a minimum amount of water. Chloride anion exchange was accomplished using Amberlite IRA-400 (Cl) yielding a white solid. Continuous extraction of the resulting solid from a 5N aqueous sodium hydroxide solution using dichloromethane gave **3.17** as a foamy solid (3.9 g, 92%). ^{1}H NMR (300 MHz, $CDCl_3$) δ (TMS) 8.35 (d, 2H, *J* = 7.9 Hz), 7.99 (t, 1H, *J* = 7.9 Hz), 7.54 (bs, 2H), 4.63 (d, 4H, *J* = 4.9 Hz), 3.83 (s, 8H), 2.82 (d, 4H, *J* = 7.6 Hz), 2.7 (q, 8H, *J* = 7.4 Hz), 1.86 (bs, 8H), 1.2 (t, 12H, *J* = 7.4 Hz); ^{13}C (75 MHz, $CDCl_3$) δ 163.56, 149.33, 142.22, 139.08, 131.52, 125.58, 39.61, 38.44, 23.12, 17.06, 16.85; IR (deposit from $CDCl_3$ on NaCl) 3294 cm^{-1} (NH) and 1659 cm^{-1} (C=O); HRMS (CI^+) calcd for $C_{37}H_{56}N_7O_2$ 630.449; found 630.449.

(3.12)

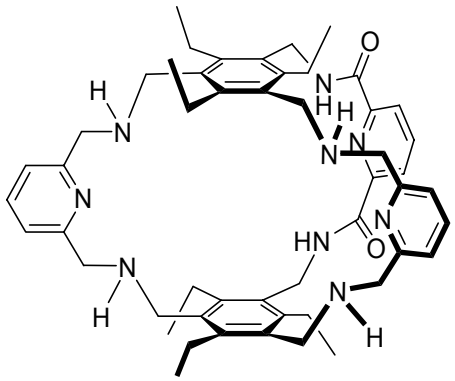

To a 500 mL round-bottomed flask equipped with an addition funnel, a condenser and a Dean-Stark trap was added **3.17** (0.50 g, 0.79 mmol) followed by 550 mL of toluene. The solution was heated to reflux and the azeotrope of water was received over calcium hydride in the Dean-Stark trap. To the solution was added 2,6-pyridine dicarboxaldehyde dissolved in 275 mL of toluene over 6 hours at room temperature. The reaction was heated to reflux for 18 hours. The remaining dialdehyde was added over 6 hours and the solution again heated to reflux for 18 hours. The solution was cooled to room temperature and the toluene removed in vacuo. To residue was dissolved in 100 mL anhydrous methanol under argon. To the solution was added $NaBH_4$ (365 mg, 9.65 mmol). The solution was then stirred for three hours under argon. The reaction was quenched with water and the methanol removed *in vacuo*. The residue was dissolved in 1N aqueous NaOH and extracted with dichloromethane (3 x 100 mL). The combined organic layers were washed with saturated brine, dried over $MgSO_4$, filtered and the solvent removed under vacuum. The resulting solid was purified *via* column chromatography (silica, 1% ammonia saturated methanol in dichloromethane) to

yield **3.12** as a yellow solid (496 mg, 75%). ^{1}H NMR (300 MHz, $CDCl_3$) δ (TMS) 8.35 (d, 2H, *J* = 7.4 Hz), 8.16 (bs, 2H), 8.06 (t, 1H, *J* = 7.4 Hz), 7.59 (t, 2H, *J* = 7.4 Hz), 7.08 (d, 2H, *J* = 7.4 Hz), 4.64 (d, 4H, *J* = 4.6 Hz), 3.93 (s, 8H), 3.78-3.77 (m, 8H), 2.88-2.74 (m, 8H), 2.62-2.55 (m, 4H), 1.82 (s, 4H), 1.17-1.08 (m, 18 H); ^{13}C (75 MHz, $CDCl_3$) δ 164.4, 159.8, 150.3, 144.3, 138.8, 137.5, 135.22, 132.0, 129.3, 126.3, 120.9, 118.3, 56.2, 48.6, 38.7, 23.3, 23.2, 16.9, 16.6; HRMS (CI^+) calcd for $C_{51}H_{66}N_9O_2$ 836.533; found 836.534.

General Procedure for the Preparation of Sodium Enolates and Phenoxides.

Sodium enolates and phenoxides were synthesized from sodium ethoxide in ethanol. One equivalent of sodium metal (from mineral oil) was placed into a tared, three-neck round-bottomed flask under argon. The mineral oil was removed by washing with 1.0 mL portions of petroleum ether and decanting the solvent under argon after each wash. After washing, the metal was dried under a stream of argon and the weight obtained by difference. The flask was cooled in an ice-water bath and ethanol was added dropwise from an addition funnel under argon. After the metal dissolved, one equivalent of β-diketone or phenol was added as a solution in ethanol. Subsequent removal of the ethanol under vacuum produced the enolate (or phenoxide) as a solid. To remove any unreacted starting material, the resulting solid was washed with anhydrous acetonitrile in a glovebox under nitrogen. The purified solid was stored in a glovebox under nitrogen.

3.4.5.2 Spectrophotometric Titrations.

General Considerations. The spectrophotometric studies were carried out on a DU-640 Beckman spectrophotometer. All Hamilton gas-tight syringes and volumetric flasks were dried in a dessicator for 24 hours prior to use. Septa and argon ballons were used to exclude water outside of the dry box. The sodium enolates were stored in a glovebox under nitrogen. The enolate-[2.2.1]cryptand solutions and host solutions were freshly prepared in acetonitrile prior to each titration. Reagents were obtained from Aldrich Chemical Co. and used as received, except for 2,6-lutidine which was obtained from Eastman Kodak. Reagents and solutions were stored in a dessicator.

Procedure for the Titration of Enolates. For a typical experiment, a stock solution of 0.25 M enolate-[2.2.1]cryptand was prepared by diluting 0.50 mM of the sodium enolate and 0.25 M of [2.2.1]cryptand to 2.0 mL in acetonitrile. A stock solution of 5.5 mM host complex was prepared by dissolving 0.010 mmol of **3.12** in 2.0 mL of acetonitrile. To 1.0 mL of the host stock solution was added 5.0 μL of a 2.0 M stock solution of $CuCl_2$ in methanol and the resulting **3.12**-$CuCl_2$ solution diluted to 2.0 mL in acetonitrile. For the titrant solution, 1.0 mL of the **3.12**-$CuCl_2$ solution was added to 0.20 mL of the enolate-[2.2.1] cryptand stock solution. The titrand was prepared by diluting 1.0 mL of the **3.12**-$CuCl_2$ solution with 0.20 mL of acetonitrile, such that in both the titrant and titrand, the

concentration of the **3.12**-$CuCl_2$ complex was equal. The absorbance spectrum of 1.0 mL of the titrand was recorded. Spectra were then recorded after 5.0 μL additions of the titrant, until a total volume of 1.20 mL was obtained.

Procedure for the Titration of Amine Bases. A 2.0 M stock solution of $CuCl_2$ in methanol was prepared by diluting 0.995 mmol of $CuCl_2$ to 0.5 mL in acetonitrile. A 1.07 M stock solution of 2-acetylcyclopentanone was prepared by diluting 0.13 mL of the diketone to 1.0 mL in acetonitrile. A 6.94 mM stock solution of 3.10 was prepared by diluting 0.0139 mmol in 2.0 mL of acetonitrile. A 0.25 M stock solution of each base was prepared prior to each titration. The complex $(Cu_2$:**3.12**$)^{4+}$ was prepared by adding 2.5 uL of the $CuCl_2$ stock solution to 0.35 mL of the stock solution of **3.12** with 5.0 uL of the 2-acetylcyclopentanone stock solution and diluting to 2.0 mL in acetonitrile. The titrant was prepared by adding 0.25 mL of the base stock solution to 1.0 mL of this solution. The titrand was prepared by adding 0.25 mL of acetonitrile to the $(Cu_2$:**3.12**$)^{4+}$ and 2-acetylcyclopentanone solution to give an initial concentration of 0.968 mM of $(Cu_2$:**3.12**$)^{4+}$, 2.14 mM 2-acetylcyclopentanone and 1.99 mM $CuCl_2$ in both the titrant and titrand. The absorbance spectrum of 1.0 mL of the titrand was recorded. Spectra were then recorded after 5.0 μL additions of the titrant, until a total volume of 1.09 mL was obtained.

3.5 REFERENCES

[1] Easton, C. J.; Lincoln, S. F. In *Modified Cyclodextrins*; Imperial College Press: London, 1999.

[2] a) Tabushi, I.; Shimizu, N.; Sugimoto, T.; Shiozuka, M.; Yamamura, K. *J. Am. Chem. Soc.* **1977**, *99*, 7100-7102. b) Tabushi, I.; Kuroda, Y.; Mizutani, T. *Tetrahedron* **1984**, *40*, 545-552.

[3] Breslow, R.; Dong, S. D. *Chem. Rev.* **1998**, *98*, 1997-2011.

[4] Breslow, R.; Overman, L. E. *J. Am. Chem. Soc.* **1970**, *92*, 1075-1077.

[5] Martell, A. E.; Motekaitis, R. J. *J. Am. Chem. Soc.* **1988**, *110*, 8059-8064. b) Bazzicalupi, C.; Bencini, A.; Bianchi, A.; Fusi, V.; Garcia-España, E.; Giorgi, C.; Llinares, J. M.; Ramirez, J. A.; Valtancoli, B. *Inorg. Chem.* **1999**, *38*, 620-621. c) Pauwels, T. F.; Smet, P. W.; Goeminne, A. M. *Polyhedron* **2001**, 2457-2466. d) Pauwels, T. F.; Lippens, W.; Smet, P. W.; Herman, G. G.; Goeminne, A. M. *Polyhedron* **1999**, 1029-1037. e) Gale, P. A. *Coordination Chemistry Rev.* **2001**, *213*, 79-128. f) Fitzmaurice, R. J.; Kyne, G. M.; Douheret, D.; Kilburn, J. D. *J. Chem. Soc., Perkin Trans. 1* **2002**, 841-864.

[6] Chin, J.; Lee, S. S.; Lee, K. J.; Park, S.; Kim, D. H. *Nature* **1999**, *401*, 254-257.

[7] Greenstein, J. P.; Winitz, M. In *Chemistry of the Amino Acids,* Vol. 1; Wiley and Sons: New York, 1996.

[8] Chin, J.; Chung, S.; Kim, D. H. *J. Am. Chem. Soc.* **2002**, *124*, 10946-10948.

[9] Albelda, M. T.; Burguete, M. I.; Frías, J. C.; García-España, E.; Luis, S. V.; Miravet, J. F.; Querol, M. *J. Org. Chem.* **2001**, *66*, 7505-7510.

[10] Darbre, T.; Dubs, C.; Rusanov, E.; Stoeckli-Evans, H. *Eur. J. Inorg. Chem.* **2002**, 3284-3291.

[11] a) Alhambra, C.; Gao, J.; Corchado, J. C.; Truhlar, D. G. *J. Am. Chem. Soc.* **1999**, *121*, 2253-2258. b) Liu, H.; Zhang, Y.; Yang, W. *J. Am. Chem. Soc.* **2000**, *122*, 6560-6570.

[12] a) Guthrie, J. P.; Kluger, R. *J. Am. Chem. Soc.* **1993**, *115*, 11569-11572. b) Maurice, M.; Bearne, S. L. *Biochemistry* **2000**, *39*, 13324-13335. c) Glavas, S.; Tanner, M. E. *Biochemistry* **2001**, *40*, 6199-6204.

[13] a) Dreyer, M. K.; Schulz, G. E. *J. Mol. Biol.* **1996**, *259*, 458-466. b) Fessner, W.-D.; Schneider, A.; Held, H.; Sinerius, G.; Walter, C.; Hixon, M.; Scholss, J. V. *Angew. Chem. Int. Ed. Engl.* **1996**, *35*, 2219-2221.

[14] Kobes, R. D.; Simpson, R. T.; Vallee, B. L.; Rutter, W. J. *Biochemistry* **1969**, *8*, 585-588.

[15] Joerger, A. C.; Gosse, C.; Fessner, W.-D.; Schulz, G. E. *Biochemistry* **2000**, *39*, 6033-6041.

[16] Kimura, E.; Gotoh, T.; Koike, T.; Shiro, M. *J. Am. Chem. Soc.* **1999**, *121*, 1267-1274.

[17] Kelly-Rowley, A. M.; Lynch, V. M.; Anslyn, E. V. *J. Am. Chem. Soc.* **1995**, *117*, 3438-3447.

[18] Robertus, J. D.; Kraut, J.; Alden, R. A.; Birktoft, J. J. *Biochemistry* **1972**, *11*, 4302.

[19] Vock, P.; Engst, S.; Eder, M.; Ghisla, S. *Biochemistry* **1998**, *37*, 1848.

[20] Snowden, T. S.; Bisson, A. P.; Anslyn, E. V. *J. Am. Chem. Soc.* **1999**, *121*, 6324-6325.

[21] Benning, M. M.; Taylor, K. L.; Liu, R.-Q.; Yang, G.; Hong, X.; Wesenberg, G.; Dunaway-Mariano, D.; Holden, H. M. *Biochemistry* **1996**, *35*, 8103.

[22] Rockcliffe, D. A.; Martell, A. E.; Reibenspies, J. H. *J. Chem. Soc., Dalton Trans*. **1996**, 167-175.

[23] Bisson, A. P.; Lynch, V. M.; Monahan, M. C.; Anslyn, E. V. *Angew. Chem. Int. Ed. Engl.* **1997**, *36*, 2340.

[24] a) Iverson, D.; Hunter, G.; Blount, J. F.; Damewood, Jr., J. R.; Mislow, K. *J. Am. Chem. Soc.* **1981**, *103*, 6073. b) Stack, T. D. P.; Hou, S.; Raymond, K. N. *J. Am. Chem. Soc.* **1993**, *115*, 6466.

c) Walsdorff, C.; Saak, W.; Pohl, S. *J. Chem. Res. Synop.* **1996**, *33*, 2313.

[25] Hanes, R. E., Jr.; Lavigne, J. J.; Anslyn, E. V.; Kilway, K. V.; Siegel, J. *Org. Syn.* **2003**, In preparation.

[26] Vaultier, M.; Knouzi, N.; Carrie, R. *Tetrahedron Let.* **1983**, *24*, 763.

[27] Tsukube, H.; Furuta, H.; Odani, A.; Takeda, Y.; Kudo, Y.; Inoue, Y.; Liu, Y.; Sakamoto, H.; Kimura, K. In *Comprehensive Supramolecular Chemistry*, Vol. 8; Davies, J. E. D., Ripmeester, J. A., Eds. Pergamon Press: Oxford, 1996; Chapter 10.

[28] Bell, D. A.; Anslyn, E. V. *J. Org. Chem.* **1994**, *59*, 512-514.

[29] Hannon, C. L.; Bell, D. A.; Kelly-Rowley, A. M.; Cabell, L. A.; Anslyn, E. V. *J. Phys. Org. Chem.* **1997**, *10*, 396-404.

[30] Serjeant, E. P.; Dempsey, B. In *Ionization Constants of Organic Acids in Aqueous Solutions*; Pergamon: Oxford, 1979.

Bibliography

Carey, F. A. Sundberg, R. J. *Advanced Organic Chemistry, Part B: Reactions and Synthesis*, 2nd edition; Plenum Press: New York, 1983.

Connors, K. A. *Binding Constants: The Measurement of Molecular Complex Stability*; Wiley-Interscience: New York, 1987.

March, J. *Advanced Organic Chemistry*, 3rd edition; Wiley and Sons: New York, 1985.

Zumdahl, S. S. *Chemistry*; D. C. Heath and Company: Lexington, Massachusetts, 1986.

Cervinka O. *Enantioselective Reactions in Organic Chemistry*; Academia Publishing House of the Academy of Sciences of the Czech Republic: Prague, Czech Republic, 1995.

Smith, M. B. *Organic Synthesis*; McGraw-Hill, Inc.: New York, 1994.

Lowry, T. H., Richardson, K. S. *Mechanism and Theory in Organic Chemistry*, 3rd edition; Harper Collins Publishers: New York, 1987.

Paesler, M. A., Moyer, J. P. *Near Field Optics: Theory, Instrumentation and Applications*; John Wiley and Sons: New York, 1996.

Augustine, R. L. *Carbon-Carbon Bond Formation*, Vol. 1; Marcel Dekker: New York, 1979.

Jacobsen, E. N., Pfaltz, A., Yamamoto, H. *Comprehensive Asymmetric Catalysis*, Vol. I; Springer, Berlin: 1999.

Morrison, J. D. *Asymmetric Synthesis*, Vol. 3; Academic Press: New York, 1984.

Trost, B. M., Fleming, I. *Comprehensive Organic Synthesis*, Vol. 3; Pergamon Press: Oxford, 1991.

Bueche, F. J. *Principles of Physics*, 5th Edition; McGraw-Hill: New York, 1988.

Vita

Brenda Jean Postnikova was born in Dallas, Texas on November 10, 1974, the daughter of Gary E. Holtzman and Lea Royce Holtzman. After graduating Valedictorian from Van Alstyne High School in Van Alstyne, Texas in 1993, she entered Austin College in Sherman, Texas. In the summer of 1996, she participated in a research program sponsored by the National Science Foundation at Texas A&M University. In January 1997, she graduated Summa Cum Laude with a Bachelor of Arts in Chemistry. She entered graduate school at The University of Texas at Austin and received a Master of Arts in Chemistry in December 1999. In August 2000, she joined Professor Eric V. Anslyn's research group at The University of Texas at Austin.

Permanent address: 800 West 38th Street, #8205, Austin, Texas 78705.

This dissertation was typed by the author.